Understanding Disease Progression and Target Identification for Multiple Myeloma

Murat Cem Köse

Faculty of Medicine

Laboratory of Hematology

Academic Year: 2022-2023

Promoter: Prof. Yves Beguin Co-Promoter: Dr. Jo Caers

Acknowledgements

As I come to the end of this special chapter in my life, I would like to acknowledge everyone who has been with me along this long and difficult journey.

First of all, I would like to express my deepest thanks to those who made this work possible. Their hard work and dedication opened the doors of research for young scientists like me. I would like to thank Prof. Yves Beguin for this unique opportunity to do my PhD in the laboratory of Hematology. He has always been very supportive of each of us. A special thanks to Dr. Jo Caers, Dr. Tine Casneuf, and Dr. Dries De Maeyer. Their belief in my skills and their guidance through challenging times have been a great motivation and encouragement for me. I learned so much from them, both professionally and personally, and I am extremely grateful to have met and worked with each of them.

I would like to thank all members of my thesis committee and jury for evaluating my work and providing constructive feedback. The discussions we had during our meetings have been greatly inspiring.

Another special thanks to Dr. Isabelle Bergiers, with whom I have worked together on a daily basis. She has been a great colleague to me, and I have learned so much from her. I would also like to thank Dr. Sheri Skerget, who coached me towards the end of my PhD.

Moreover, I would like to express my gratitude to Prof. Frederic Baron and my colleagues at the laboratory of Hematology: Lorenzo, Benoit, Greg, Caroline, Elodie, Margaux, Justine, Michelle, Megane, Louise, Charline, Oswin, Bianca, Valentina, Coline, and Sophie. As a team, we have been very productive.

Their supportive and friendly attitude towards me greatly helped me, for which I am sincerely grateful.

Finally, I want to thank my family and friends, including Luca Balazs, Ramon Duran, Alp Tetikel, and Baturay Ofluoglu, for their moral support. Their presence in hard times gave me the motivation to keep going.

List of Contents

List of Abbreviations

MM	Multiple myeloma
BM	Bone marrow
PC	Plasma cell
Ig	Immunoglobulin
BCR	B-cell receptor
CDR3	Complementary determining region 3
VDJ	Variable diversity joining
MGUS	Monoclonal gammopathy of unknown significance
SMM	Smoldering multiple myeloma
PCL	Plasma cell leukemia
MRI	Magnetic resonance imaging
PET/CT	Positron emission tomography-computed tomography
AL	Light chain amyloidosis
DSS	Durie-Salmon staging
ISS	International staging system
RISS	Revised international staging system
IGH	Ig heavy chain
RB1	Retinoblastoma 1
FGFR3	Fibroblast growth factor receptor 3
MMSET	Multiple myeloma SET domain
CNV	Copy number variation
1q	Q arm of chromosome 1
NK	Natural killer
MHC	Major histocompatibility complex
MICA	MHC Class I Polypeptide-Related Sequence A
Treg	Regulatory T-cell
Breg	Regulatory B-cell

DC	Dendritic cell
MDSC	Myeloid-derived suppressor cell
NOS	Nitric oxide synthase
ROS	Reactive oxygen species
MSC	Mesenchymal stromal cell
ASCT	Autologous stem cell transplantation
CAR	Chimeric antigen receptor
scRNA-seq	Single cell RNA sequencing
FACS	Fluorescence activated cell sorting
cDNA	Complementary DNA
PCR	Polymerase chain reaction
IVT	In vitro transcription
UMI	Unique molecular identifiers
GEM	Gel beads in emulsion
SAM	Sequence alignment/map
BAM	Binary alignment/map
CPM	Counts per million
HVG	Highly variable genes
PCA	Principal component analysis
tNSE	T-distributed stochastic neighbor embedding
UMAP	Uniform manifold approximation and projection
DGE	Differential gene expression
GSEA	Gene set enrichment analysis
CITE-seq	Cellular indexing of transcriptomes and epitopes by sequencing
READ-seq	RNA expression and protein sequencing assay
ADT	Antibody derived tag
TCR	T-cell receptor
scVDJ-seq	Single cell VDJ sequencing
iMSC	Inflammatory mesenchymal stromal cell

PFS	Progression-free survival
RP	Rapid progressor
NP	Non-progressor
10xWGS	10x Genomics linked-read whole genome sequencing

Multiple Myeloma

Multiple myeloma (MM) is a hematologic cancer of bone marrow (BM) plasma cells (PC). The name "multiple myeloma" refers to the first observations in patients who presented multiple bone lesions in their BM[1]. It is the second most common hematologic malignancy[2] and is known to be treatable but incurable due to high relapse rate[3]. It is a disease that is more common in elderly patients with the median age of 69 and most patients are diagnosed at a higher age than 65.[2] Every year, approximately 100 000 people lose their lives from MM.[2] Extraordinarily, the disease is twice more frequent in Black ethnicity[4] and observed at a younger age[5], compared to White ethnicity. It also has a higher incidence in men than in women.[6]

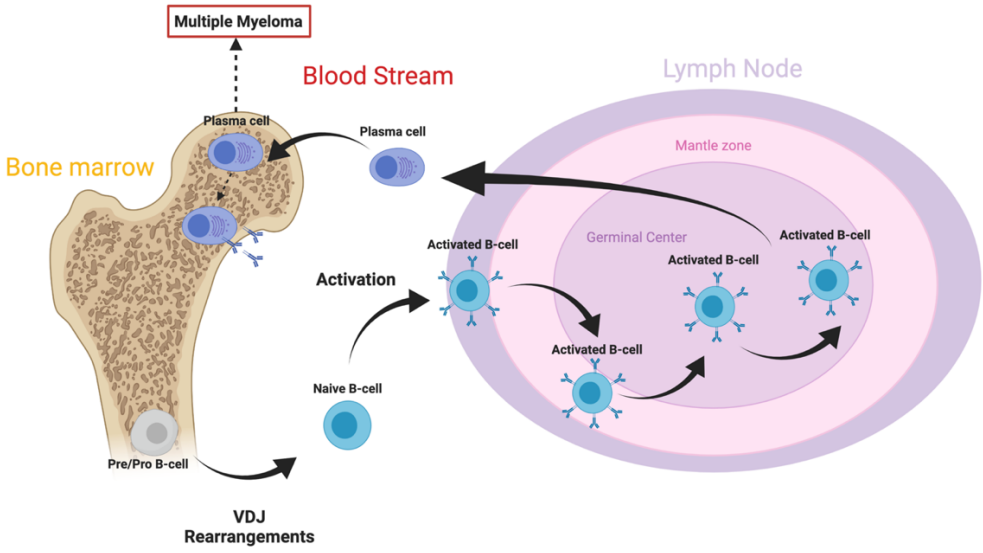

Figure 1. Life cycle of B-cells. Figure is adapted from Lejeune et al. [7]

To comprehend MM, it is important to understand how PCs mature and function. PCs belong to a larger family called B-cells. B-cells are characterized by their cell-specific immunoglobulins (Ig), B-cell receptors (BCR). These receptors build up a diverse repertoire for immune reactions against pathogens. When B-cells

encounter a foreign antigen through BCR, they get activated and expand clonally.[8] BCRs are composed of two chains, a heavy chain and a light chain, each of which has constant and variable regions. The complementary determining region 3 (CDR3) in the variable region of the chains are highly diverse, which allows for the generation of a large immune repertoire. This diversity is achieved through the recombination of different variable (V), diversity (D), and joining (J) segments, resulting in unique immune receptors.

The life of B-cells starts in the bone marrow, as hematopoietic stem cells initially differentiate into pre-B-cells (Figure 1). Along their maturation, these cells gain the ability to produce BCR, differentiate into naive B-cells and migrate to blood stream. When naive B-cells encounters a pathogen antigen, they get activated and migrate to lymph nodes. In lymph nodes, they differentiate into mature B-cells, initiating rapid proliferation. Some B-cells further maturate into memory B-cells, long-lived circulating B-cells that can generate an acute response in the future, when encountered with the same pathogen. The remaining, on the other hand, migrate to bone marrow and differentiate into short-lived antibody-secreting plasma cells.

The cause of MM is unknown. Yet, uncontrolled proliferation of defective plasma cells in the bone marrow results in excessive production of aberrant antibodies. As the disease progresses, the accumulation of tumor burden, the activation of bone-resorbing osteoclasts and production of excessive amounts of antibodies causes multiple tissue damages including bone lesions, kidney failure, and anaemia.[6,9]

Characteristics of MM

Progression Stages

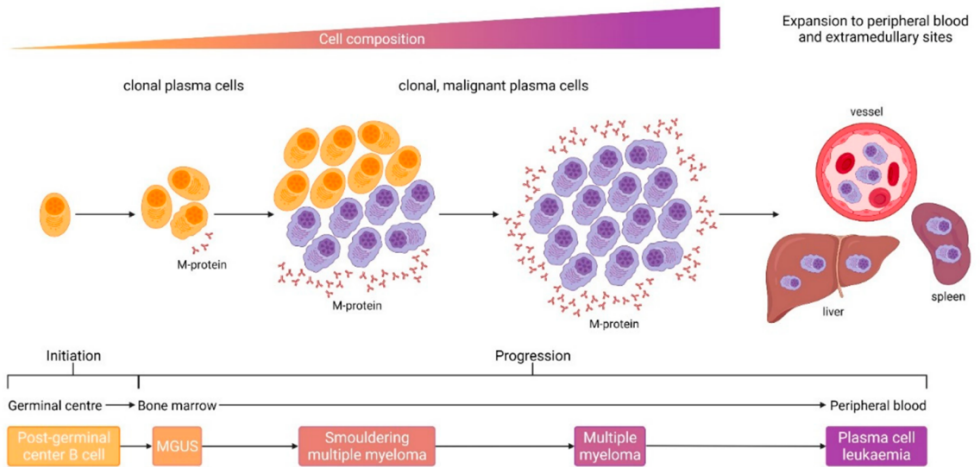

Figure 2. MM progression steps. The figure is adapted from Neumeister et al.[10]

MM is an advanced plasma cell disorder, resulting in tissue damages. Between the initial event and MM stage, alterations take place in genome and proteome, accumulating in abnormal cells. These events cause them to branch into new clonotypes, some of which become more aggressive over time. There are two precursor stages of MM, where aberrant plasma cells are observed but not causing symptoms (Figure 2). Monoclonal gammopathy of unknown significance (MGUS) patients are characterized by low levels (<10%) of aberrant plasma cells, which are identified by the abnormal levels of M (monoclonal) protein in the blood.[11] At this stage, there are no symptoms observed that harms the body. Nevertheless, every year, 1-2% of these patients progress to MM.[11] Smoldering multiple myeloma (SMM) is an advanced stage of MGUS. There are higher levels of circulating M proteins observed in these patients as well as >10% plasma cells in the bone marrow.[3] About 10% of SMM patients progress to MM each year.[3] When the patients develop symptoms that meet CRAB

criteria (hypercalcemia, renal impairment, anemia, bone lesions), they are diagnosed as MM. A detailed comparison of the precursor stages and MM is shown in Table 1.

Moreover, around 2-4% of plasma cell dyscrasias are observed in the form of plasma cell leukemia (PCL), where the plasma cells are also observed to be circulating in the peripheral blood.[12] PCL could emerge with or without progressing from MM. Those appear without previous evidence of MM are called primary PCL and constitute about 65% of the patients. On the other hand, 35% of PCL cases develop from MM and called secondary PCL.[12]

Light chain amyloidosis (AL) is another disorder caused by abnormal plasma cells. Similar to MM, abnormal antibodies, monoclonal light chain fragments accumulate in distant organs and cause various problems, such as heart and kidney damages. It is important to note that diagnosis of MM requires accumulation of tumor cells in the bone marrow, while AL can develop independent of tumor formation. Nevertheless, around 10-15% MM patients also develop AL.[11]

Symptoms and Diagnosis

Table 1. National Comprehensive Cancer Network and International Myeloma Working Group Diagnostic Criteria for MGUS, SMM and MM.[13] The table is adapted from Cowan et al.[11]

Criteria	Monoclonal gammopathy of undetermined significance	Smoldering multiple myeloma	Multiple myeloma
Monoclonal protein quantification	<3 g/dL	≥3 g/dL[a]	Typically present[b]
Bone marrow plasma cells by CD138 IHC	<10%	≥10%[a]	≥10%[c]
Urinary monoclonal protein (Bence Jones protein)	<500 mg/24 h	≥500 mg/24 h	Typically present[b]
Myeloma-defining events	Absent	Absent	End-organ damage attributable to the plasma cell neoplasm[d]: Hypercalcemia (serum calcium >1 mg/dL higher than upper limit of normal or >11 mg/dL) Kidney injury (serum creatinine >2 mg/dL or creatinine clearance <40 mL/min/1.73 m2) Anemia (hemoglobin >2 g/dL below lower limit of normal or <10 g/dL) Bone lesions (≥1 osteolytic lesions on osseous radiograph, computed tomography, or PET-CT) More than 1 of the following biomarkers of myeloma[d]: Clonal bone marrow plasma cells ≥60% Ratio of involved to uninvolved serum free light chains ≥100 and involved FLC concentration 10 mg/dL or higher >1 focal lesion on MRI ≥5 mm

Abbreviations: FLC, free light chains; MRI, magnetic resonance imaging; PET-CT, positron emission tomography–computed tomography.

SI conversion factors: To convert calcium values to mmol/L, multiply by 0.25; creatinine values to μmol/L, multiply by 88.4; creatinine clearance values to mL/s/m^2, multiply by 0.0167.

[a] For smoldering multiple myeloma, either monoclonal protein level 3 g/dL or greater or bone marrow plasma cells 10% or greater fulfills the diagnostic criteria.

[b] A monoclonal protein in the serum or urine, identified by serum protein electrophoresis or urine protein electrophoresis, is typically present in patients with multiple myeloma; however, in 1% to 2% of patients it is absent (termed "nonsecretory multiple myeloma").

[c] This requirement is not necessary for patients who have more than 1 biopsy-proven plasmacytoma, although bone marrow involvement is common.

[d] A diagnosis of multiple myeloma is confirmed in patients with 10% or greater abnormal plasma cells in the bone marrow and at least 1 of the end-organ events or myeloma-defining biomarkers shown.

The most common symptoms of MM include fatigue, bone pain and anemia.[14] The diagnosis of multiple myeloma requires the presence of one or more myeloma-defining CRAB events as well as evidence of 10% or greater abnormal plasma cells in the bone marrow. After an initial examination, patients are subjected to various diagnostic evaluations, including laboratory studies, urine studies, bone marrow biopsy, and radiology.[3] Serum and urine assays are used to assess the levels of serum calcium as well as creatinine, hemoglobin and M proteins.[11] The evaluation of bone disease can be conducted by magnetic resonance imaging (MRI) or positron emission tomography-computed tomography (PET/CT) imaging.[11] Further assessments of disease biology can be conducted with genetic and molecular studies. FISH assay and karyotyping can be used for cytogenic abnormality evaluation.[11]

Staging

The staging in MM is traditionally assessed by the Durie-Salmon Staging (DSS)[15] or International Staging System (ISS)[16]. While both staging systems take into account tumor burden, they lack the element of disease biology, which has a high impact on overall survival.[17,18] In 2014, the revised international staging system (RISS)[19] is announced. Unlike ISS, RISS also considers disease biology, involving cytogenetic risk stratification (Table 2). As a result of this combination, the 5-year survival rate of the Stage I, II, III patients were estimated as 82%, 62%, and 40%, respectively.[19]

Table 2. Revised International Staging System for Myeloma. The table is adapted from Rajkumar et al.[18]

Stage	Frequency (% of Patients)	5-Year Survival Rate (%)
Stage I	28	82
ISS stage I (serum albumin > 3.5, serum beta-2-microglobulin < 3.5) and		
No high-risk cytogenetics		
Normal LDH		
Stage II	62	62
Neither stage I or III		
Stage III	10	40
ISS stage III (serum beta-2-microglobulin > 5.5) and		
High-risk cytogenetics [t(4;14), t(14;16), or del(17p)] or elevated LDH		

Abbreviations: LDH, lactate dehydrogenase; ISS, International Staging System.

Prognostic factors

MM is a complex and multi-factorial disease, and its exact cause is not fully understood. Yet, there are common mechanisms observed among the patients that take place along disease progression (Figure 3). The events that are commonly observed at early disease stages are called primary events and they have a significant impact on disease biology, affecting the course of the disease, response to therapy and prognosis (Table 3).[18] Thus, they are frequently used for the categorization of patients. As the disease progresses, additional abnormalities are observed in abnormal plasma cells. These are called secondary events.

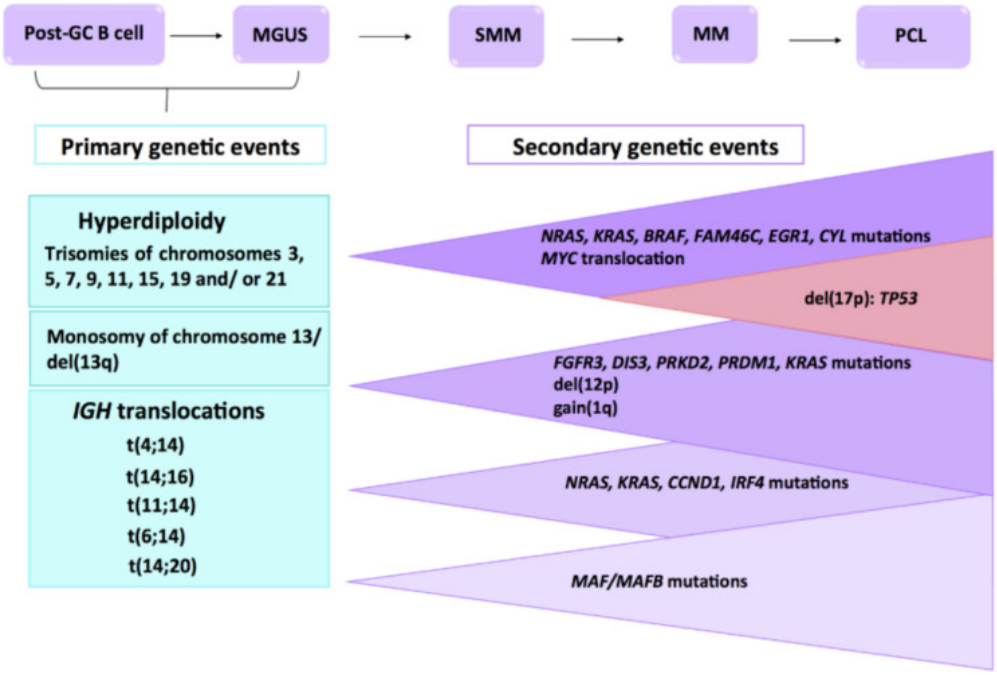

Figure 3. Intra-tumoral abnormalities that takes place along MM disease progression. Figure adapted from Cardona et al.[20]

Primary Genetic Events

Plasma cells are specialized cells producing very high amount of Igs and the most common abnormalities observed in MM are translocations related to Ig heavy chain (IGH), located on chromosome 14. However, translocations are not the only cytogenetic abnormalities observed in MM. Partial and/or complete chromosomal gains and deletions are also frequently detected, resulting in significant losses or gains of functionality as well as increased genomic instability. Thus, these events are also considered primary drivers in development of MM.[20,21]

Table 3. MM cytogenetic risk assessment. Table adapted from Wallington et al.[22]

Cytogenetic abnormality	Genes affected	Percentage in MM	Prognosis
Trisomies	Odd-numbered chromosomes	40–50	Favourable
Monosomy 13	*RB1*	45–50	Intermediate
1q gain	*CKS1B* and others	35–40	Poor
1p del	*FAM46C*, *CDKN2C* and *FAF1*	30	Poor
MYC 8q24	*MYC*	15–20	Poor
t(4;14)	*FGFR-3* and *MMSET*	15	Poor/Intermediate
t(11;14)	*CCND1*	15	Favourable
17p del	*TP53*	10	Poor
t(6;14)	*CCND3*	5	Favourable
t(14;16)	*c-MAF*	5	Poor
t(14;20)	*MAFB*	1	Poor

IGH translocations

These translocations involve up-regulation of key oncogenes under influence of IGH enhancer.[20] Translocations t(11;14) and t(6;14) elevate the expression of the cyclin genes CCND1 and CCND3 respectively, inactivating retinoblastoma 1 (RB1) and causing dysregulation in cell cycle control.[20,23] Similarly, t(4;14) causes overexpression of fibroblast growth factor receptor 3 (FGFR3) and multiple myeloma SET domain protein (MMSET), which results in overexpression of CCND2.[24] Moreover, increased MMSET expression is reported to be associated with dysregulation in DNA repair mechanism and demethylation of histone H3K36, leading to increased chromosomal instability.[25,26] Translocations t(14;16) and t(14;20)

deregulate MAF and MAFB genes respectively. Up-regulation in MAF gene family also induces CCND2 expression, leading to accelerated proliferation.[24] An overview of cytogenic abnormalities and their prognostic effects are listed in Table 3.

Chromosomal abnormalities

Hyperdiploidy is observed in approximately half of MM cases. It is characterized by extra copies of the odd chromosomes, 3, 5, 6, 7, 9, 11, 15, 19, 21.[20] The underlying mechanism of these chromosomal gains and how they contribute to MM progression remain unclear.[24] The most frequently occurring hyperdiploidy case is trisomy 11, which is known to increase the expression of CCND1 that is located on chromosome 11.[24] In addition to chromosomal gains, loss of the q arm or monosomy of chromosome 13, where the tumor suppressor gene RB1 is located, is considered a high-risk factor in MM.[22]

Secondary Genetic Events

MM development is a multistep process. Along transition from MGUS to MM, additional genomic abnormalities accumulate in abnormal plasma cells, providing additional advantages, such as increased survival and proliferation, leading towards a more aggressive disease. These events include key mutations and additional chromosomal changes.

The mutational diversity is very high in MM, with around 250 mutated genes described, 60 of which are considered to be driver genes.[27,28] Yet, only a few of them are mutated in more than 5% of patients, including KRAS (20–25%), NRAS (20–25%), TP53 (8–15%), DIS3 (11%), FAM46C (11%) and BRAF (6–15%).[20] Most of the mutations observed are related to key pathways, such as MAPK, MYC, DNA repair mechanism, NF-kB, JAK-STAT and cell cycle control.

Among the most commonly observed mutations in MM, proto-oncogenes KRAS, NRAS, BRAF, and DIS3 are associated with the activation of the ERK/MEK pathway. Disruption in the ERK/MEK pathway trigger a cascade of kinase activity. As a consequence, several transcription factors (including MYC) become activated, ultimately leading to uncontrolled cell proliferation and growth.[29–31]. Another key mutation frequently observed in MM is the TP53 tumor suppressor gene. It can occur as monoallelic mutations, where a single allele is affected, or biallelic mutations, where both alleles are affected. Monoallelic mutations pose a significant risk for patients, while biallelic mutations result in the inactivation of TP53 function, disrupting the cell-cycle control mechanism. This disruption facilitates tumor formation by promoting uncontrolled cell proliferation, dysregulating DNA repair mechanism, and disabling apoptosis.[32,33]

Copy number variations (CNV) are another group of abnormalities frequently observed in MM. Amplification on the q arm of chromosome 1 (1q) is observed in 40% of the patients and considered a poor prognosis risk factor.[22] There are many genes on the 1q region that are potentially contributing to myelomagenesis through cell growth and survival, and drug resistance.[20] Similarly, deletion of the p arm of chromosome 17, where a key tumor suppressor gene TP53 is located, together with TP53 mutation in the other allele, they cause its biallelic inactivation leading to impairment in DNA damage and cell cycle control.[20]

Molecular Classification

In 2006, Zhan et al.[34] conducted a comprehensive transcriptomics analysis, using microarrays, involving a large group of newly diagnosed MM patients. A total of 414 patients were categorized into training (n=256) and test (n=158) sets. They applied unsupervised clustering on the training set and tested the performance of their analysis using a prediction model on the test set by using 50 up- and 50 down-regulated genes in each cluster. As a result, they have identified 7 distinct molecular classes that

can be used to categorize MM patients (Figure 4). This analysis also allowed the detection of characteristic transcriptomic differences between these classes. Some categories are strongly linked to specific genetic alterations described above. For example, the group with high expression of MAF and MAFB is connected to t(14;16) and called MF. CD-1 and CD-2 groups are related to t(11;14) and t(6;14), respectively. The "MS" group is associated with the up-regulation of FGFR3 and MMSET, which are related to t(4;14). The HY group is comprised of over 90% of patients with hyperdiploidy, and the up-regulated genes in this cluster are FRZB, DKK1, TRAIL (TNFSF10), and CCR5. PR group showed high expression of cell-cycle related genes, as well as a gene expression profile indicating a higher proliferative index. LB group is characterized by the expression of EDN1, which is associated with an osteoblastic phenotype. Furthermore, the patients in this group have significantly fewer bone lesions. Survival analysis revealed low- and high-risk subgroups, where CD-1, CD-2, LB, and HY groups categorized as low-risk while MF, MS, and PR cases, high-risk.

The findings of Zhan et al. are further extended by the study conducted by Broyl et al.[35] In a similar setting, they identified 10 clusters, 6 of them are matching with previously described molecular subtypes, except for the LB subgroup. It was later detected as a subcategory within the MF group. Moreover, four additional subgroups were defined. One subgroup characterized by elevated expression of both erythroid and myeloid markers, demonstrated a high myeloid signature. Another cluster was defined by overexpression of PRL3. Additionally, a cluster with increased cancer testis antigens was identified, which exhibited a similar expression profile to a previously defined PR cluster. Finally, a separate cluster, was distinguished by differential expression of genes involved in the NFKB pathway, including regulatory genes CD40 and TRAF3.

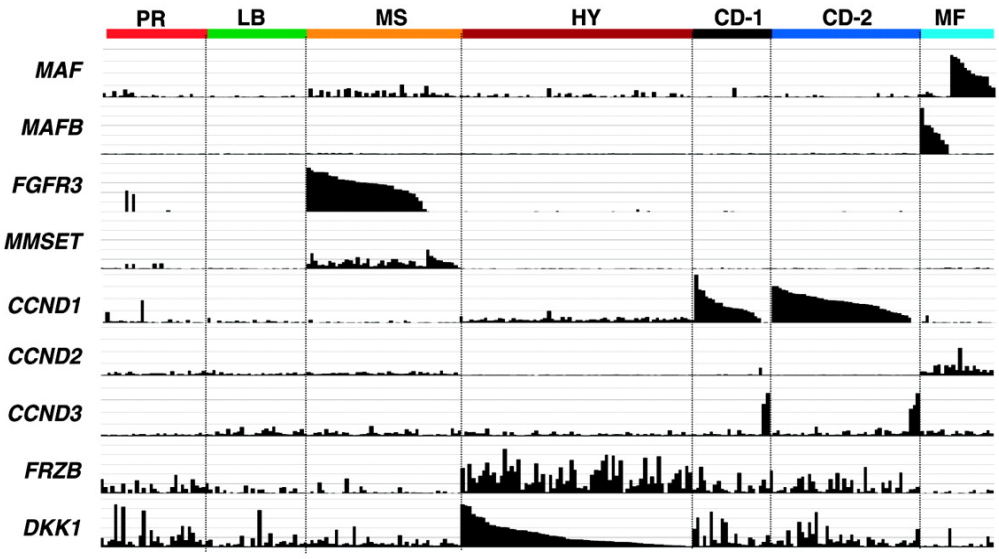

Figure 4. Marker gene expression profiles in molecular classes. Figure adapted from Zhan et al.[34] PR; Proliferation, LB; Low Bone, MS; MMSET, HY; Hyperdiploid, CD-1; CCND1, CD-2; CCND3, MF; MAF,

Tumor Micro-environment

The fate of a cell is highly influenced by the external signals and interactions from its surrounding micro-environment. MM cells are no exception to this paradigm. At the initial stage of the disease, high survival pressure is inflicted on MM cells, induced by immune surveillance. Clones that can reduce this pressure gain a significant survival advantage. In later stages, changes in the microenvironment provide MM clones additional benefits from their surrounding cell populations including immune protection and survival (Figure 5).

Bone marrow is a complex organ, hosting diverse cell types that perform a variety of crucial functions. These include the production of blood cells, immune responses, and maintenance of the skeletal system. Therefore, there is a complex network of inter-cellular interactions that is altered during MM progression (Figure 6).

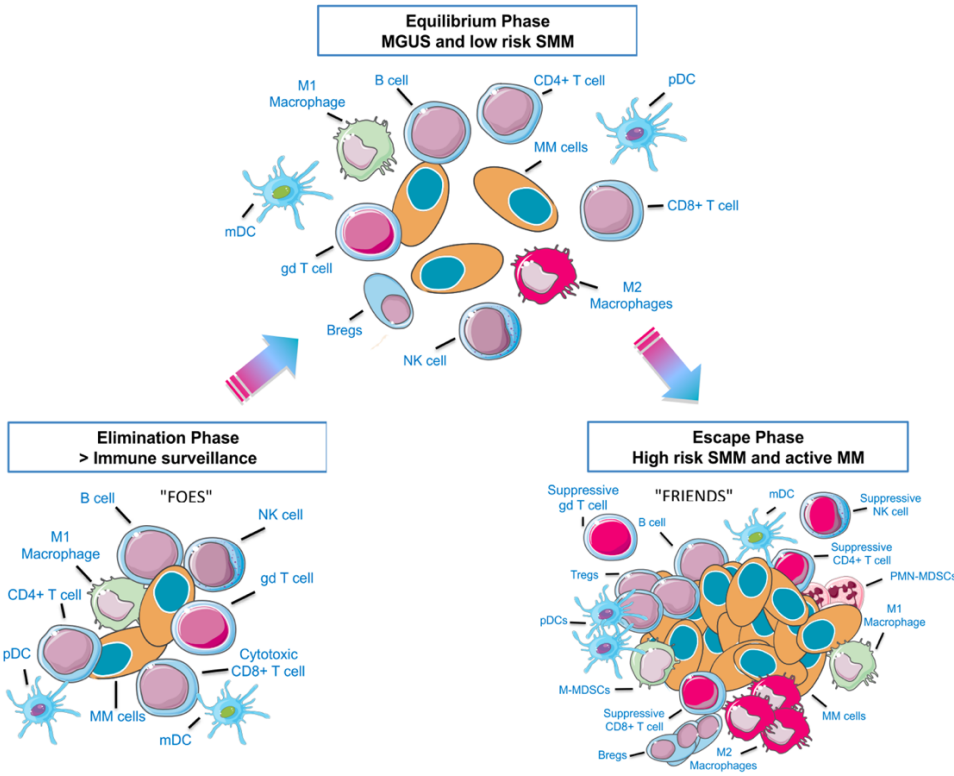

Figure 5. By nature, the immune system has the capacity to detect and eliminate abnormal plasma cells (Elimination Phase). In case these cells develop mechanisms to balance immunosurveillance by rapid proliferation or emergence of immune-resistant clones, a suitable environment for further progression emerges (Equilibrium Phase). Along their progression to MM, abnormal plasma cells gain additional mechanisms receiving pro-survival signals, additional energy sources, immunosuppression, and increased mobility (Escape Phase). Figure adapted from Lopes et al. [36]

Immune Compartment

Bone marrow contains hematopoietic stem cells that give rise to hematopoietic immune populations, as well as red blood cells and platelets. Immune populations are responsible for the detection and elimination of pathogens as well as abnormal cells,

including tumors. To do so, they need to go through a complex process that involves detection of tumoral antigen, antigen presentation, effector cell activation, and elimination of the tumor cell. Dysregulation in these mechanisms leads to immune evasion as well as promotion of tumor growth and survival.

CD8+ T-cells and natural killer (NK) cells are essential components of the immune system that can recognize and eliminate tumor cells through cytotoxic mechanisms. However, both cells express immune checkpoint inhibitors, such as PD1, CTLA4, TIGIT, TIM3, and LAG3, which induce impairment in cytokine secretion and proliferative capacity.[10,36] Moreover, NK cell activity is also suppressed by increased STAT3 activity in the tumor micro-environment which leads to shedding of major histocompatibility complex (MHC) Class I Polypeptide-Related Sequence A (MICA), causing down-regulation and blockage of activating receptor of NKG2D on NK cell surface.[37] Macrophages are another group of cells having killer activity, specialized for phagocytosis. There are two major macrophage subtypes. M1 macrophages are characterized by their anti-tumor activity, expressing high levels of MHC Class II and pro-inflammatory cytokines. On the other hand, M2 phenotype is specialized in immunosuppression and tissue repair, which may assist tumor development via secretion of immunosuppressive molecules, such as IL10 and angiogenic elements such as VEGF.[38] It was observed that the balance between the M1/M2 populations shifts towards the M2 subtype, favoring MM progression.[38]

Within the immune system, there are specialized cells called regulatory B (Breg) and T (Treg) cells, which can modulate the immune response by secreting molecules that are mainly known to suppress the activity of other immune cells. In general, an increase in the number of these cells is associated with a reduced immune response. In case of MM, increased proportions of both Bregs and Tregs were observed.[39,40] They produce high levels of immunosuppressive IL10 and TGFB cytokines that can inhibit the function of T-cells, dendritic cells (DCs), and macrophages.[10,36] Another fundamental regulator cell type is myeloid-derived

suppressor cells (MDSCs). It was shown that they benefit MM cells by creating a protective environment by suppressing NK and T-cell activity through production of nitric oxide synthase (NOS), reactive oxygen species (ROS), and immunosuppressive cytokines, including IL6 and IL10. Moreover, activation of STAT3 and STAT1 pathways further aid MM cells by induction of VEGF secretion and increased expression of anti-apoptotic proteins.[10,36]

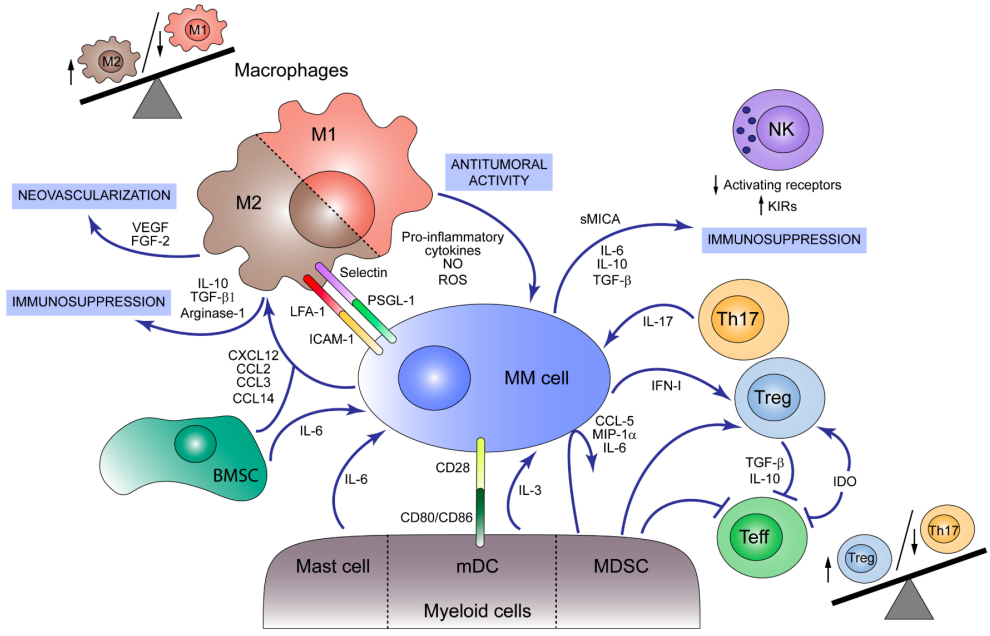

Figure 6. Alternations in the BM micro-environment along MM progression. Figure adapted from Encinas et al.[38] Teff; effector T-cell, MDSC; myeloid derived suppressor cell, mDC; myeloid dendritic cell, BMSC; bone marrow stromal cell.

As professional antigen-presenting cells, DCs have the crucial role of recognizing and presenting tumor-specific antigens for identification of tumor cells. However, it is believed that DCs are dysfunctional in MM, lacking antigen presentation capabilities.[41,42] Moreover, it was shown that pro-tumorigenic interactions take place between MM cells and DCs through the CD80/CD86 and CD28 axis, RANK-RANK interaction and APRIL-BCMA interaction. These communications

lead to tumor growth, survival, and drug resistance by increased expression of soluble factors, such as IL3, IL6, IL10, IL8, IL15, VEGF, MCP1, and CXCL12.[36,38]

Non- Immune Compartment

In addition to the dysregulation in the immune compartment, various interactions with neighboring cells support MM development.

Mesenchymal stromal cells (MSC) are multipotent cells that can differentiate into a variety of cell types including endothelial cells, adipocytes, chondrocytes, osteoblasts, and fibroblasts.[43] In healthy bone marrow, MSCs aid hematopoietic differentiation, maintain bone homeostasis, and support formation of the spatial structure of cellular niches.[44] However, within the MM micro-environment, they support MM development via multiple mechanisms. MSCs interact with MM cells through adhesion molecules, such as VCAM1, ICAM1, and CD40, which induce angiogenic and proliferative activity by up-regulation of growth factors, such as HGF and VEGF. They also contribute to an immunosuppressive micro-environment by secretion of various cytokines, such as IL6, IL10, and TGFB. CXCL12 expressed by MSCs, interacting with CXCR4 on plasma cells, modulates homing to bone marrow in healthy individuals. However, in MM, elevated levels of CXCL12 lead to increase in survival, proliferation, angiogenesis, and drug resistance.[44,45] Elevated levels of pro-inflammatory and pro-angiogenic factors in the tumor micro-environment induce activation of endothelial cells, leading to increased vessel density and IL6 production.

Osteoclasts and osteoblasts are key populations for maintenance of skeletal integrity of bone. Osteoclasts are myeloid-derived cells that are responsible for breakdown of bone matrix. Increased levels of RANKL and MIP-1 within the tumor micro-environment increase osteoclast activity in MM.[46] They play an immunosuppressive role by the production of APRIL, a ligand of BCMA, which induces up-regulation of TGFB, and IL10. In addition, they support MM cell survival

and proliferation.[47] Moreover, the interaction of tumor cells and the micro-environment with osteoclasts leads to their activation, which results in bone destruction.[48] Conversely, osteoblasts are responsible from maintenance of the bone structure, while adipocytes are fat cells that form the adipose tissue. Increased DKK1 secretion by MM cells acts as a suppressor for osteoblast differentiation while favoring adipocyte differentiation.[44] These events cause impairment in maintenance of the bone structure and lead to formation of bone lesions. In addition, increase in adipocytes aids tumor growth, survival, and migration through secretion of adipokines.[49]

Treatment strategies

The treatment of MM has evolved significantly over the past few decades, with the development of novel therapies that have improved survival rates and quality of life for patients. These strategies aim to reduce disease-related complications by decreasing the amount of plasma cells in the bone marrow. Although treatment protocols may vary among countries, the standard approach for multiple myeloma typically involves induction therapy including a combination of chemotherapeutic agents (Alkylators), proteasome inhibitors, immunomodulatory agents, and corticosteroids (Figure 7). More recently, monoclonal antibodies have also been approved for use in this setting. For eligible patients, autologous stem cell transplantation is recommended following induction therapy to further enhance treatment efficacy. Additionally, maintenance therapy with low-toxicity medications is often administered to prevent disease relapse after initial treatment.

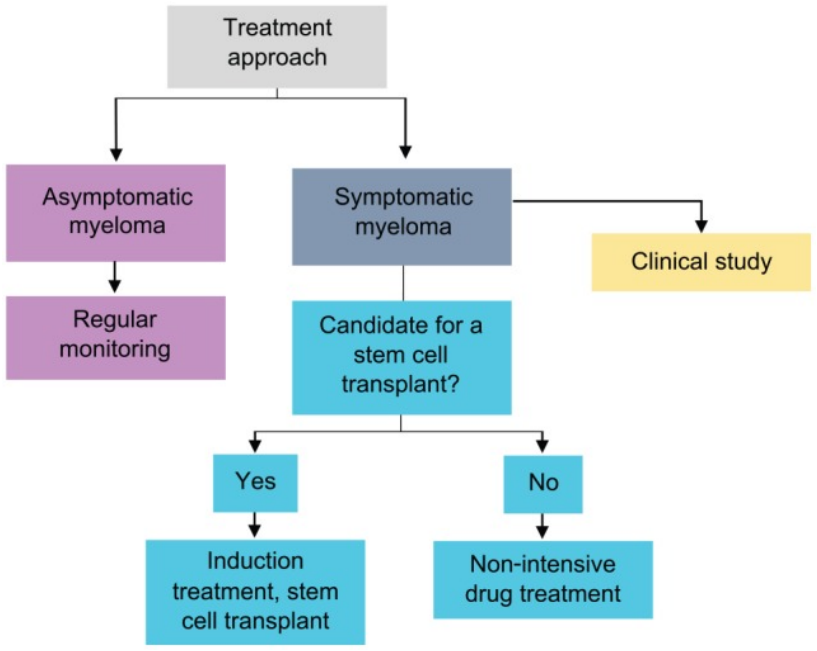

Figure 7. Decision making steps for MM therapy. Figure adapted from Bird et al.[9]

Induction Therapy

Proteasome inhibitors

MM cells generate significant quantities of antibodies. In addition, cancer cells produce a high volume of abnormal or misfolded proteins, which can lead to cell stress. MM cells rely on proteases and proteasomes to break down these proteins, which makes them ideal targets. Moreover, the proteasome plays a vital role in cell-cycle by catalyzing key proteins in cell cycle control.[50] Proteasome inhibitors, such as bortezomib, carfilzomib, and ixazomib, block proteasome activity, leading to increased cell stress and ultimately the induction of apoptosis.[51]

Immunomodulatory drugs and corticosteroids

In previous chapters, it has been demonstrated that the MM tumor micro-environment is highly altered and involves multiple mechanisms to support MM development. In this regard, application of immunomodulatory agents has shown significant benefits for the treatment of MM. Currently, three immunomodulatory drugs, thalidomide, lenalidomide and pomalidomide, are approved for the treatment of MM.[52] Their mechanism of action includes enhancement of killer cell activity, induction of apoptosis, inhibition of angiogenesis and anti-inflammatory regulation.[52] Similarly, corticosteroids, particularly glucocorticoids dexamethasone or prednisolone, are used for MM treatment to block pro-inflammatory cytokine release.[9,53]

Autologous Stem Cell Transplantation (ASCT)

ASCT is currently a part of the standard therapy for MM treatment for eligible patients. The application involves the following steps: stimulation of migration of peripheral blood stem cells to the blood stream, collection and storage of stem cells, induction of high-dose chemotherapy, and reinjection of the stem cells. The added

value of ASCT is that it enables effective killing of tumor cells via high-dose chemotherapy and results in long-term disease control. Moreover, patient autologous stem cells can effectively restore healthy blood cell production.[11]

ASCT is highly beneficial for patients. Yet, due to the high median age of disease onset, not all patients are eligible to receive such a heavy treatment. Although there is no specific age limit, for patients above age 65-70, the application of ASCT is generally conditional. For ASCT application, two major requirements are cardiac functionality and absence of any severe comorbidities.[54]

Immunotherapeutic Approaches in Clinical Trials

Immunotherapy is a promising approach to treat multiple myeloma that aims to use the patient's own immune cells to target cancer cells. The main idea behind immunotherapy is to guide immune cells specifically to target cancer cells, excluding healthy cells and reducing the risk of side effects. Therefore, immunotherapy has the potential for a more personalized and potentially more effective treatment option for patients with MM. There are novel and innovative approaches being developed to make this possible. Three of these methods will be covered in the following paragraphs: monoclonal antibodies, chimeric antigen receptor (CAR) T-cells and bispecific antibodies.

Monoclonal antibodies

Monoclonal antibodies are engineered molecules that bind to a specific cell surface antigen. Such specificity is particularly valuable for cancer treatment for minimizing the off-target effects and maximizing the efficacy of the treatment. For optimal effectiveness, the target antigen should be highly expressed by cancer cells and absent from other cell types in the body. Monoclonal antibodies work through various mechanisms of action, including attracting immune cells to kill cancer cells or directly inducing apoptosis (Figure 8).[55] In the context of MM treatment, multiple

monoclonal antibodies have been developed to target different antigens. Two promising products are daratumumab and elotuzumab. Elotuzumab, targeting SLAMF7, became the first approved monoclonal antibody for treating relapsed/refractory MM patients, and daratumumab, targeting CD38, was the first to receive FDA approval for treatment of transplant-ineligible patients.[55]

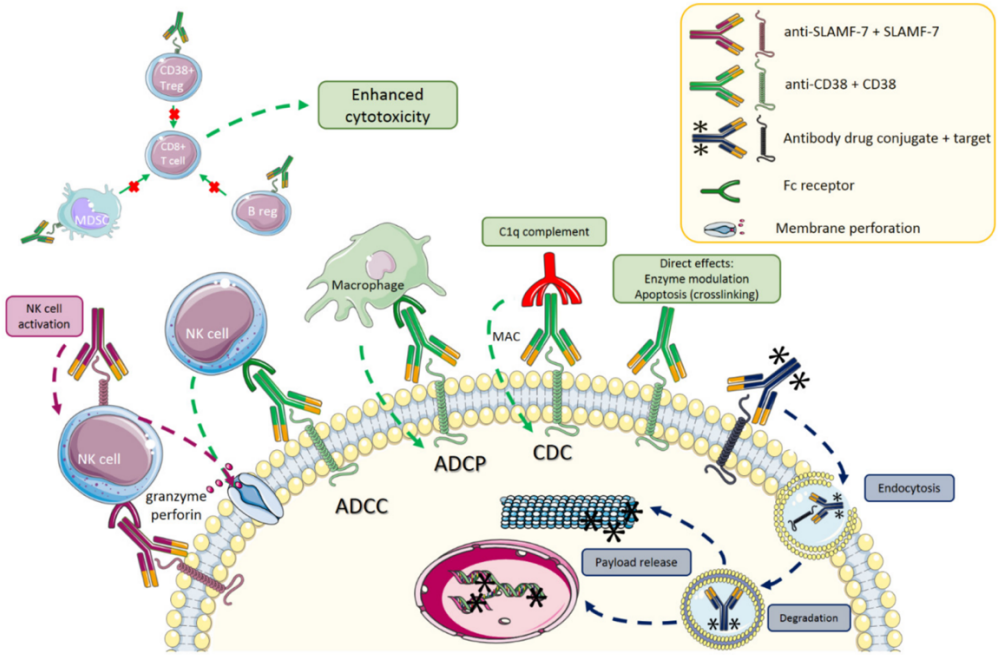

Figure 8. Mechanisms of action of monoclonal antibodies. Figure adapted from Radocha et al.[56] ADCC; antibody dependent cellular cytotoxicity, ADCP; antibody dependent cellular phagocytosis, CDC; complement dependent cytotoxicity, MAC; membrane attacking complex.

Chimeric antigen receptor T-cells

CART strategy relies on engineering the patient's own T-cells to target tumor-specific antigens, resulting in the activation of T-cells and subsequent destruction of tumor cells. For this purpose, T-cells are collected from patients, engineered using a viral CAR vector, cultured for expansion, and then infused back into the patient's blood stream. CARs are composed of four subunits. The extracellular targeting

domain, specifically designed for biding to the cancer-specific antigen, is bound to a transmembrane domain, located on the cell membrane (Figure 9). Binding to the target antigen induces T-cell activation by the internal signaling domain (in CD3 subunits) and by a second costimulatory domain from CD28, 4-11B or OX40.[57,58] While most CAR studies focus on T-cells, a similar strategy can also be adapted to NK cells.[59] Many CART studies focus on BCMA as target antigen. Yet, other targets such as CD138, CD19, GPRC5D and SLAMF7 have also been investigated.[57,60] The potential of CART therapy to provide personalized treatment and long-term immunity makes it a highly active area of research.

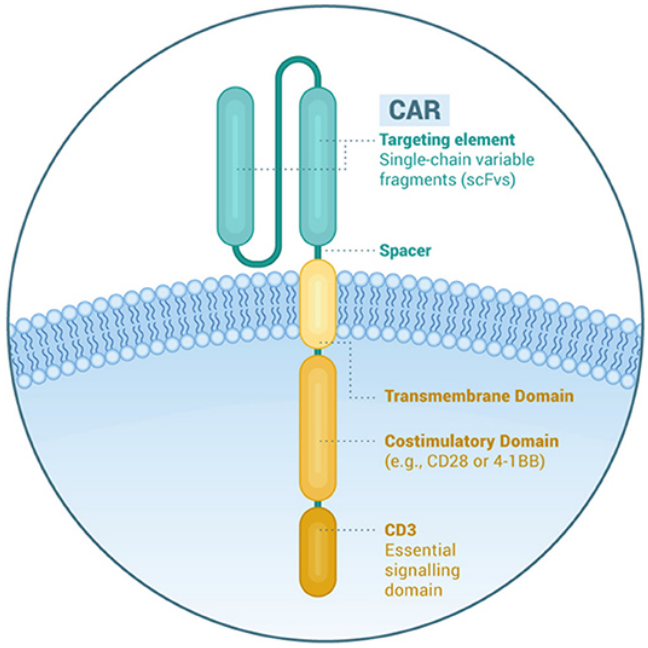

Figure 9. Structure of a chimeric antigen receptor. Figure adapted from Rodriguez et al.[58]

Bispecific antibodies

Bispecific antibodies are engineered molecules, designed to target two antigens at once (Figure 10). One side of the antibody targets a tumor-specific antigen. There are various candidate antigens in clinical trials for MM targeting, such as

BCMA, CD138, CD38, SLAMF7 and GPRC5D.[61] The other side induces activation of an immune cell population, a T-cell, or a NK cell, through binding to CD3, CD16 or NKG2D.[36,62] Bispecific antibodies trigger a strong immune response with high specificity. Compared to CART, they have a particular advantage in terms of the manufacturing process, as they are directly available, low-cost and can be administered more quickly.[62]

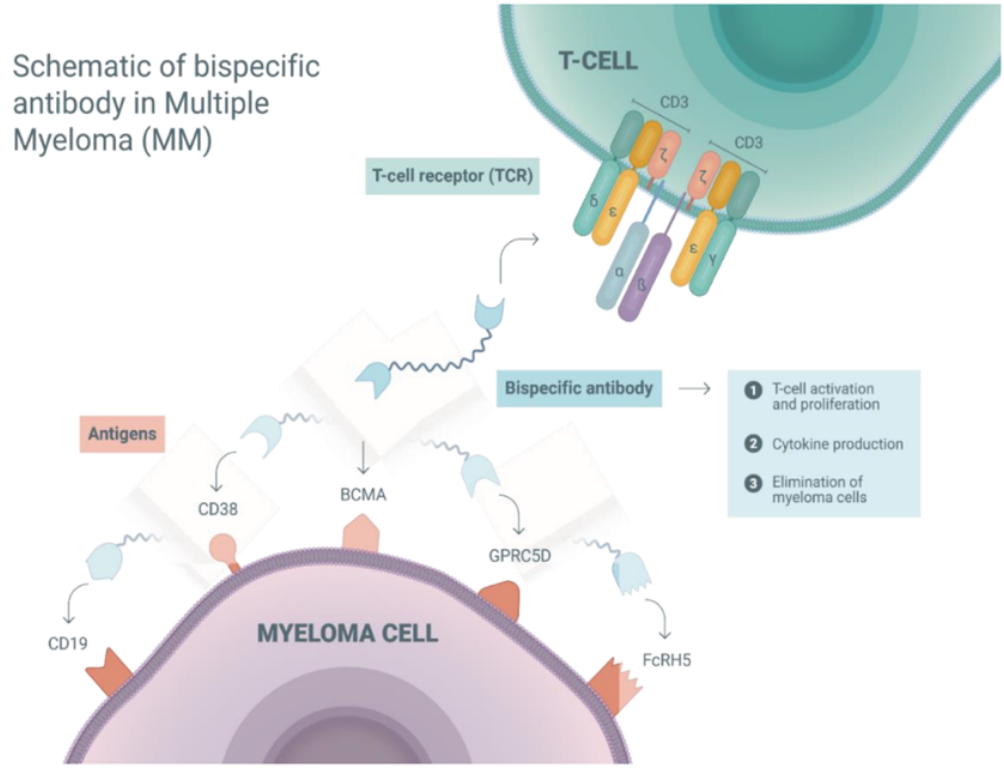

Figure 10. Bispecific antibody mechanism of action. Figure adapted from Zhou et al.[61]

One of the challenges in immunotherapy is the dysfunctional phenotype observed in cytotoxic immune cells within the tumor micro-environment. To increase the efficiency of treatment, application of the therapy can be accompanied by immune checkpoint blocking agents, such as anti-PD1/PDL1. Alternatively, for CART applications, T-cells can also be specifically engineered to be resistant to an immunosuppressive environment.[63]

Target antigens for MM immunotherapy

The success of immunotherapy is heavily reliant on finding the right target antigen. The optimal target should be highly and consistently expressed on tumor cells, reside on the cell surface, and be absent in other cell types. The expression profiles and functions of existing immunotherapeutic MM targets can be found in Figure 11.

B-cell maturation antigen (BCMA) is a highly promising target for multiple myeloma therapy, as it is specifically and globally expressed on plasma cells. Targeting BCMA with immunotherapeutic products is a highly active area of research, with several products, including Teclistamab[64], and Belantamab[56], already approved for the treatment of relapsed/refractory MM patients. Nevertheless, it should be noted that, in rare cases, parkinsonism has been observed due to BCMA expression in patient basal ganglia.[65]

CD38, CD138, and SLAMF7 were initially targeted for the treatment of multiple myeloma, and clinical trials have shown success for CD38 (Daratumumab) and SLAMF7 (Elotuzumab). While all three antigens are actively being studied for alternative targeting strategies, their expression in various other cell types, including immune cells, remains a limitation. Despite their initial success, the off-target expression of these antigens is an important concern.

GPRC5D and FCRL5 (also known as FCRH5) are two relatively new and promising antigens for targeted therapies. Compared to other targets, both antigens have low off-target expression profiles, making them attractive alternatives. Although there are currently no approved products targeting these antigens, there are two promising therapies under investigation: Talquetamab, which targets GPRC5D, and Cevostamab, which targets FCRL5.[66]

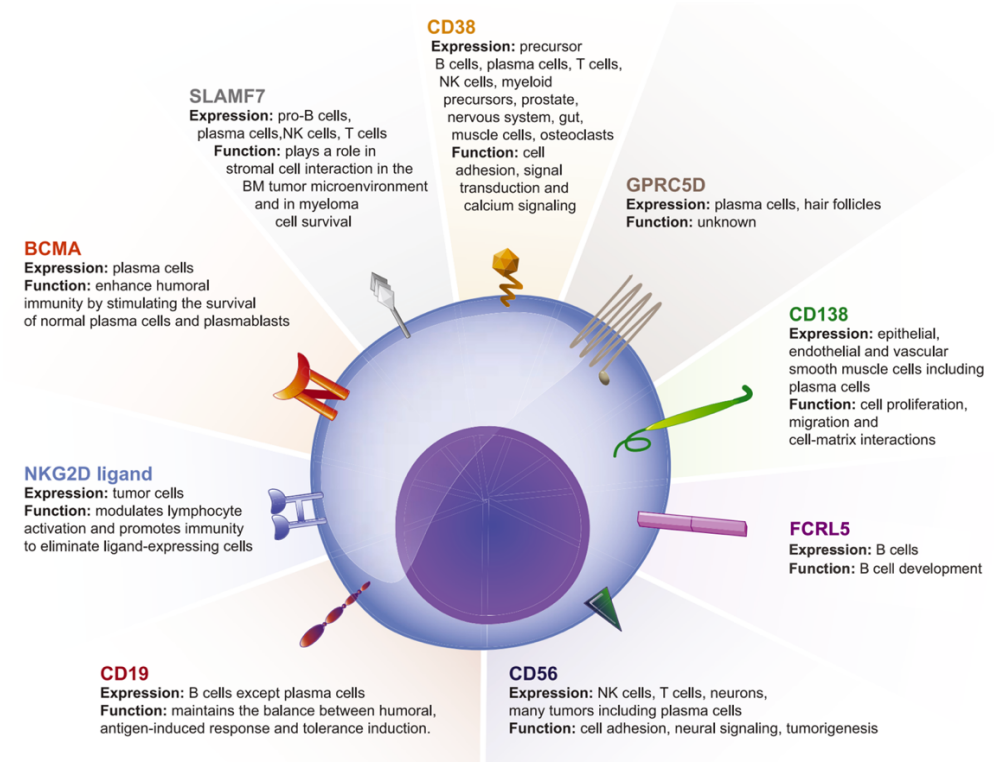

Figure 11. Immunotherapeutic targets for multiple myeloma treatment. Figure adapted from Shah et al.[67]

CD56 and CD19 are both cell surface antigens that have shown promise in the treatment of multiple myeloma (MM). While CD56 is absent on normal plasma cells, it can be detected on approximately 70% of MM patients, and similarly, CD19 is also absent on normal plasma cells but can be found on a small fraction of MM patients. [67] While these targets are currently being investigated for MM treatment, their low abundance on tumor cells and off-target expression are potential challenges that may make them less favorable than other candidates.

scRNA-seq

In the late 2000s, RNA sequencing (RNA-seq) was widely integrated as a novel cost-effective tool for the investigation of transcriptomic data[68]. It succeeded microarrays in many ways. Unlike microarrays, it did not require a prior sequencing knowledge, allowed direct measurement of the RNA levels, allowed detection of sequence variants and enabled investigation of multiple samples at once.[69] Nevertheless, in RNA-seq, all the transcriptome coming from the mixture of cells, collected from a sample, is quantified at once. Such property limits the information gain since the cellular heterogeneity cannot be captured. Due to this characteristic, it is also often referred as bulk RNA-seq. In 2009, Tang et al. overcame this limitation by isolating single cells and conducting RNA-seq per cell.[70] This strategy is commonly known as single cell RNA sequencing (scRNA-seq). Early applications were limited by the low number of cells per experiment and high experimental cost. In the last decade, with improvements in cell capture and sequencing efficiency, the number of cells investigated increased up to millions and the sequencing cost decreased significantly, enabling wide usage of the technique (Figure 12).[71] A standard scRNA-seq pipeline is composed of cell isolation, library preparation, sequencing, data processing and data analysis (Figure 13). In this chapter, the procedural steps of scRNA-seq experiments and one of the most commonly used scRNA-seq protocols, 10X Chromium[72], will be addressed.

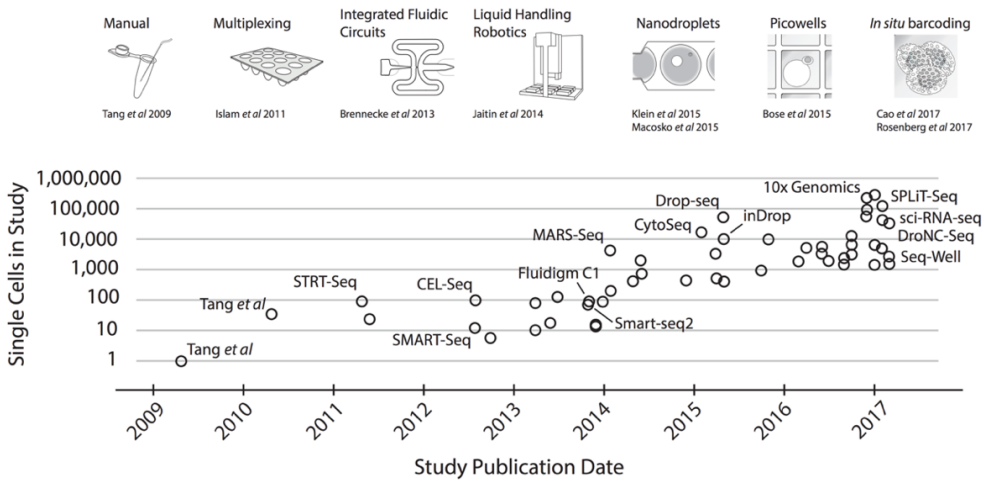

Figure 12. Timeline of the evolution of scRNA-seq methods. The figure is adapted from Svensson et al.[71]

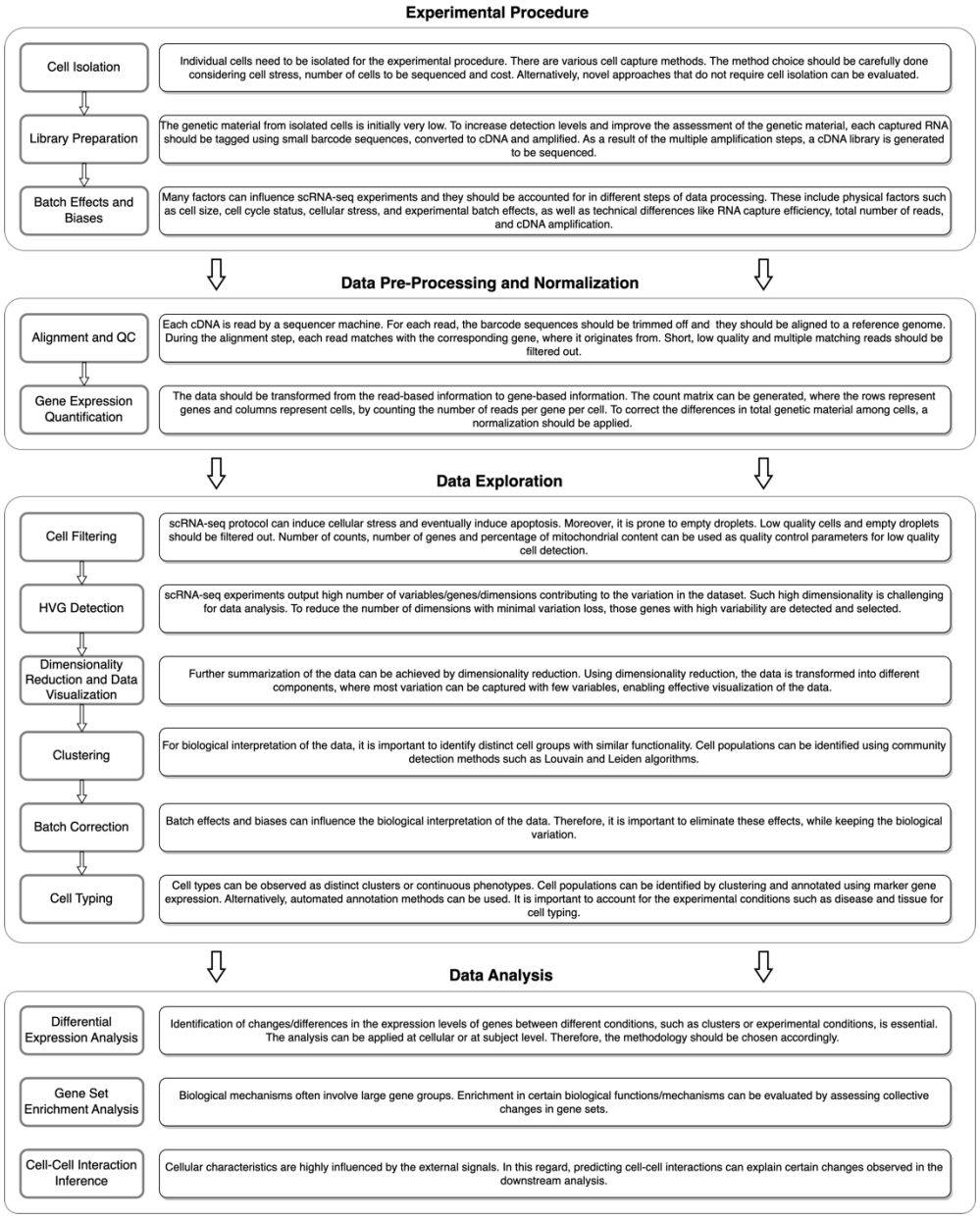

Figure 13. A detailed summary of the steps in a standard scRNA-seq procedure.

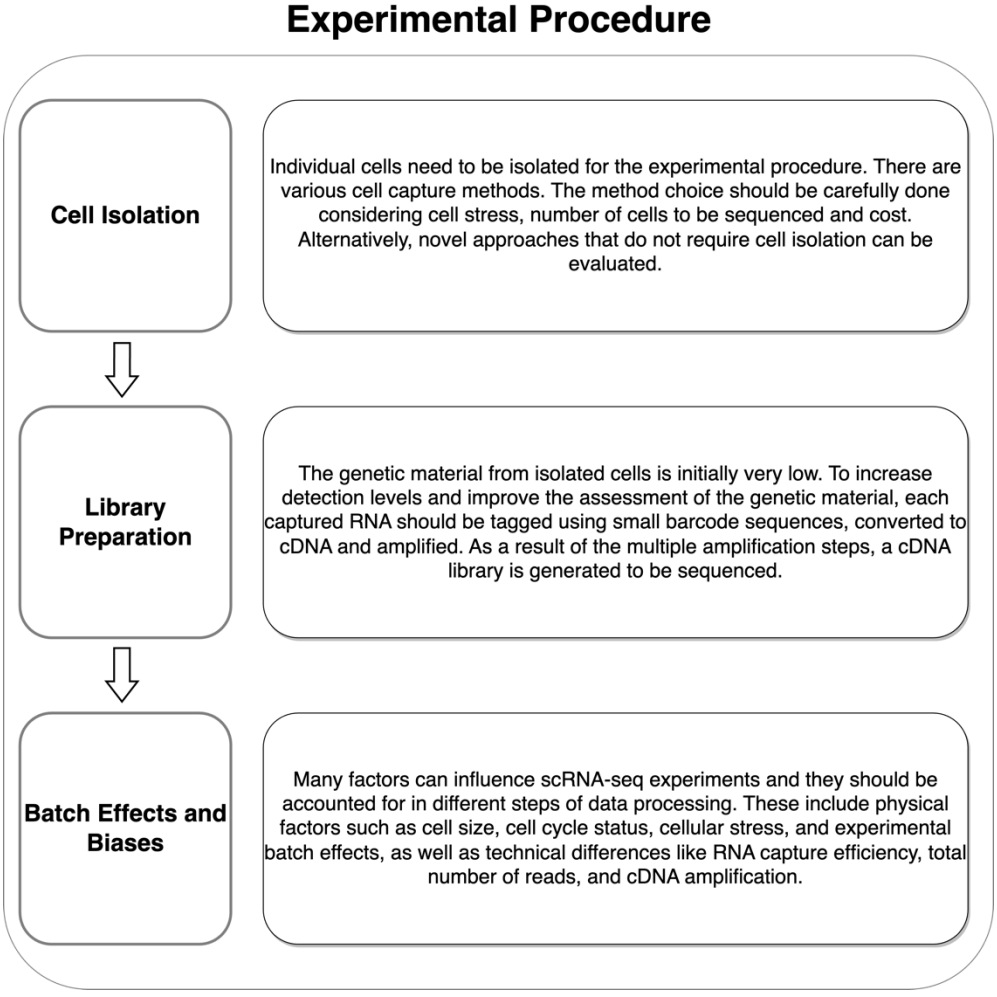
Experimental Procedure
Cell Isolation
Individual cells need to be isolated for the experimental procedure. There are various cell capture methods. The method choice should be carefully done considering cell stress, number of cells to be sequenced and cost. Alternatively, novel approaches that do not require cell isolation can be evaluated.
Library Preparation
The genetic material from isolated cells is initially very low. To increase detection levels and improve the assessment of the genetic material, each captured RNA should be tagged using small barcode sequences, converted to cDNA and amplified. As a result of the multiple amplification steps, a cDNA library is generated to be sequenced.
Batch Effects and Biases
Many factors can influence scRNA-seq experiments and they should be accounted for in different steps of data processing. These include physical factors such as cell size, cell cycle status, cellular stress, and experimental batch effects, as well as technical differences like RNA capture efficiency, total number of reads, and cDNA amplification.

Experimental Procedure

Cell Isolation

The novelty of scRNA-seq experiments, compared to traditional bulk RNA-seq, is the isolation of single cells. This way, several cell populations can be collected and analyzed individually within the same experimental setup. The following steps rely on this initial selection. Therefore, the cell isolation method should be chosen carefully, based on the experimental setup. Currently, existing cell isolation methods are micro-pipetting, fluorescence-activated cell sorting (FACS) into microwell plates, microwell encapsulation and droplet encapsulation (Figure 14).

In micro-pipetting, the cells are collected using micro-pipettes which can be applied manually or in an automated fashion. Although the method yields high quality cell isolation, it is time consuming and is limited to small number of cells. Hence, it is a method preferred for segregation of rare or very fragile cell types.[73,74]

FACS into microwell plates relies on selection of cells using florescence labelling and isolation of them using laser-based detection.[75] FACS can be used for selection of populations based on phenotypical markers.[76] For the other scRNA-seq methodologies, FACS phenotypical selection can be applied before the cell sorting, while for FACS into microwell plates-based methodologies, it can be applied during cell isolation. Although, it provides good quality whole transcriptome of captured cells, it is expensive compared to other alternatives and limited by low number of cells per experiment.[76]

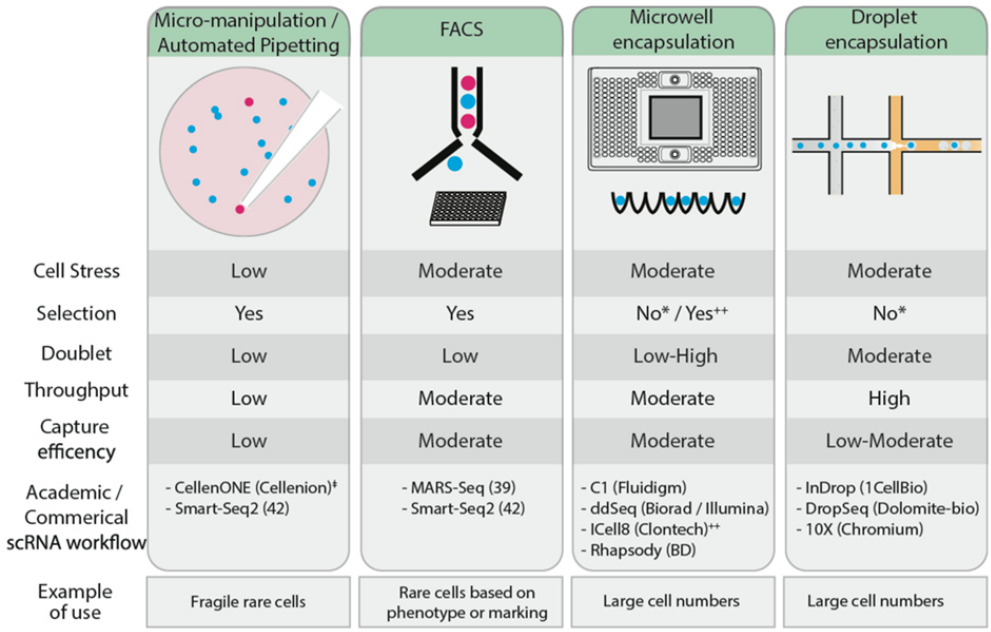

Figure 14. The summary of cell sorting methods. The figure is adapted from Nguyen et al.[74]

In the microwell encapsulation method, the cells are run through a fluidic circuit, ending up sorted into single chambers.[76] The size and the structure of the circuit is a limiting factor on the identified number of cells, capture efficiency and the doublets.[73,76] Two widely used applications of microwell encapsulations are DB Rhapsody[77] and CEL-Seq2[78].

In cases where high a number of cells needs to be analyzed, droplet-based methods have different advantages. In this method, the cells are run through micro-tubes and captured by oil droplets including the library preparation material.[79] Such a strategy uses minimal material with maximum efficiency.[80] Moreover, the methodology can induce stress on fragile cells, it captures only a fraction of the transcriptome and is prone to empty droplets and doublets. Nevertheless, it can be applied to samples with hundreds of thousands of cells, making it ideal for high throughput sequencing.[74]

Recently, combinatorial barcoding methods such as SCI-seq[81] and SPLIT-seq[82], emerged as low-cost alternatives which enable the scRNA-seq to be conducted with basic lab equipment, without the need of a sorter machine. These methods aim to use the cells as the containers, like the droplets, and combine rounds of barcoding to index each cell. This eliminates the need for cell sorting. However, the increased complexity of the experiments, barcoding errors, and lack of bioinformatics tools for combinatorial demultiplexing are limiting factors for their use.

Library Preparation

The quantity of genetic material, obtained from the individual cells, is very low. To effectively quantify the RNA levels, an amplification step is applied during sequence library preparation (Figure 15).[83] The captured material is transformed into a more stable double stranded structure using reverse transcription via binding of poly T primers and the obtained complementary DNA (cDNA) is further amplified. Notably, the starting amount of each gene creates a bias in this procedure. Those genes that are highly expressed are also more likely to be captured. Hence, it should be noted that the capture of lowly expressed genes remains a challenge.[79]

The library generation strategies vary based on the cDNA amplification strategy and the length of the sequencing (weather it is full-length, 5' end or 3' end). cDNA amplification can be done by polymerase chain reaction (PCR) or in vitro transcription (IVT).[76,79] An essential difference between the two methods is that the amplification takes place in a linear trend with IVT while exponential with PCR. In addition, IVT requires an extra reverse transcription step.[79]

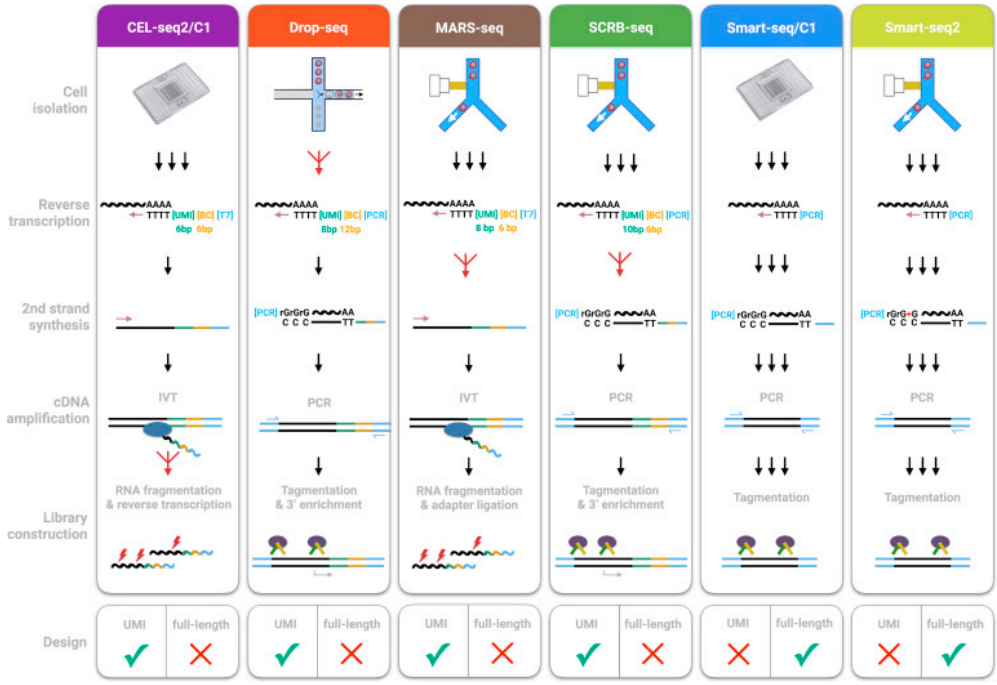

Figure 15. Overview of library preparation steps of various scRNA-seq technologies. The figure is adapted from Ziegenhain et al.[84]

Mapping of transcript reads to specific genes does not require complete gene sequence. Hence, it is often preferred to sequence a small section of 3' or 5' end of the transcript to reduce sequencing cost. Nevertheless, the full-length transcriptome sequencing is required in certain cases, including investigation of splice variants, and can be obtained by Nextera technology.[76,79]

Unique molecular identifiers (UMI) can be used for the identification of individual mRNA reads.[73,84] These are unique, short sequences of 4-10 bp that can be inserted on the 3' or 5' end of the transcript during reverse transcription. The number of identified UMIs is valuable for the assessment of captured genetic material and initial library size.[76] Likewise, barcode sequences, also consisting of unique short sequences and are used for molecular identification of cells and samples (for samples it is also referred as sample index). While UMI sequences are random, barcode

sequences are specific for each cell and each sample. They are used for identification of individual cells and samples.[85] Such characterization enables parallel sequencing of multiple cells and samples, reducing experimental costs.[71]

Batch Effects and Biases in scRNA-seq

Even though scRNA-seq experiments provide a comprehensive insight of cellular transcriptome, it is prone to technical noise. The biases and noises can be observed within- and between-samples. To prevent incorrect biological inferences, it is essential to correct these technical variations in the downstream analysis.[86,87]

The variations from the experimental procedure can be due to biological diversity, such as cell size, cell cycle state and cellular stress, or can originate from technical variables like personnel and lab conditions.[88–90] Additionally, differences in RNA capture efficiency, sequencing depth (number of reads) and cDNA amplification can also cause unwanted variation in data.[86,91] Throughout data processing and exploration, we will talk about these biases and how to correct them.

10x Chromium scRNA-seq

10x Chromium uses a droplet-based strategy for the isolation of individual cells. In this technique, the cells are captured within droplets, together with gel beads that contain the barcode sequence, while running through the microfluid chip, and form gel beads in emulsion (GEMs) (Figure 16). GEMs include all the necessary material to perform the sequencing: barcode sequences, UMIs, poly-T primer and adapter sequences for PCR. GEMs provide nano level material usage, enabling minimum cost with maximum throughput.[92]

Once the cells are captured in GEMs, cell lysis begins. Barcode sequences attach the mRNA from the poly-T primer and reverse transcription takes place (Figure 16b and c). From the obtained cDNA, the sequencing library is generated and

the sequencing takes place using Illumina short read sequencing. Obtained reads can be further pre-processed by CellRanger software for mapping to a reference genome, quantification, and quality control (QC).[92]

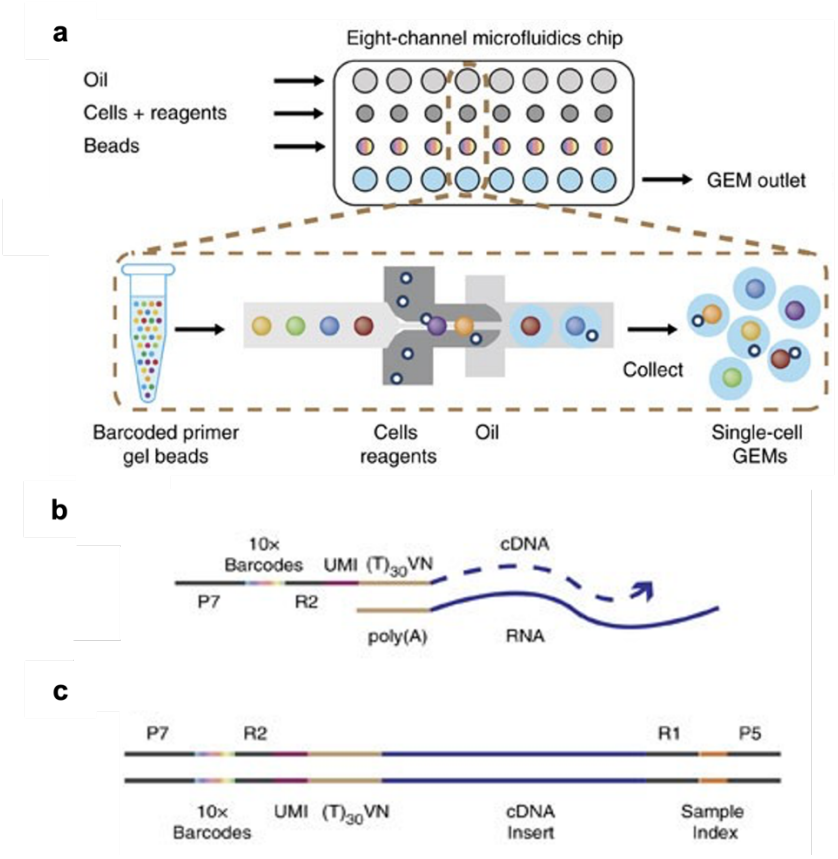

Figure 16. 10x Chromium library generation procedure. The figure is adapted from Zheng et al.[92]

Data Pre-Processing and Normalization

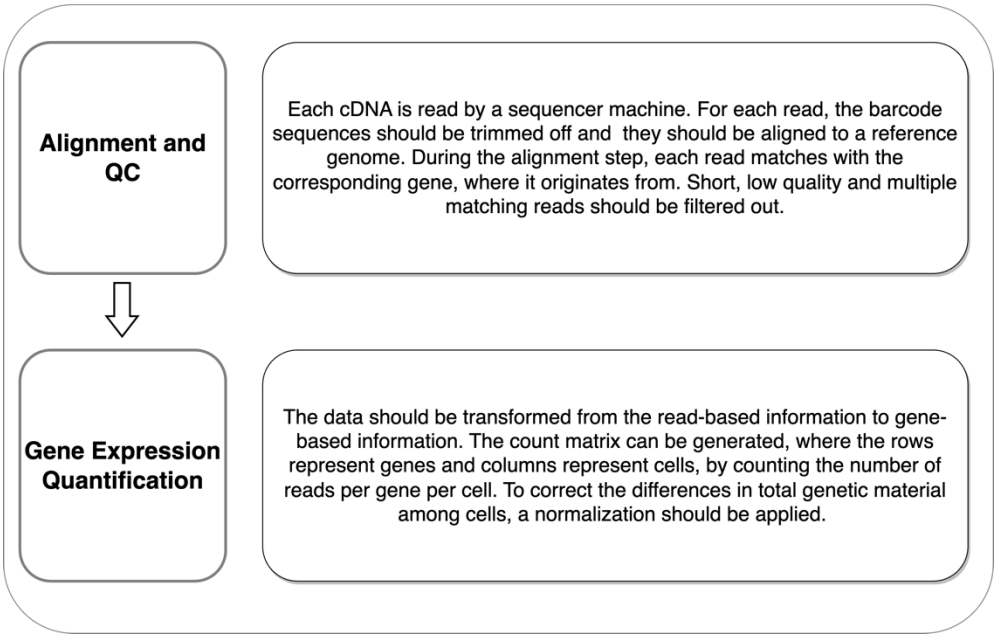

Data Pre-processing and Normalization

Illumina short read sequencing produces fastq files where each file contain reads of the amplified cDNAs. To match the short sequencing reads to their corresponding gene, they need to be mapped to a reference genome. Ultimately, quantification of mapped reads enables assessment of gene expression levels.[76,90]

Alignment and QC

Genes and their sequences vary among the species. Therefore, it is essential that the reads are aligned to a reference genome from the species where the sequenced cells originate from.[90,93] Since quality of reads can affect consistency of mapping, the reads shorter than 100 bp and low quality reads should be excluded.[74,94] In addition, prior to alignment, synthetic sequences such as barcode sequences, UMIs and adapter sequences should be trimmed off from the sequence reads.[74,95] Finally, following alignment, reads with multiple gene overlaps should also be filtered out. These steps can be performed by CellRanger.

Considering batch effects, assessment of the quality of the sequenced material is important per sample. Sample quality can be evaluated by sequencing depth, library complexity and mitochondrial percentage. Samples with a low number of reads or genes should be treated carefully. Low genetic material capture and low number of genes, as well as high number of read and low UMI number can be signs of poor sample quality. Similarly, samples with a high number of cells with high mitochondrial percentage can indicate high cellular stress. Such stress could be due to sampling and should be carefully evaluated.[96] In case there are high variations among samples, after a careful evaluation, repeating the experiment or excluding these samples could be possible solutions.

Gene Expression Quantification

The output of the alignment step is Sequence Alignment/Map (SAM) or Binary Alignment/Map (BAM) files. These files include mapping results of individual reads. In order to obtain gene expression levels, they need to be transformed into an expression matrix by quantifying read-gene pairs. Usage of UMIs makes an important difference for quantification step by regressing out PCR bias can be observed between cells and genes. For those experiments, where full length transcript is sequenced, the variation among the transcript lengths can create a bias. Therefore, it is essential to regress out these variations using one of the normalization methods of transcript per million, fragments per kilobase million or reads per kilobase million.[76,86,91] Tools such as scran[97], and SCnorm[98] are specifically designed for the normalization of scRNA-seq experiments. In case UMIs are used, methods such as UMI-tools[99], zUMIs[100], or dropEst[101] are applicable for the data pre-processing.[102] CellRanger generates the gene count matrix by counting UMIs aligned to each gene. In case a UMI is aligned to multiple genes, those UMIs are discarded. Sequencing depth bias can be overcome by counts per million (CPM) normalization.[97] Moreover, it is a common practice to transform the normalized values into a logarithmic scale. Log-transformed expression values represent log fold changes, the widely used measure for expression changes, while reducing data skewness to approximate the assumption of normal distribution in downstream analysis tools.[96,103] To avoid infinite values due to log(0), the log transformation is applied by adding one (+1 log transformation).

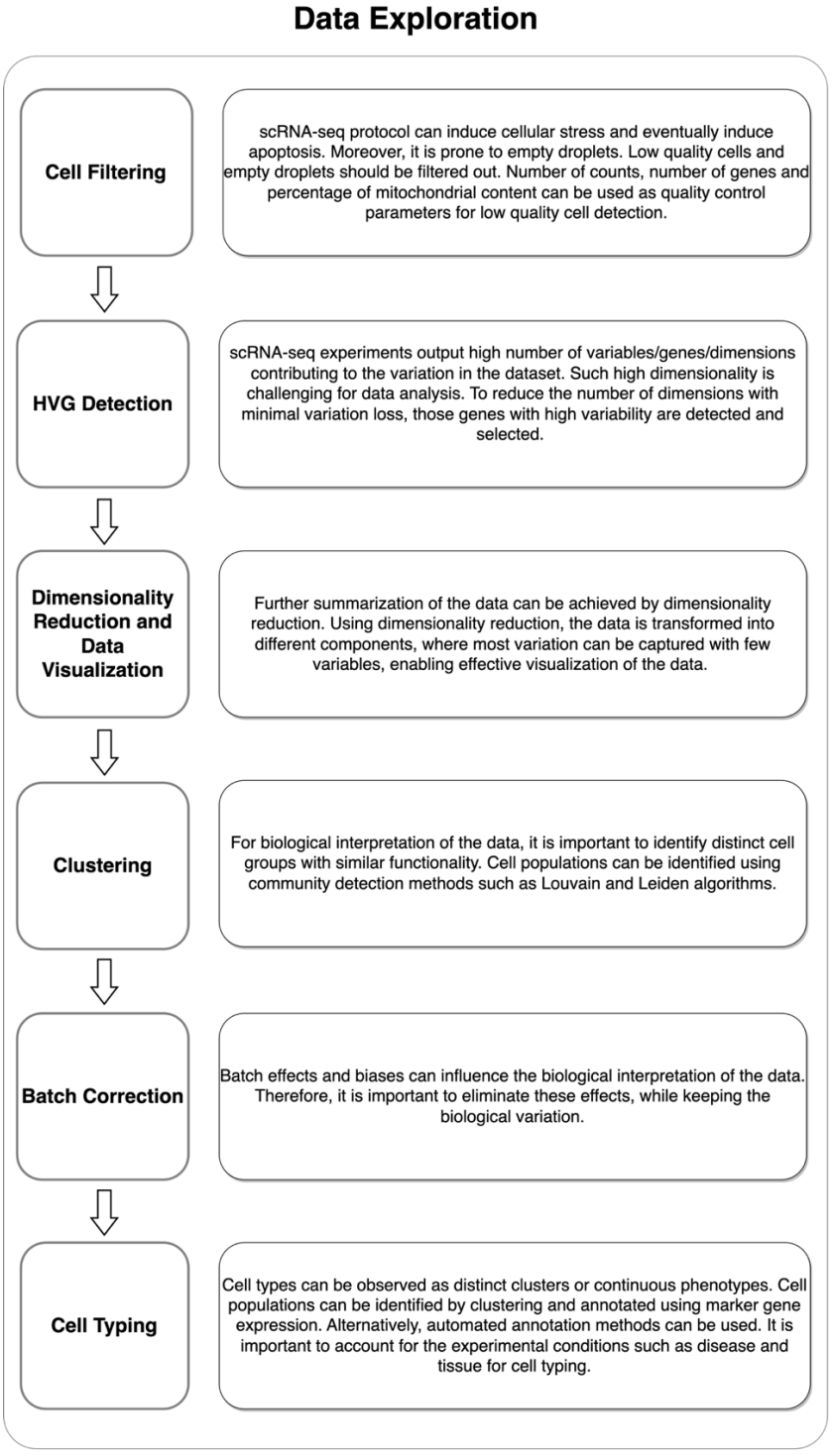
Data Exploration
Cell Filtering
scRNA-seq protocol can induce cellular stress and eventually induce apoptosis. Moreover, it is prone to empty droplets. Low quality cells and empty droplets should be filtered out. Number of counts, number of genes and percentage of mitochondrial content can be used as quality control parameters for low quality cell detection.
HVG Detection
scRNA-seq experiments output high number of variables/genes/dimensions contributing to the variation in the dataset. Such high dimensionality is challenging for data analysis. To reduce the number of dimensions with minimal variation loss, those genes with high variability are detected and selected.
Dimensionality Reduction and Data Visualization
Further summarization of the data can be achieved by dimensionality reduction. Using dimensionality reduction, the data is transformed into different components, where most variation can be captured with few variables, enabling effective visualization of the data.
Clustering
For biological interpretation of the data, it is important to identify distinct cell groups with similar functionality. Cell populations can be identified using community detection methods such as Louvain and Leiden algorithms.
Batch Correction
Batch effects and biases can influence the biological interpretation of the data. Therefore, it is important to eliminate these effects, while keeping the biological variation.
Cell Typing
Cell types can be observed as distinct clusters or continuous phenotypes. Cell populations can be identified by clustering and annotated using marker gene expression. Alternatively, automated annotation methods can be used. It is important to account for the experimental conditions such as disease and tissue for cell typing.

Data Exploration

Generation of the count matrix is a milestone in a scRNA-seq pipeline. Up until this point, the objective of the steps taken was to capture the biological information and transform it into a quantitative data format. With the count matrix, the underlying biology can be explored by using scRNA-seq tools Seurat[104] and Scater[105] in R, and Scanpy[106] in Python.

Cell Filtering

Due to the nature of the experimental procedure, scRNA-seq experiments are prone to errors. It is essential to assess the quality of the cells before starting investigation of the biological variation. Empty droplets, doublets, dying cells, cells with high proportion of unmapped reads, cells with low number of expressed genes should be filtered out.[90,107] It is important to assess these categories carefully. The filtering parameters should be chosen carefully, considering the experimental conditions.[93] For example, the percentage of the mitochondrial genes are often used to identify dying cells. Yet, in tumor cells, it is expected to observe a higher mitochondrial gene expression due to rapid proliferation. Hence, a higher threshold for tumor-specific experiments can prevent exclusion of tumor cells.

The segregation of real cells from empty droplets can be done manually by clustering. Clusters with very low RNA quantities are expected to group together in PCA or in UMAP. Moreover, certain thresholds can be used for quality control measures. Number of UMI counts, number of genes and mitochondrial percentage are commonly used features.[108108] Alternatively, the original EmptyDrops[109] tool or its adaptation in CellRanger can be used. The floating RNAs captured by empty droplets are called ambient RNA. EmptyDrops generates an ambient gene expression profile using the droplets with small amount of UMI and categorizes those with a significantly different profile than the ambient profile as real cells.

Like empty droplets, doublets also often stand out in clustering and quality control measures. Alternatively, doublet detection methods Scrublet[110] and DoubletFinder[111] can be used. Scrublet simulates possible doublets by combining random observations and generates a final score, which represents the likelihood of a cell to be a doublet, based on the relative density of generated doublets around each cell. Likewise, DoubletFinder also simulates doublets and identifies those cells having high numbers of artificial doublet neighbors as doublets.

Highly Variable Gene Detection

The transcriptomic landscape of cells often includes large numbers of genes (~20.000) and analyzing such a high dimensional data is a challenging task. Summarizing of the data without losing the essential information is required. During summarization, the aim is to conserve the biological variation within the data and to reduce the number of features. Therefore, highly variable genes (HVG) within the dataset are identified[112]. HVGs can be identified either based on the relation between mean and variance[104,112] or mean and dropout rate, as in M3Drop[112].

Dimensionality Reduction & Data Visualization

Even though feature selection reduces the number of dimensions significantly, selected highly variable genes are expected to be still too numerous, due to the high complexity of biological mechanisms. Therefore, there is further need for the summarization of the data. A linear dimensionality reduction technique, principal component analysis (PCA) transforms the data into components (Figure 17). Each gene contributes to each component in different weights. So, components are new features, generated on the basis of the weighted sum of the original features (genes). The first component explains the highest variance and the explained variance decreases in the following components.[93] Such property enables the representation of a large portion of the variance in the data using few components. Since they represent

the highest variance in the data, visualization of the first two components can provide insights into different groups within the dataset. Therefore, it is commonly used for high level data representation and low-quality cell identification.[90] Nevertheless, it is important to note that the underlying assumptions of PCA, the normality and linearity of the data, are limiting factors, since the underlying biology does not necessarily have to fit the expected trends[113]. For scRNA-seq datasets, commonly preferred methods are T-distributed stochastic neighbor embedding (tSNE)[114] and Uniform Manifold Approximation and Projection (UMAP)[115,116].

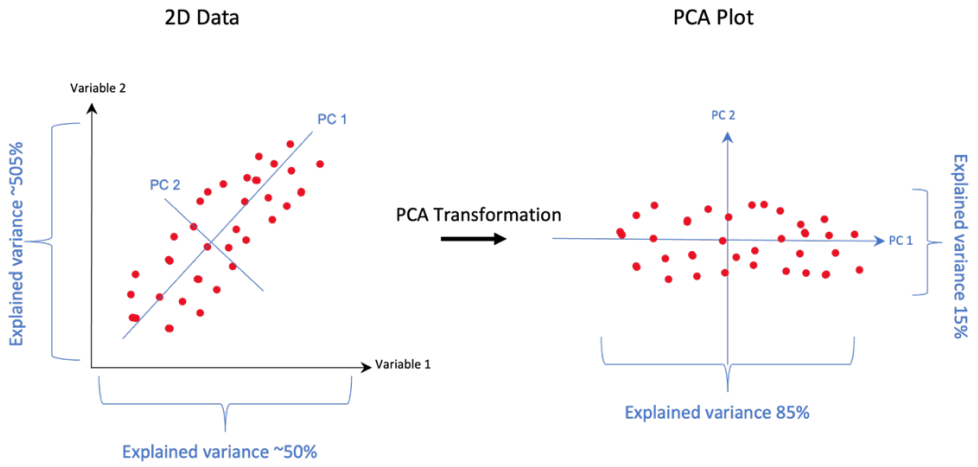

Figure 17. Illustration of a PCA transformation. In this example, the dataset consists of two variables, each explain ~50% of the variation. There is no single variable that can capture the most variance in the dataset. Using PCA transformation, the variables are transformed into principal components (PC). Using only PC1, 85% of the variation in the dataset can be explained. Therefore, it can be used to summarize the dataset as a single variable.

Stochastic neighbor embedding (SNE) algorithm is designed as a dimensionality reduction method aiming to conserve the proximity information among the neighbors in the lower dimensional representation. In SNE, a Gaussian distribution, representing the similarities between each point, is generated by the conversion of Euclidian distances into conditional probabilities. Within each distribution, generated for each instance, those instances that are located closely in

the high dimensional data will have closer proximity to the mean of the distribution. Hence, it is more probable that these instances are the closest neighbors. During the mapping of the high dimensional data to a low dimensional representation, the algorithm randomly generates a low dimensional representation and aims to minimize the difference between the conditional probabilities (cost function) of the high and low dimensional representations. An optimization step, using gradient descent, minimizes the outcome of the cost function and the low dimensional data points are obtained. A downside of this approach is that the optimization step is complex and challenging. In tSNE, instead of Gaussian distribution, Student-t distribution is applied, simplifying the optimization step.[114] It is a non-linear dimensionality reduction method, capable of conserving complex relations together with the local clusters.[113,117] Therefore, there is extensive usage of tSNE in scRNA-seq applications.[113] One limitation of tSNE is that there is information loss for the long-distance relationships.

Uniform manifold approximation and projection (UMAP)[115] is a machine learning method, used for dimensionality reduction, where the features are transformed into manifolds. The topology of each data point is captured based on the proximity of its k nearest neighbors, capturing the neighboring information between all points. An initial low dimensional representation is generated using spectral embedding and the entropy between the low and high dimensional spaces is minimized using an optimization algorithm. The resulting low dimensional representation is highly dependent on the selected k value. A smaller k results in focusing closer relations while a large k focuses on a larger perspective, preserving a more global structure.[115]

UMAP and tSNE are two techniques that are widely used in scRNA-seq studies.[117] Although the algorithms share similarities in terms of methodology, UMAP performs faster in large datasets and keeps the long-distance relations between the data points (Figure 18).[116] Yet, it should be noted that the algorithm is

designed to represent the local relations. Interpretations for the long-distance relations may not reflect the reality in the original space and subject to further validation.[116]

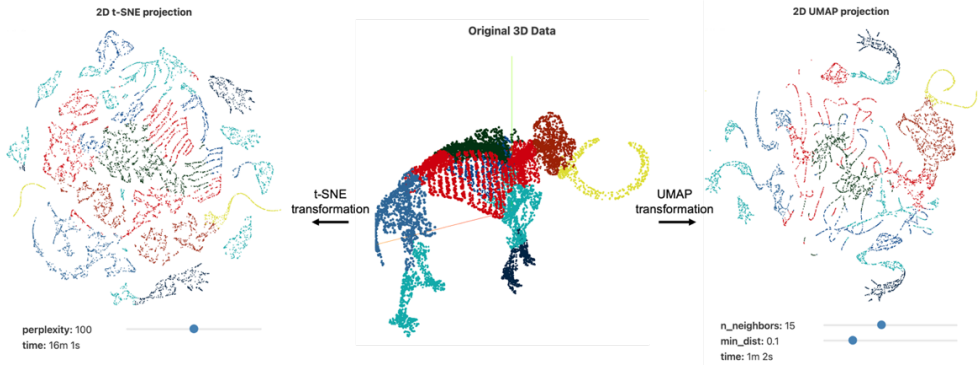

Figure 18. A case example for the comparison of tSNE and UMAP. In this example, we observe dimensionality reduction applied to a 3D dataset (middle) to project onto 2D space using tSNE (left) and UMAP (right) algorithms. It can be observed that in tSNE, although the local structures (body parts with same colors) are conserved, the global structure (the shape of a bull) is not conserved. On the other hand, although UMAP prioritizes the local structure conservation, it still keeps a similar global structure as well. This can be observed through proximity of the horns and head as well as the arms and legs. The figure is adapted from https://pair-code.github.io/understanding-umap/.

Clustering

Identification of cell groups, sharing similar transcriptomic properties, is an essential step in scRNA-seq analysis. To detect cell clusters, community detection algorithms Louvain and Leiden are widely used.[118,119]

Louvain clustering is an approximation algorithm where the aim is to maximize the modularity.[120] The algorithm consists of two steps: modularity optimization and community aggregation. Initially, an optimization algorithm is applied to generate optimal local communities. In the second step, these communities are aggregated into larger communities. The algorithm continues applying the same

steps iteratively until all data points are merged into a single cluster. The number of clusters obtained by Louvain method is controlled by the resolution parameter that varies between 0 and 1. The smaller the parameter is set, the larger the clusters form, resulting in lower number of clusters.[120]

Leiden clustering[121] is an improved version of the Louvain clustering[122]. It has an additional step in between the first and second step of the Louvain algorithm; refinement of the partition. During refinement, the identified communities in the first step are further partitioned into smaller communities to increase stability in further steps. Such application increases the accuracy and the runtime speed.[121,122]

Batch Correction

In the previous chapter, possible reasons for batch effects and the necessity for the elimination of these variations were discussed. The data visualization and the community detection are sensitive to these variations. Both methods focus on the similarity between the cells and the batch effects can easily derive this similarity. Instead of biological similarity, cells can group based on their experimental conditions. Therefore, it is essential that the batch effects are corrected before data visualization and clustering.[113,118] There are various batch correction methods. Although the methodologies highly differ among each other, the generic strategy includes generation of a low-dimensional representation of the data (using dimensionality reduction), identification of commonalities/neighbors between the batches and generation of the corrected data/representation prioritizing these similarities. Among batch correction algorithms, widely used ones can be listed as BBKNN[123], Harmony[124], Liger[125] and Seurat 3[126]. A comprehensive overview of these methods and their comparison can be found in Tran et al. study[127].

Cell Typing

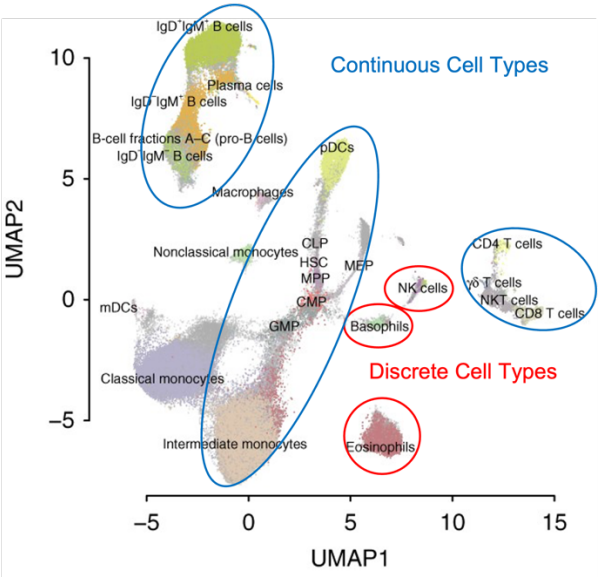

Figure 19. An illustration, depicting the two observed cell type categories. The figure is adapted from Becht et al.[116]

The characteristic of a cell is determined by many factors, including its location, interactions with neighboring cells and external signals.[128] These factors initiate the mechanisms, causing the cell to undergo a series of changes, and end up in different cellular states called cell types.[128] Definition and identification of the cell types in a micro-environment is a challenging task. There are many different characteristics that can define a cell state. Cells can be categorized based on their cell cycle state, their maturation levels or based on expression of different marker genes or proteins.[129] Therefore, the definition of cell types differs based on the experimental conditions and the data available.[129] Moreover, the transition from one cell type to another is not always definitive. In some cases, the transformation is decisive and discrete cell types are observed (Figure 19). In other cases, the transition involves smaller changes spread over time, where continuous phenotypes are observed.[128–130]

Depending on the experimental setup, cell typing can be done either manually or automated classification methods can be used. In cases where a rare subpopulation is being investigated or identification of a new population is aimed for, manual annotations can be preferred[74]. In this strategy, the cells are clustered based on their transcriptional profile and annotated depending on the expression levels of differentially expressed genes.[130,131] There are many automated annotation methods developed for scRNA-seq. These methods can be classified into four categories: correlation-based, such as SingleR[1321] and CHETAH[133], projection-based, such as Scmap[134] and WNN[135], marker gene-based, such as Garnett[136] and machine learning methods. A thorough comparison of widely used automated annotation methods can be found in Abdelaal et al. 2019 [137].

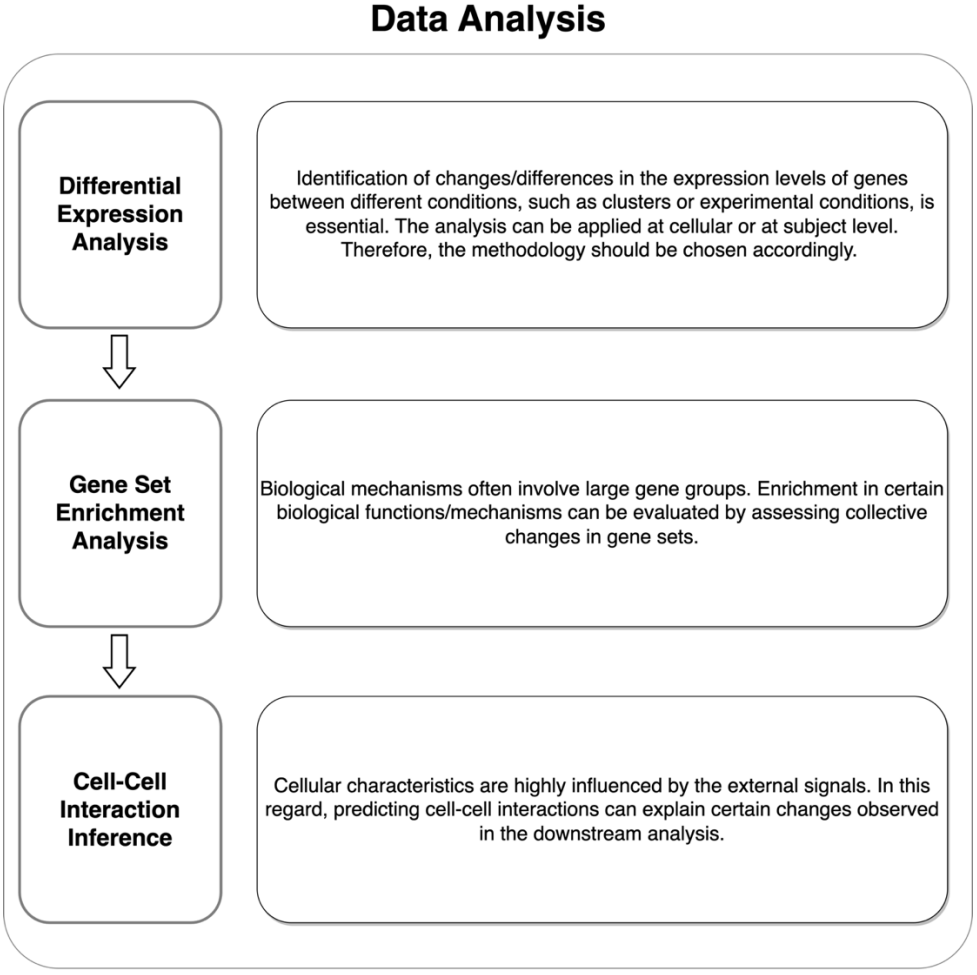
Data Analysis
Differential Expression Analysis
Identification of changes/differences in the expression levels of genes between different conditions, such as clusters or experimental conditions, is essential. The analysis can be applied at cellular or at subject level. Therefore, the methodology should be chosen accordingly.
Gene Set Enrichment Analysis
Biological mechanisms often involve large gene groups. Enrichment in certain biological functions/mechanisms can be evaluated by assessing collective changes in gene sets.
Cell-Cell Interaction Inference
Cellular characteristics are highly influenced by the external signals. In this regard, predicting cell-cell interactions can explain certain changes observed in the downstream analysis.

Data Analysis

With the knowledge obtained by the data exploration, one can start building hypotheses and conduct statistical analyses to test these hypotheses. Alternatively, the data can be used for predictive modelling, which can provide an estimation that can be used to build hypotheses to be explored in follow-up studies. In this section, we will focus on the data analysis used in this dissertation. A detailed explanation of data analysis approaches, including trajectory inference, cytogenic inferences and regulatory networks, has been covered by Chen et al.[138].

Differential Gene Expression (DGE) Analysis

To identify differences in transcriptional landscape of diverse cell types or subject groups, differential gene expression analysis can be applied. The methods to be applied depends on whether the comparison is at cellular level or at subject level. To compare different cell populations or clusters, commonly used methods include Wilcoxon rank sum test, student's t-test, Likelihood test and logistic regression.[104] For inter-subject comparisons, pseudobulk approaches are used. In pseudobulk strategy, the cellular data are initially aggregated to obtain pseudobulk data, representing subject level information. This transformation approximates bulk RNA-seq strategy and enables the use of traditional differential expression tools, such as EdgeR[139] and DEseq2[140]. Alternatively, MUSCAT[141], an adaptation of DEseq2 to scRNA-seq data, can be used.

Gene Set Enrichment Analysis

Differential gene expression analysis reveals the difference between the contrasts at gene level. However, the biological systems are complex and often large gene groups are required to function together for biological processes. Gene set enrichment analysis (GSEA) enables investigation of alterations in biological processes by evaluating collective changes in gene groups. Initially, the genes are

ranked by their expression difference between the two contrasts. Genes in the lower and upper end of the ranked list are associated with either one of the two contrasts. Therefore, the accumulation of genes of a biological process in one of the two edges indicates high correlation with the observed phenotype. To evaluate such polarization, an enrichment score is calculated by running down the ranked list and generating a running-sum score when a gene in the gene set of interest is observed. When another gene is observed, the score decreases. Finally, to determine the statistical significance of the enrichment score, a permutation test is applied.[142] The analysis can be conducted by GSEA software[142], FGSEA[143] library in R or gseapy (https://gseapy.readthedocs.io/en/latest/) in Python.

Cell-cell Interaction Inference

Cells in a micro-environment have a highly dynamic and complex communication network. The interaction between cellular groups has a major impact on their cellular state and function. Therefore, identification of such network structures has a vital role in disease biology. Although scRNA-seq experiments provide a deep understanding of intracellular changes, it has limitations on intercellular information. It only provides transcriptomic information, while intercellular interactions mostly take place in the form of protein-protein interactions. Also, it does not provide information regarding proximity between cells, which is another important effector for intercellular interactions. Nevertheless, using the central dogma, the potential interaction between different cell populations can be inferred using transcriptomics data. There are numerous databases, such as OmniPath[144], UniProt[145] and IntAct[146], that have cell-cell interaction information, enabling predictive analyses.

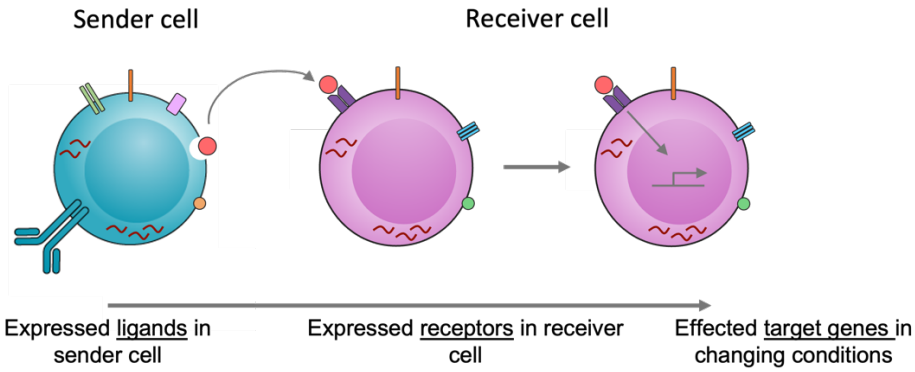

Figure 20. Visual representation of the concept of cell-cell interaction inference.

Cell-cell interaction inference algorithms initially focuses on known ligands and receptors and their expression on cell types of interests. Based on changes and/or abundance of ligands and receptors, potential interactions were predicted (Figure 20). In a recently published study, Dimitrov et al.[147] provided a comprehensive overview of ligand-receptor interaction models and databases. They also showed that the choice of database and the model have significant impact on the results. Therefore, they have implemented the Liana framework where the analysis can be conducted by model and database of preference. It also enables multiple selection of databases and models, providing a consensus decision. In addition to ligands and receptors, intercellular interactions are expected to alter downstream mechanisms in the cells of interest. Investigating these expected alterations, further evidence can be gathered. NicheNet[148] and CytoTalk[149] are two methods that also take into account downstream changes in the gene expression patterns.

CITE-seq

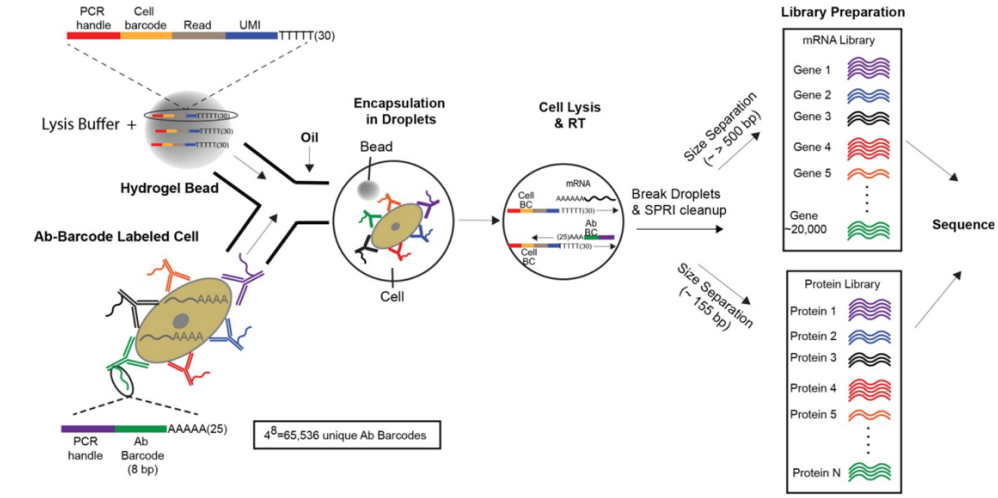

Figure 21. REAP-seq protocol. The figure is adapted from Peterson et al.[150]

In the cell typing chapter, the challenges of characterization of different cell types were discussed. In some cell types, such as T-cells, the transcriptomic information may not be sufficient to characterize all the subpopulations. In these cases, additional cell surface proteome information can facilitate accurate and deeper annotation of distinct cell groups.

Cellular indexing of transcriptomes and epitopes by sequencing (CITE-seq)[151] and RNA expression and protein sequencing assay (REAP-seq) are two adaptations of scRNA-seq with the addition of the possibility to investigate the cell surface proteome. The two approaches greatly overlap in terms of methodology. In both techniques, before encapsulation, antibodies, tagged with a DNA conjugate-including primer, antibody barcode and poly A sequences, bind to their respective antigens to capture the cell surface protein abundance (Figure 21).[150,151] Data obtained from the surface proteome is called antibody-derived tag (ADT). Such a strategy enables simultaneous quantification of both transcriptomic and cell surface proteomic

information. Once the scRNA-seq procedure is complete, both data types can be separated by the barcode sequences and analyzed. The main difference between the two strategies is the generation of the antigen-DNA conjugate. CITE-seq uses a sequence which binds to biotinylated DNA, while REAP-seq depends on the covalent bond between the antibody and aminated DNA barcode.[152] Recently, an expanded version of CITE-seq, ECCITE-seq[153], which offers additional information gain by enabling investigation of CRISPR perturbations and immune receptor clonotypes, has been announced.

Since the protocol of scRNA-seq and CITE-seq overlap greatly, the data preprocessing and data exploration strategies can be used for both, except for the data normalization. The strength of scRNA-seq data comes from the large number of identified genes, which can provide a global overview of the cellular state. However, in CITE-seq proteomics data, limited numbers of antibodies are used due to lack of antibodies to target all antigens of interest.[154] This also provides additional challenges on correcting the technical noise and data normalization. RNA data include high numbers of 0 values, making it a sparse dataset with a peak at 0 and a positive distribution. On the other hand, in ADT data, for each antigen, it is often observed that there is a non-zero negative peak, due to unbound antibodies, and a positive peak[155]. To segregate the actual distribution from the noise, different strategies, including centered log ratio transformation[156], denoised and scaled background normalization [157], ADTnorm[155] and arcsinh transformation, have been developed. A comparison of CITE-seq denoising strategies can be found in Zhen et al.[155]

scVDJ-seq

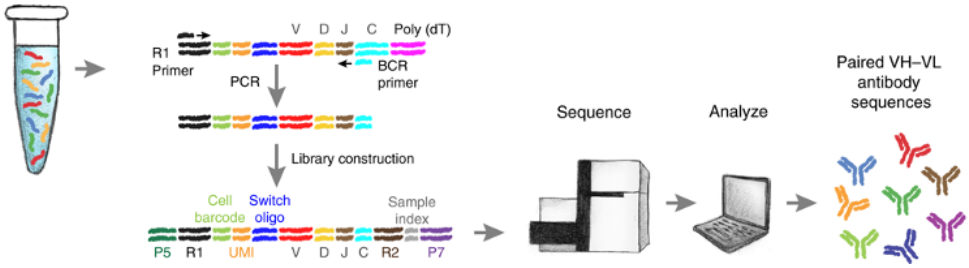

Figure 22. scBCR-seq protocol. The figure is adapted from Goldstein et al.[158]

In the first chapter, BCR, a unique antibody that can recognize the pathogen antigens was introduced. Similar to B-cells, T-cells also have unique antibodies that can recognize peptide fragments of MHC molecules, the T-cell receptor (TCR). Importantly, both receptor types gain their diversity through VDJ rearrangements. The characterization of these regions as well as their expansion status are of great importance for various fields in research.

Like the surface proteome, the characterization of individual cell BCRs or TCRs have been integrated with transcriptomic analysis via single cell technologies. Single cell VDJ sequencing (scVDJ-seq) protocol follows the 10x scRNA-seq sequencing with an additional feature of detection and amplification of BCR (or TCR) mRNA using specific primers targeting constant and VDJ regions (Figure 22).[158] After sequencing, each cell can be characterized by CDR3 regions of the heavy and light chains, and clonality can be assessed. Data analysis for scVDJ-seq data can be conducted through computational tools, such as Scirpy[159], scRepertoire[160] and Immunarch[161].

scRNA-seq applications on MM

In the previous chapters highly heterogeneous characteristics of MM were shown. There are changes involved within plasma cells as well as changes in the surrounding micro-environment that can impact the disease characteristics. Therefore, scRNA-seq experiments have wide range of applications in the field of MM. This dissertation primarily focuses on disease progression and active disease. Thus, a collection of studies that have made a significant impact in these areas are compiled here. These studies can be categorized based on whether they focused on the tumor micro-environment or plasma cells. In this section, we provide a detailed summary of the key findings from each of these studies.

Focus on Tumor Micro-environment

Zavidij et al. Study

In this study[162], the authors focused on bone marrow cells, obtained from 32 individuals, including healthy donors (n=9), MGUS (n=5), SMM-low risk (n=3), SMM-high risk (n=8) and MM (n=7) categories. They aimed to reveal changes in the tumor micro-environment along MM progression. They conducted scRNA-seq experiment with cells isolated as CD45+CD138- and identified 21 subpopulations, as a result of the clustering analysis.

Despite high heterogeneity among samples, proportional analysis showed a general trend of enrichment in NK cells, T-cells and CD16+ monocytes as well as a decrease in pDCs, neutrophils, CD14+ monocytes and progenitors. These findings were further supported by CyTOF experiments. Within NK cells, they have found that as the NK cell proportion increase, with a population shift from the CXCR1+ subpopulation towards the CXCR4+ subpopulation. They explained this shift by an increased recruitment of immature NK cells. Using non-

negative matrix factorization, a machine learning dimensionality reduction technique, they have identified components that explain large variations in the dataset. Investigating these components, they obtained different gene signatures within T-cells and monocytes. Investigation within T-cells revealed a population shift from a GZMK+ state to a more effector phenotype with a GZMB+ signature. Moreover, they observed an IFNα signature enriched along disease progression in various cell types. Interestingly, although they observed increased HLA-DR gene expression in transcriptomics analysis in CD14+ monocytes, CyTOF analysis showed decreased MHC class II presentation on the cell surface. They further conducted cell culture experiments and concluded that up-regulation of MARCH1/MARCHF1 expression resulted in internal localization of MHC class II in CD14+ monocytes in later disease stages.

De Jong et al. Study

De Jong et al.[163] investigated the bone marrow micro-environment of healthy individuals and MM patients. Using scRNA-seq analysis, they generated a paired dataset of non-hematopoietic, CD38+, CD38-, and CD138+CD38+ populations, revealing a MM-specific subpopulation within mesenchymal stromal cells (iMSC) with a high inflammatory signature. This discovery was further validated through flow cytometry and in-situ hybridization, where the iMSC cells were located in close proximity to malignant plasma cells and T-cells, indicating possible interactions with this population. The authors applied functional protein network analysis through STRING database and identified TNF and IL1B as potential drivers of this signature, which was validated using in-vitro assays. Additionally, they discovered that the inflammatory signature in iMSCs can be induced by T and NK cell subsets; NCR1+GZMB+CX3CR1+CD56dim NK cells, GZMB+ CD8B+ effector T-cells and TNF+FAS+GZMK+ Tscm, via TNF expression. Further investigation for cell-cell interactions, using CellPhoneDB, revealed that iMSCs-MM plasma cell

interactions through CCL2-CCR/CCR10 and IL6-IL6R could potentially induce proliferation in MM plasma cells, and iMSCs can modulate myeloid cell functionality. Finally, their investigation of the inflammatory signature after treatment revealed that the inflammatory response continues after therapy, even in patients with negative MRD.

Pilcher et al. Study

In a recently published study, Pilcher et al.[164] utilized the MMRF CoMMpass scRNA-seq dataset to investigate the CD138- BM tumor micro-environment. Using the progression-free survival (PFS) information, 18 newly diagnosed MM subjects were categorized into rapid-progressors (RP<18 months) and non-progressors (NP>4 years). The study compared the immune subtypes between the two conditions and identified higher levels of CD8+ Exhausted T-cells and M2 macrophages, and lower levels of CD8+ Effector T-cells and immature B-cells in the RP group. The authors also found an enrichment of IFN response (both) in the RP group and TNF response in the NP group. Cell-cell interaction analysis using CellChat[165] was applied, and three signaling pathways, BAFF, CCL, and IL16, were found to be significantly associated with patient survival. The study identified CCL5 and CCL3 interactions with CCR1 from CD8+ T-cells to monocytic cells as negative effectors of patient survival in the RP group. They observed an increase in the abundance of BAFF in the tumor micro-environment of the RP group, which can potentially enhance the survival of MM cells and negatively affect patient survival. Conversely, IL16 expression in the tumor micro-environment was found to have a positive impact on patient survival.

Focus on Plasma Cells

Ledergor et al. Study

Ledergor et al.[166] conducted one of the first single-cell RNA sequencing (scRNA-seq) studies on multiple myeloma (MM), investigating isolated CD38+CD138+ plasma cells from the bone marrow of 7 MGUS, 6 SMM, 12 MM, 4 AL, and 11 age-matched healthy controls. The authors observed minimal heterogeneity among control samples but high heterogeneity among malignant cells across individual subjects. They identified common transcriptional mechanisms among patient clusters, including overexpression of driver genes, such as CCND1, CCND2, FGFR3, FRZB, and the WNT pathway, previously associated with genomic abnormalities observed in MM. In addition, the authors identified three novel candidate genes, LAMP5, CDR1, and WFDC2. Interestingly, the study also investigated rare malignant cells in subjects post-therapy, which shared most of their transcriptional state with the original cells at diagnosis. Moreover, the researchers further profiled circulating tumor cells and showed that these cells in the blood reflected the molecular disease observed in the bone marrow, indicating that circulating tumor cells may serve as potential biomarkers for MM. Overall, this study provides a comprehensive understanding of the molecular mechanisms underlying MM and identifies potential biomarkers for diagnosis and monitoring of the disease.

Boiarsky et al. Study

Boiarsky et al.[167] conducted a comprehensive study using single cell RNA-sequencing of CD138+ plasma cells from 26 patients at varying disease stages (MGUS = 6, SMM = 12, newly diagnosed MM = 8) and 9 healthy donors. They observed a common transcriptomic profile among the normal plasma cells across all subjects. On the other hand, abnormal clones showed a diverse profile. The within-patient abnormal vs. normal cell comparisons highlighted inter-

patient heterogeneity and patient-specific disease characteristics. The patients could be categorized based on cytogenic abnormalities using translocation target genes, and the performance of the experiment was benchmarked using interphase fluorescence in situ hybridization to identify large-scale structural genomic variants. Moreover, Boiarsky et al. identified 15 gene signatures using non-negative matrix factorization, representing common profiles among patients including t(11;14), t(14;20) and normal plasma cells. They observed high heterogeneity of activation of these signatures among plasma cell subpopulations. Interestingly, the study found that the normal plasma cell signature was uniformly down-regulated in abnormal plasma cells, while t(11;14) and interferon-inducible signatures were correlated with disease progression.

Liu et al. Study

Liu et al.[168] conducted a longitudinal study of 14 patients at different stages of MM using scRNA-seq and 10x Genomics linked-read whole genome sequencing (10xWGS). They identified patient-specific plasma cell profiles and immune cell expression changes, analyzing potential driver events. The composition of the immune cell populations varied among the different patients, highlighting the diverse nature of the disease. In addition, they examined the copy number variations in plasma cells, finding chromosome 13 deletion in 17 out of 21 samples. They found that distinct plasma cell subpopulations remained stable during the transition from SMM to primary MM, while emerging subpopulations with increased genomic instability were observed from primary MM to relapse. Differential expression analysis revealed high expression of JUN, FOS, FOSB, and JUND in certain plasma cell populations, which assemble the AP-1 transcription factor. They validated AP-1 complex differential expression (JUN and FOS) in plasma cell subpopulations using CyTOF. Integrated analysis of scRNA-seq and CyTOF data revealed AP-1 downstream targets (IL6 and IL1B) that potentially regulate inflammation.

Purpose of This Study

Development of novel immunotherapeutic applications, combined with the recent advancements in next generation sequencing, has opened new opportunities for gaining a more comprehensive insight of disease biology, as well as to increase the effectiveness of treatment. In this context, the current dissertation focuses on employing multi-modal analyses to explore the unexplored areas of MM disease biology and the potential of immunotargeting. By integrating different techniques, this research aims to provide a comprehensive landscape of MM and explore innovative strategies for targeted immunotherapy.

Multiple myeloma is a cancer where much of the focus is concentrated on elimination of the tumor cells. However, it is crucial to recognize that the disease can often be detected at premalignant stages. Therefore, understanding the disease progression and identifying possible ways to prevent it holds great importance. Despite the extensive literature on MM disease biology, there is still much to discover, particularly regarding the changes in the bone marrow micro-environment during disease progression. The primary objective of the first chapter is to gain an in depth understanding of the changes occurring in both the tumor cells and the tumor micro-environment as well as to identify potential molecules and/or interactions that have a driver effect in disease progression.

In the field of multiple myeloma treatment, various candidate antigens have been proposed. However, the issue of off-target toxicity remains a significant concern when it comes to immunotherapeutic applications. In addition, solely relying on the expression of a single target is vulnerable to antigen escape mechanisms. Combinatorial antigen targeting can potentially address these issues. Antigen combinations can reduce toxicity by increasing tumor-

specificity, which leads to applicability of multiple antigen combinations to be used at once to overcome antigen escape. The second chapter of this dissertation is centered around target antigens in MM treatment. The objective of this study is to conduct a multi-omics approach to identify novel antigens and antigen pairs that can be utilized in a combinatorial method, followed by evaluation of these targets using external datasets and in vitro assays.

Chapter I: Understanding MM Biology

Dynamic Interplay Between Tumor and Micro-environment During Multiple Myeloma Disease Progression

Murat Cem Köse[1*], Isabelle Bergiers[2*], Sheri Skerget[3] , Milan Malfait[4], Nele Fourneau[2], Jenna-Claire Ellis[2], Greet Vanhoof[2], Tina Smets[2], Bie Verbist[2], Dries De Maeyer[2], Jeroen Van Houdt[2], Koen Van der Borght[2], Raluca Verona[3], Bradley Heidrich[3], William Kurth[5], Michel Delforge[6], Nathalie Meuleman[7], Jan Van Droogenbroeck[8], Philip Vlummens[9], Christoph J. Heuck[3], Yves Beguin[1], Nizar Bahlis[10], Jo Caers[1+], Tineke Casneuf[2+]

[1]Department of Hematology, CHU of Liège, Liège, Belgium
[2]Janssen Research & Development, Beerse, Belgium
[3]Janssen Research & Development, Spring House, PA, United States of America
[4]Department of Applied Mathematics, Computer Science and Statistics, University of Ghent, Ghent, Belgium
[5]Department of Orthopedic Surgery, CHU de Liège, Liège, Belgium
[6]University Hospital Leuven, Leuven, Belgium
[7]Service d'Hématologie, Institut Jules Bordet, Université Libre, Bruxelles, Belgium
[8]Department of Haematology, AZ Sint-Jan Brugge-Oostende AV, Brugge, Belgium
[9]Department of Clinical Hematology, Ghent University Hospital, Gent, Belgium
[10]Department of Hematology and Oncology, University of Calgary, Calgary, AB, Canada
**shared first authorship*
+shared senior authorship

Abbreviations

- Multiple myeloma (MM)
- Bone marrow (BM)
- Healthy volunteer (HV)
- Monoclonal gammopathy of undetermined significance (MGUS)
- Smoldering multiple myeloma (SMM)
- Single cell RNA sequencing (scRNA-seq)
- Cellular indexing of transcriptomes and epitopes by sequencing (CITE-seq)
- B-cell receptor sequencing (BCR-seq)
- International Myeloma Working Group (IMWG)
- BM mononuclear cell (BM-MNC)
- Phosphate-buffered saline (PBS)
- Fetal bovine serum (FBS)
- Bovine serum albumin (BSA)
- Dimethyl sulfoxide (DMSO)
- Antibody derived tag (ADT)
- Cell per million (CPM)
- Immunoglobulin genes (IG)
- Centered log-ratio (CLR)
- Principal component analysis (PCA)
- Differential expression (DE)
- Biological process (BP)
- Gene set enrichment analysis (GSEA)
- Gene Expression Omnibus (GEO)
- Multiple Myeloma Research Foundation (MMRF)
- Dendritic cell (DC)
- Interferon alpha (IFNα)

- Interferon gamma (IFNγ)
- Tumor necrosis factor alpha (TNFα)
- CD8+ activated T-cells (CD8+ ATC)
- Classical DCs (cDC)
- Progression free survival (PFS)
- Overall survival (OS)
- Myeloid-derived suppressor cells (MDSCs)
- Normalized enrichment score (NES)

Abstract

Background: The investigation of the cellular and molecular mechanisms of progression from precursor plasma cell disorders to active disease increases our understanding of multiple myeloma (MM) pathogenesis and helps further identify novel preventive and therapeutic strategies. Single cell transcriptomics is an opportune tool to facilitate the study of tumor cells, tumor micro-environment, and their molecular interactions.

Methods: Using single cell RNA sequencing, surface proteome profiling, and B lymphocyte antigen receptor profiling of unsorted, whole bone marrow samples, we generated a cell atlas of the BM micro-environment from 123 individuals. These subjects included healthy volunteers (HV), and patients with monoclonal gammopathy of unknown significance (MGUS), smoldering MM (SMM) and MM.

Results: Despite high transcriptional heterogeneity in malignant plasma cell composition among patients, our analyses revealed commonality in molecular pathways, including MYC signaling, E2F targets and interferon alpha response, altered during disease progression. We found evidence of early dysregulation of the immune system in MGUS and SMM, which increases and impacts many cell types as the disease progresses. In parallel with disease progression, we observed population shifts in CD8+ T-cells, macrophages and classical dendritic cells, and found that the resulting differentiation in CD8+ T-cells and macrophages were associated with poor overall survival outcomes. Modelling cell-cell interactions between tumor plasma cells and the immune micro-environment, we identified potential ligand receptor interactions that may play role during the transition from precursor stages to MM and identified potential biomarkers of disease progression, some of which may represent novel therapeutic targets. MIF, IL15, CD320, HGF, and FAM3C were detected as potential regulators of the tumor microenvironment by plasma cells, while SERPINA1 and BAFF (TNFSF13B)

were found to have the highest potential to contribute to the downstream changes observed between precursor stage and MM cells.

Conclusions: Our findings show that myeloma tumorigenesis is associated with dysregulation of molecular pathways driven by gradually occurring immunophenotypic changes in the tumor and tumor micro-environment.

Background

Multiple myeloma is a hematological malignancy of bone marrow plasma cells [1]. It is the second most common blood cancer and is primarily a disease of the elderly. Over the past 15 years, the prognosis of patients with MM has improved due to the emergence of new therapies and therapeutic platforms providing deep and durable responses [2,3]. However, patients still relapse and for most patients, MM remains incurable, underscoring the urgent need for new treatment options and a better understanding of the disease.

MM has two precursor stages: starting with MGUS, an indolent condition relatively common among elderly individuals with a rate of progression to MM of 1% per year; and SMM with a rate of progression to MM of 10% per year [4]. During MGUS and SMM, patients present clonal bone marrow plasma cells and elevated levels of monoclonal protein in the blood, but are typically asymptomatic, lacking MM-defining symptoms of hypercalcemia, renal impairment, anemia, and bone lesions (CRAB criteria) that are commonly observed in MM [5,6].

MM is a complex disease that exhibits high inter- and intra-patient variability. The identification of tumor intrinsic driver events, and a better understanding of the interaction between the tumor and the micro-environment, is important for the discovery of new MM treatments. MM has also been shown to be not a single disease but one in which multiple molecular subtypes exist that share a similar clinical presentation [7,8]. Previous studies have shown that genomic alterations of plasma cells characteristic of MM are already detectable at MGUS and SMM stages, highlighting the contribution of tumor extrinsic factors in progression to MM [7–11]. Notably, changes in the bone marrow micro-environment at different stages of MM have also been described [6,12,13]. Exploring the BM

resident plasma and immune micro-environment cells, Zavidij et al. found evidence of increased NK cell proportions, altered chemokine receptor expression upon disease progression [12] and provided evidence of myeloma-associated events, such as loss of GZMK+ memory cytotoxic T-cells and MHC class II dysregulation in CD14+ monocytes, in the precursor stages. A study performing single cell transcriptomic analysis of plasma cells demonstrated high variability between individuals and even within subjects and could further associate this variability with the expression of known genomic drivers of MM and potential new drivers [13]. Spatial colocalization of transcription of genes involved in tumor survival and immune modulation in tumor cells and immune cells predicted a role for mesenchymal stromal cells in the disease [14]. Although many studies highlight the value of single cell profiling in understanding inter- and intra-patient tumor heterogeneity as well as the contribution of the tumor micro-environment across different stages of the disease, most have focused solely on plasma cells [13,15] or on the surrounding immune cells [12], lacked inclusion of precursor stages [14], or had been conducted on a limited number of subjects [12,13,16,17].

In this study, we collected BM samples from HV, as well as MGUS, SMM and newly diagnosed MM patients from a large set of 123 subjects, balanced across the 4 cohorts (Table 1). Samples were profiled using multi-modal single cell omics techniques including single cell RNA sequencing (scRNA-seq), cellular indexing of transcriptomes and epitopes by sequencing (CITE-seq), and B-cell receptor sequencing (BCR-seq) to investigate the status of the bone marrow micro-environment, dysregulation of the immune system, and interaction between BM immune cell populations and tumoral plasma cells to better understand progression to MM.

Through this study, we confirm the observed high plasma cell heterogeneity among subjects, but also reveal shared features in the immunophenotypic changes of the BM micro-environment that take place during

progression to MM. Along the clinical stages of the disease, we identified increased inflammatory response in the tumor micro-environment and population shifts in specific immune cell types, some of which were also found to be associated with overall survival. Our cell-cell interaction modelling identified ligands and receptors that induce tumor growth and promote survival, which we hypothesize play a role during disease progression to MM. Our findings highlight the dynamic relationship between plasma cells and the micro-environment and show that the alterations in the tumor micro-environment are already initiated in the precursor stages which likely contributes to progression to MM.

Methods

Sample collection

BM aspirates were collected at 6 Belgian centers from subjects of 4 cohorts: 31 HV, 28 MGUS, 32 SMM and 32 newly diagnosed MM patients (Figure 1a). Updated Criteria for the Diagnosis of Multiple Myeloma were used as defined by the International Myeloma Working Group (IMWG)[18]. To isolate the BM mononuclear cell (BM-MNC) fractions, BM aspirates were diluted at a ratio of 7:1 with phosphate-buffered saline (PBS) and filtered through 100µm filter to remove bone fragments and/or cell clumps. BM-MNC layers were isolated after Ficoll-plaque^{TM}PLUS (density 1.077+/-0.001g/ml) gradient separation and washed three times with PBS. Samples were frozen at 5-8x10^6 cells/ml in freezing medium (90% fetal bovine serum (FBS) + 10% DMSO) and stored in liquid nitrogen.

Single Cell Sequencing

Samples were thawed at 37ºC and diluted in pre-warmed RPMI-1640 medium before centrifugation. Cell pellets were resuspended in cold PBS + 1% BSA and kept on ice for the remainder of the procedure. For each sample, 0.2x10^6 cells were stained using the CITE-seq antibody pool following the manufacturer procedure (BioLegend). After staining, cells were resuspended in PBS +0,04% bovine serum albumin (BSA) at a concentration of 1000 cells/µl. Cells were filtered using a FACS tube with a cell strainer cap and processed immediately according to the 10x Genomics Chromium single cell V(D)J with Feature Barcoding protocol. Viability was assessed by Moxi Flow™ Flow Cytometer using propidium iodide, where median 89.2%, min 60.4% and max 99.4% was observed. Twenty thousand cells were loaded onto 10x chips. For each chip, one sample from each cohort was processed and loaded in a randomized order. Single

cell multi-omics profiling, including RNA, BCR and antibody derived tagged (ADT) 10x sequencing, was conducted according to the 10x Genomics manufacturer instructions (10x Genomics, CG000186 Rev C). Library pools were sequenced using an Illumina NovaSeq6000 following 10x Genomics' instructions to reach a median sample sequencing saturation of 90.7% for the whole dataset (lowest sample saturation observed was 63.5%).

Single Cell Multi-Omics Data Analysis

Sample demultiplexing, barcode processing, alignment to the human transcriptome (GRCh38), single-cell 5′ gene, V(D)J and feature barcode counting were performed using Cell Ranger Single-Cell Software Suite (cellranger-4.0.0, 10x Genomics). Each data type (RNA, ADT, BCR) was then pre-processed per sample independently and subsequently concatenated into a single dataset for further downstream analysis. Unless stated otherwise, for each data analysis step, related functions from the *scanpy* [19] (v1.6.1) Python package were used with default parameters.

RNA data pre-processing

Empty droplets and dying cells were filtered out based on UMI counts < 650, minimum number of genes < 300 and mitochondrial gene expression > 20%. Doublet detection was conducted by *Scrublet* [20] (v0.2.1). Droplets with a Scrublet doublet score > 0.3 and genes expressed in <3 cells were excluded. Following the initial filtering, a count per million (CPM) normalization was applied with a scale factor of 10^4 and the data were log transformed. Highly variable genes were detected with *Seurat* flavor [21]. For the downstream analyses, immunoglobulin genes (IG) were removed from the dataset. Cell cycle scores were calculated using *score_genes_cell_cycle* function from scanpy using the gene sets identified by Kowalczyk et al. [22].

ADT data pre-processing

Droplets with UMI counts < 500 were excluded. The data were normalized using centered log-ratio (CLR) transformation [23].

BCR data pre-processing

Cell Ranger filtered BCR-seq output contig files from individual samples were concatenated into a single file. Using the *scirpy* [24] (v0.6.1) library, with parameters *receptor_arms=all* and *dual_ir=primary only*, observed clonotypes were defined based on CDR3 nucleic acid sequences. To assess clonal expansion, per-sample-clonotype definitions were generated using both CDR3 nucleic acid sequences and sample IDs. Per-sample-clonotypes observed in ≥ 10 cells were considered expanded malignant clonotypes.

Dataset integration and visualization

ADT and RNA data were integrated independently for all samples. For both ADT and RNA integrated datasets, principal component analysis (PCA) and *Harmony* [25] (v1.0) batch correction, using theta=0, was performed. Nearest neighborhood networks were constructed using a cosine distance. Each integrated dataset was projected onto 2D space applying the UMAP [26] algorithm based on the standard settings of scanpy. The data were grouped by *Leiden clustering* [27] within scanpy via multiple resolutions.

Cell typing

To generate a reference dataset for automated cell typing, the data analysis pipeline was initially run using 12 samples comprised of 3 patients from each cohort. We defined the cell types in three annotation steps (Figure S1a). At level 1, to avoid inconsistency between scRNA-seq and ADT data, we first annotated the whole dataset for major cell types using both data types

independently. The cells whose annotation does not overlap between the two data types were marked as “inconsistent” and represented 3.35% of the dataset. Since scRNA-seq data provides more insight for the cellular state due to high feature coverage, for cell typing we prioritized the transcriptional data to define the subtypes and identified the transcriptionally distinct subtypes. At level 2, each major cell type was isolated, reprocessed (HVG gene selection, PCA generation, batch correction, umap generation), Leiden clustered, and annotated based on highly ranked genes. At level 3, for those subtypes that could be further subtyped based on ADT data, we conducted the same methodology using only ADT data. Using this method, we managed to classify T-cells based on both transcriptional markers and cell surface protein markers.

To save time and computational resources, we adapted *SingleR* (v1.4.1) [28] to our cell typing strategy (Figure S1b). *SingleR* was initially run on scRNA-seq data to detect the cell types identified on the second level of our reference generation, where the subtypes were identified using only scRNA-seq data. Next, for each subtype that can be further sub-categorized using ADT data, SingleR was run using ADT data for each cell type. Finally, the annotations were concatenated as a single annotation output. Consequently, we have applied further Leiden clustering for the identified cell groups in the whole dataset. The clusters that showed distinct characteristics were considered as independent cell types and misclassifications were corrected. In cases where certain clusters were characterized by high mitochondrial percentage and/or low number of genes within a cell population, they were labeled as low quality and removed from downstream analyses. Using both the RNA and cell surface protein data, we have identified 10 major and 30 minor cell types (Figures 1b and 1c). Inconsistent cells represented 0.0007% of the dataset.

Proportional comparison analysis

Proportional changes among cohorts were assessed using Mann-Whitney U test, comparing data from MGUS, SMM, and MM with HV. Changes were considered significant at a threshold of $p<0.05$.

Differential expression analysis

Two types of differential expression (DE) methodologies were applied. For contrasts involving comparisons at subject level, we applied a pseudobulk approach using the *muscat* [29] (v1.4.0) R package. To compare cell clusters, Wilcoxon rank sum tests were applied. Significantly down- and up-regulated genes were identified based on adjusted p-val (padj <0.05).

Briefly, muscat applies the quasi-likelihood method from the standard edgeR [30] pipeline on sum-aggregated counts across subjects and cell types. Before aggregation, a gene filtering step was performed at the single-cell level, excluding the IG genes and retaining only genes with at least 1 count in 10 cells across all samples. We further used the standard muscat sample filtering, where for each cell type tested, only subjects with at least 10 cells were used for that contrast. Cell types represented by less than 3 subjects after this step were not considered for DE testing. Finally, to avoid any genes expressed in just a few cells, we applied a post-hoc gene filtering step; removing any genes from the DE list expressed in less than 10% of the cells for a given cell type-cohort combination, followed by re-calculation of the FDR-corrected p-values.

Gene set scoring and enrichment analyses

Hallmark and biological process (BP) gene sets were obtained from MsigDB [31] web site and gene set scores were calculated using scanpy *score_genes* function with normalized counts. Gene set enrichment analysis (GSEA) was conducted by R package *FGSEA* [32] (v1.12.0) with *nperm=10000*, using the test

score, obtained from the Wilcoxon rank sum test, for the ranking variable. Due to high variation in the number of genes among the gene sets, we required a minimum of 30 genes and a maximum of 200 genes for the analysis of BP gene sets.

Ligand-receptor interaction modelling

MultiNichenet [33] (v1.0.0), an improved version of the original NicheNet [34] algorithm, was used following the *detailed_analysis_steps_MISC.md* vignette, provided by developers, with the differential expression results from the muscat differential gene expression analysis for the contrast MM vs precursor stages ((MGUS+SMM)/2). We selected the top 12 cell types with the highest numbers of significantly differentially expressed genes and conducted the ligand-receptor modelling analysis.

Survival regression analysis

Survival data were evaluated using the Kaplan-Meier method. A Cox proportional hazards modeling was used to assess the association of cell type abundance with progression-free (PFS) and overall survival (OS). The analyses were conducted using Python's *lifelines* (v0.27.4) library.

Validation studies using external datasets

Three external datasets were used to validate our findings. Data from all 3 studies were run through the same pipeline used to analyze our data and the cell types of interest were identified using Leiden clustering. To accommodate the lack of cell surface protein information in the external datasets, we applied manual gating ((CD3E+ or CD3D+) and CD4- and (CD8A+ or CD8B+)) for the identification of CD8+ T-cells.

Zavidij et al. Data

Cell Ranger output (mtx) files were obtained from Gene Expression Omnibus (GEO, GSE124310). This dataset included 25142 cells from 32 subjects including 9 HV, 5 MGUS, 11 SMM and 7 MM patients.

CoMMpass Data

Raw immune cell scRNA-seq data (IA-001) of patients from the CoMMpass study (NCT01454297) was obtained from the Multiple Myeloma Research Foundation (MMRF). Survival analysis was conducted using the *ttcos*, *ttcpfs*, *censos* and *censpfs* fields using data from the IA20 release. Only newly diagnosed MM samples were used: 516394 cells from 92 subjects.

de Jong et al. Data

The fastq files were obtained from ArrayExpress (E-MTAB-9139). We detected 346673 cells from 25 individuals composed of 12 HV and 13 MM patients.

Results

Decrease in antigen-presenting cell populations and increase in T-cell subtypes observed during MM progression

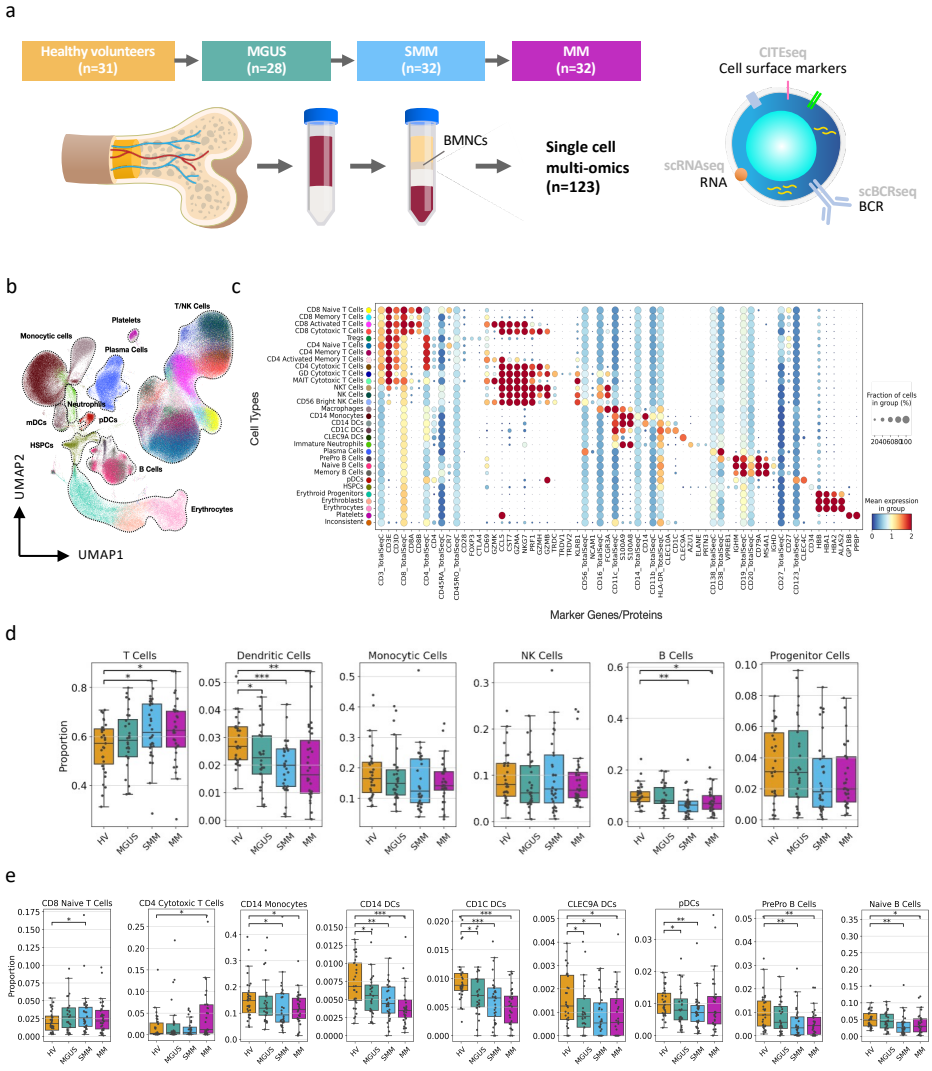

Fig. 1 Single cell atlas of BMNCs shows proportional changes in key immune cell populations. (**a**) Study design. BMNCs were collected from 123 subjects in four cohorts (Healthy Volunteers (HV), Monoclonal gammopathy of undetermined significance (MGUS), smoldering multiple myeloma (SMM) and active multiple myeloma (MM)) and further analyzed using scRNA-seq, CITE-seq, and scBCR-seq. (**b**) UMAP representation of the scRNA-seq dataset, colored by identified cell types. (**c**) Expression profile of marker genes/proteins fort each cell type. The "TotalSeqC" extension designates the proteins. (**d**) Proportions of major cell types in each patient cohort. (**e**) Proportions of minor cell types in each patient cohort. Only cell populations where significant proportional changes were observed, are displayed. For both sections **d** and **e**, each dot represents an individual subject. The proportional differences between each disease state vs HV are compared and the significance was calculated using the Mann–Whitney U test: *P < 0.05; **P ≤ 0.005; ***P ≤ 0.005.

Our single cell atlas of multiple myeloma of 355857 single cells was generated using BM aspirates from 123 subjects of 4 cohorts: HV, MGUS, SMM and active MM (Figure 1a, Table 1). Using Ficoll gradient separation, bone marrow mononuclear cells (BMNCs) were isolated and profiled using scRNA-, CITE- and BCR-sequencing. These multi-modal single cell omics technologies allowed us to identify the major BM cell subsets based on their gene and protein expression patterns (Figures 1b and 1c).

Through analysis of proportional changes of immune populations among cohorts, we found evidence of a gradual decrease in the B-cell and dendritic cell (DC) populations and a gradual increase in total T-cells when comparing MGUS, SMM and MM with HV (Figure 1d). At the subtype level, proportional decreases were observed in pre-pro B-cells, naive B-cells, all DC subtypes and CD14+ monocytes while the proportional increases were detected for CD8+ naive and CD4+ cytotoxic T-cells (Figure 1e). Interestingly, these changes were observed

to be highly variable among subjects of each category. Our observations regarding gradual increase in T-cells as well as the gradual decrease in CD14+ Monocytes, DCs and pre-pro B-cells highly correlate with the findings of Zavidij et al. Additionally, we observed a decrease in the naive B-cell population in SMM ($p<0.005$) and MM ($p<0.05$) subjects compared to HV.

Table 1. Subject characteristics

Characteristics	HV	MGUS	SMM	MM
Number of subjects	31	28	32	32
Age				
Median	70	61.5	63	70
Range	59-89	38-85	50-86	45-86
Gender				
Male	16	17	20	20
Female	15	11	12	12
ISS* Stage				
NA				4
I				9
II				10
III				9

*ISS: international scoring system; NA: Not available

Inter-patient transcriptional diversity and commonalities in molecular alterations in plasma cells across disease stages

Our dataset included the transcriptomes of 20,759 single plasma cells from 121 subjects (Figure 2). From 1 HV and 1 SMM sample, no plasma cells were isolated. As expected, we found no expansion of plasma cells in the HV subjects except for 2 individuals. In one of them the number of clonal cells was low (n=15) whereas in the other subject we observed a considerably higher number of clonal cells (n=130) which may be the result of an acute infection or other immune reaction. In a few patients, no clonal expansion was observed (In Figure 2a, patients lacking colored bars, except for light blue and light grey). A low number or lack of plasma cells can be due to the rarity of plasma cells or sampling at a location outside the tumor area.

Unsupervised dimensionality reduction revealed interesting patterns of both transcriptional heterogeneity and similarity patterns (Figure 2b). For example, non-clonal plasma cells (light blue, right panel) localize in the center, independently from patient subgroups (Figure 2b, left and right panels). Clonal cells (light brown, right panel) of MGUS subjects (in green) localize close to those of HV (in orange), while clusters of MM patients (in magenta) predominantly locate on the periphery (Figure 2b, left panel). Notably, cells of individual patients clustered together and away from those of other patients (Figure 2b, center panel), illustrating the gradual divergence of MGUS, SMM, and MM plasma cell transcriptomes. Further, most plasma cells of individual patients clustered together, however for a few patients we observed subclusters, which points out inter- as well as intra-patient diversity of transcriptomes.

Pathway enrichment analysis at the subject (Figure 2c) and cohort (Figure 2d) levels revealed the presence of both within-cohort heterogeneity and similarity. Using GSEA, we found MYC signaling (MGUS, $p<0.05$) [35], cell cycle related E2F targets (SMM, $p<0.05$) and interferon alpha (IFNα) response (SMM, $p<0.05$) pathways to be enriched early in the disease and increased along MM progression (Figure 2e). Oxidative phosphorylation ($p<0.005$) [36] and G2M Checkpoint ($p<0.05$) pathways were only observed to be significantly enriched in MM patients, while a decrease is observed in IL6/JAK/STAT3 ($p<0.05$) signaling, KRAS signaling ($p<0.05$) and complement ($p<0.05$) pathways. Using per sample gene set scoring, despite heterogeneity among subjects, the alterations in these pathways could also be observed at patient level. Notably, even though WNT signaling [37] and NOTCH signaling [38] did not meet the significance threshold, they were observed to be enriched in individual subjects and showed positive enrichment scores in MGUS, SMM and MM stages.

Comparing the malignant plasma cells from diseased subjects (expanded clones) with the normal plasma cells from all patients (non-expanded), we identified 439 significantly differentially expressed genes ($p<0.05$, $|logFC|>1$, $logCPM>1$) including up-regulation of the known MM markers [6,8,39] FRZB, DKK1, MYC, CCND1, CCND3 as well as proto-oncogene KIT [40] and down-regulation of the B-cell antigens CD27, CD19, CD79A as well as tumor suppressor genes CD81 [41] and CD99 [42] (Figure 2f).

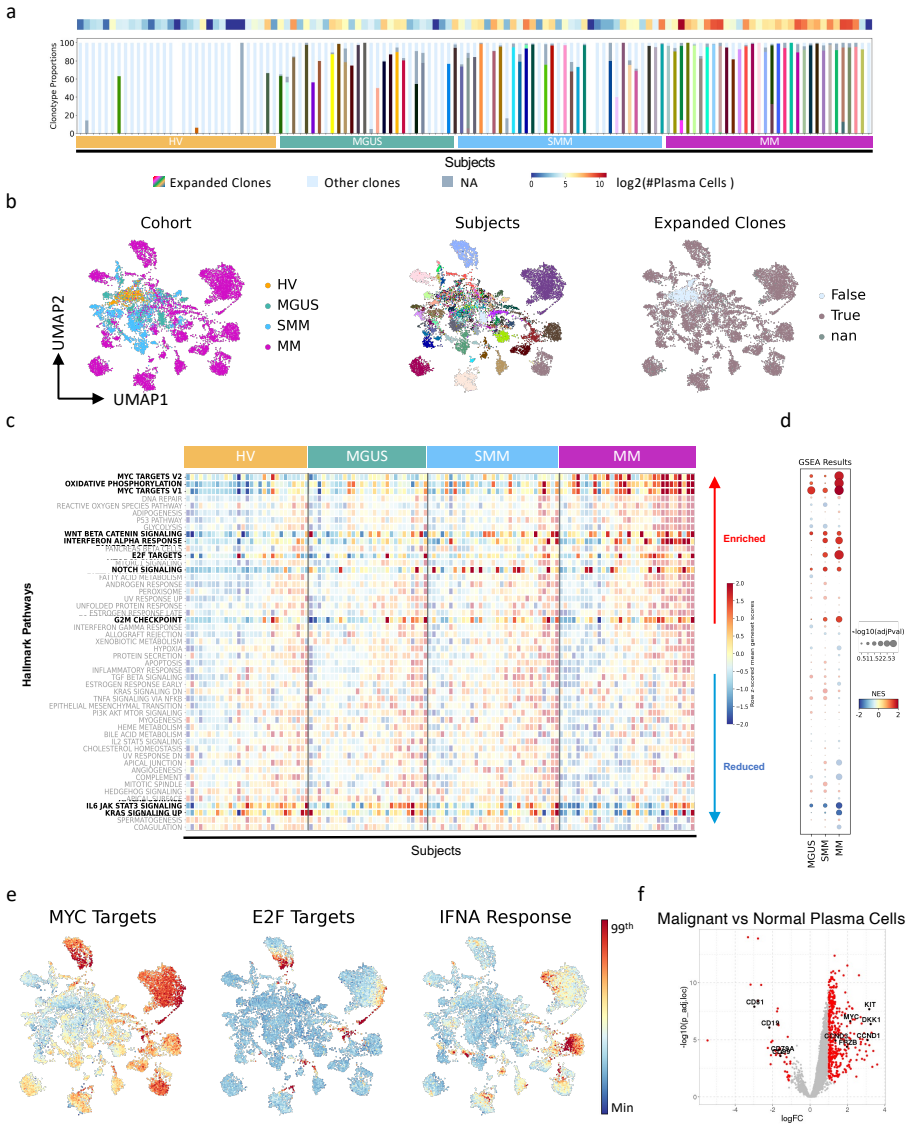

Fig. 2 Transcriptional similarities and differences are observed in plasma cells across disease stages. (**a**) Cell number proportions of plasma cell clonality within subjects, obtained by BCR-seq. The heatmap on the top of the stacked bar plot shows the number of cells per sample. Expanded clones: per subject clones with 10 cells; Other clones: identified clones with no expansion; NA: cells with no clonal information captured by BCR-seq (**b**) UMAP representation of plasma

cell transcriptome, colored by cohort (left), subject (center) and expanded clonality (right) information. True: per subject clones with at least 10 cells; False: identified clones with no expansion; NA: cells with no clonal information captured by BCR-seq. (**c**) Within and between cohort diversity is represented by hallmark gene set scores, where x-axis is categorized by cohort and sorted based on mean NES score, whereas y-axis is sorted by mean normalized enrichment score (NES) in MM subjects. (**d**) GSEA results where each disease state is contrasted with HV. Gene sets highlighted in both panels c and d show gradual divergence at both patient and cohort level. (**e**) UMAP representation of transcriptome of plasma cells colored by gene set scores of hallmark gene sets enriched in precursor stages. The figure colors range from minimum value (blue) to the 99th percentile of the value distribution (red). (**f**) Differential expression results of the contrast diseased (MGUS, SMM, MM) vs non-diseased (HV) plasma cells. Points colored in red represent significantly down- (negative logFC) and up-regulated (positive logFC) genes. Significantly down- and up-regulated genes were identified based on adjusted p-val<0.05, absolute value of logFC >1 & logCPM>1.

Dysregulation of inflammatory response is initiated early and gradually detected across the tumor micro-environment

Contrasting each disease stage to HV, using muscat and FGSEA, highlighted the activation of numerous inflammatory pathways, such as interferon gamma (IFNγ) signaling, IFNα signaling, tumor necrosis factor alpha (TNFα) signaling, KRAS signaling, inflammatory response and apoptosis (Figure 3). Intriguingly, the dysregulation of the inflammatory response can already be observed in the micro-environment of MGUS patients with high (TNFα) signaling activity throughout the majority of cell types. With disease progression, further dysregulation of the inflammatory pathways was detected across the many

cell types of the BM. IFNα signaling, IFNγ signaling, KRAS signaling and apoptosis pathways were rarely observed in MGUS stage while their activation in multiple immune cell types was observed in the SMM and MM stages. Interestingly, IFN pathways were observed to be highly enriched in all cell types in the tumor micro-environment in MM stage, particularly IFNα in plasma cells.

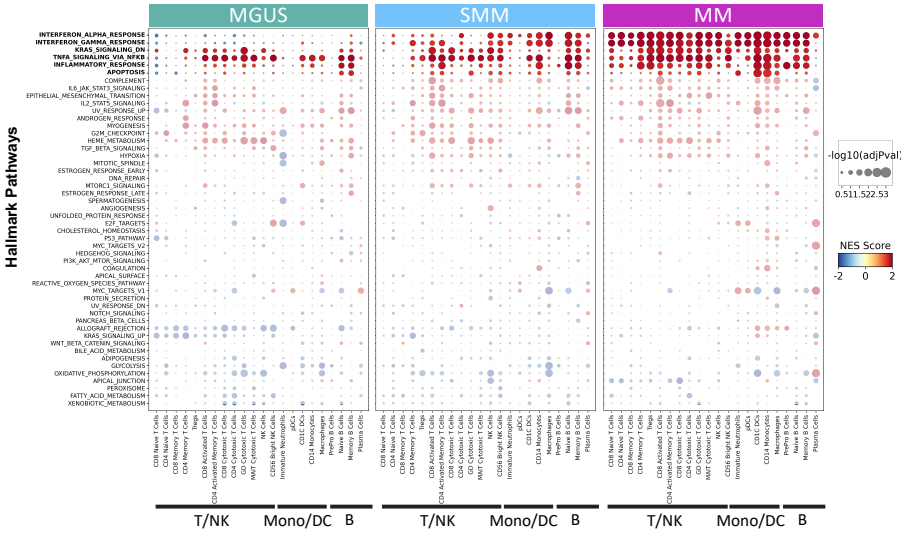

Fig. 3 Proportional and transcriptional changes in the immune micro-environment shows early dysregulation of inflammatory response. GSEA results of hallmark gene sets where the expression profile of each disease state is contrasted by HV per immune cell type. On x-axis, the cell types are grouped by their corresponding major cell type category. The y-axis is sorted based on average NES score in MM. Gene sets, enriched along disease progression, are highlighted at the top.

Pre-dysfunctional characteristics in highly immune-responsive CD8+ activated T-cells along disease progression

We contrasted cell proportions across the precursor stages to MM spectrum, comparing MGUS, SMM and MM with HVs, and found significant population shifts in CD8+ T-cells, CD1C+ DCs and macrophages.

CD8+ T-cells were identified by the T-cell markers CD3 and CD8, whereas activated T-cells (ATC) can be categorized by their expression of activation markers GZMK, CD69 and CCL4. Their cell state forms a trajectory from an activated intermediate state towards a cytotoxic state which can be identified using the expression of GZMB and PRF1 (Figure 4a). We further subtyped CD8+ ATC by Leiden clustering where 3 sub-populations form a trajectory from a naive-like population (characterized by the expression of IL7R, CCR7 and TCF7), over a cytotoxic-like population (specified by GNLY, CX3CR1, GZMB and PRF1), towards a highly active population with high expression of CXCR4, RGS1, NR4A2, CCL3, low levels of some of the exhaustion markers [43,44] TOX, TIGIT, PD1 and low levels of the pro-inflammatory cytokine TNF (Figures 4a-c). This highly active population shows high TNF response (Figure 4b). Moreover, GSEA analysis demonstrated down-regulation of translational and metabolic mechanisms including translation elongation, translation initiation, oxidative phosphorylation, protein localization to endoplasmic reticulum and cellular respiration in this population (Figure S2). These changes may be associated with increased exhaustion in CD8+ T-cells [45,46]. Recently, Yan et al. [45] demonstrated the rapid decrease in translational and metabolic pathways in the pre-dysfunctional state along T-cell differentiation towards exhaustion. We identified this cell population as “pre-dysfunctional” based on the expression of exhaustion associated genes RGS1 [47] and NR4A2 [48],

the expression of some but not all of the exhaustion markers, their highly active TNF response and the down-regulation of translational and metabolic pathways in these cells. We found evidence for a gradual shift from the naive-like phenotype towards the pre-dysfunctional phenotype that tracks with the disease progression stages (Figures 4d and 4e).

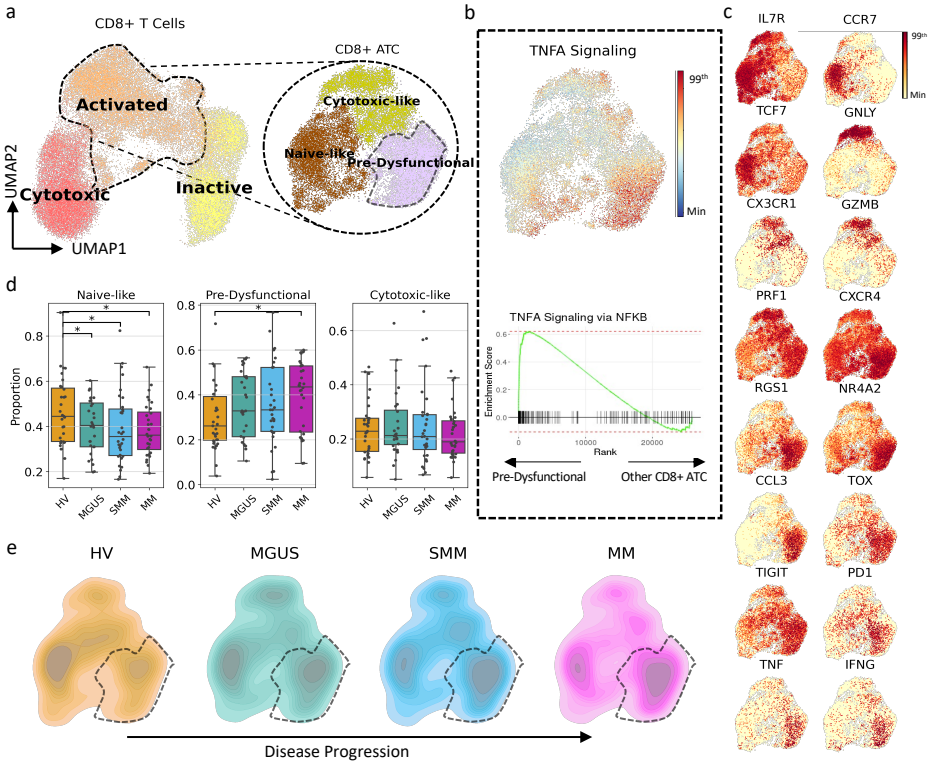

Fig. 4 Increase in pre-dysfunctional phenotype within CD8+ ATCs observed during disease progression. (**a**) UMAP representation of transcriptome of CD8+ T-cells and CD8+ ATCs colored by cell groups in per cell type analyses. (**b**) Gene set scores and GSEA plots of TNFα signaling highlighting enrichment of TNFα signaling in pre-dysfunctional CD8+ ATCs. The figure colors range from minimum value (blue) to the 99th percentile of the value distribution (red). In the GSEA analysis, the gene expression levels of pre-dysfunctional cells are compared against other CD8+ ATCs. (**c**) Gene expression profiles of marker

genes define CD8+ ATC subtypes. The figure colors range from minimum value (yellow) to the 99th percentile of the value distribution (red). (**d**) Proportional differences among cohorts for CD8 ATC subtypes. Each dot represents an individual subject. The proportional differences between each disease state vs HV are compared and the significance was calculated using the Mann–Whitney U test: *P < 0.05; **P ≤ 0.005; ***P ≤ 0.005. (**e**) Density plots showing the transcriptomic landscape of CD8+ ATCs per cohort. The highlighted area represents the region where the pre-dysfunctional cells reside. A transcriptional shift with disease progression was observed.

Macrophages polarize towards a M1 phenotype with increased BAFF expression along disease progression

We subclustered the macrophage population with Leiden clustering into five distinct molecular subtypes and annotated the populations largely based on their gene expression profile (Figure 5a-b). The cluster with relatively low expression of CD14 and MS4A7 was annotated as maturating macrophages (Figure 5b). One cluster, annotated as M1 macrophages, exhibited high IFN response expression (Figure 5c, Figure S3) and expressed IFN-related genes including IFI6, IFI44L IFIT1, TNFSF10 and STAT1. The cluster annotated as M2 macrophages was characterized by the expression of the C1Q gene family and M2 markers CD163, CD5L, CXCL12. Although the M2-like group lacked most of the M2 markers, they exclusively expressed C1Q family genes. Finally, the M0 state was characterized by the expression of macrophage markers FCGR3A and MS4A7 while lacking expression of CD14 as well as M1 and M2 markers.

The proportional analysis demonstrated an inverse relation between M0 and maturating macrophages versus M1 phenotype (Figure 5d). Compared to HV,

there is a highly significant ($p<0.0005$) decrease of M0 macrophages and an increase of M1 macrophages in MM patients. Moreover, a significant ($p<0.05$) decrease of maturating macrophages was observed in SMM and MM patients, while a significant ($p<0.05$) increase of M1 macrophages was observed in MGUS and SMM. From our analyses, it was evident that during disease progression, M0 and maturating macrophages differentiate towards a M1 phenotype (Figure 5e). Notably, this was not observed for the M2 phenotype as the proportion of M2 macrophages did not differ significantly among disease categories (Figure S4a). These findings suggest that, at early stages of multiple myeloma and in the active disease, the balance between M1 and M2 macrophages shifts towards the M1 phenotype. Interestingly, in line with this population shift, elevated expression of BAFF (TNFSF13B) was observed. BAFF has been shown to interact with BCMA, which is known to enhance the growth and survival of plasma cells [49,50]. To illustrate elevated BAFF expression, macrophages are divided into BAFF-low and BAFF-high groups based on the local minimum of 0.92 from the distribution of BAFF expression levels (Figure 5f). It can be observed that the BAFF-high region highly overlaps with M1 macrophages and the BAFF-low region highly overlaps with M0 macrophages (Figure 5g).

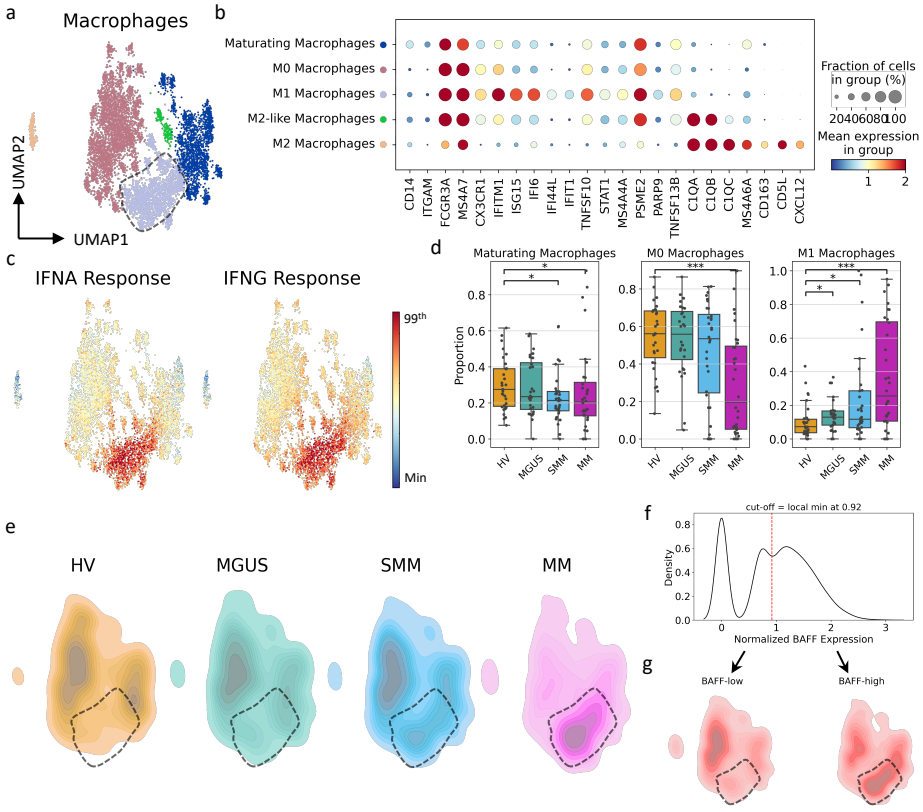

Fig. 5 Macrophages polarize towards a M1 phenotype during myeloma disease progression. (**a**) UMAP representation of transcriptome of the macrophage population, colored by subtype annotations. (**b**) Expression profiles of marker genes that define macrophage subpopulations. (**c**) Gene set scores of IFNα and IFNγ highlight IFN-responsive regions in macrophages. The figure colors range from minimum value (blue) to the 99th percentile of the value distribution (red). (**d**) Proportional differences among cohorts for macrophage subtypes. Each dot represents an individual subject. The proportional differences between each disease state vs HV are compared and the significance was calculated using the Mann–Whitney U test: *P <0.05; **P ≤ 0.005; ***P ≤ 0.005.(**e**) Density plots showing the transcriptomic landscape of macrophages per cohort. The highlighted area represents the region where M1 macrophages reside.

(**f**) The distribution of BAFF gene expression within the macrophage population. The cut-off value was defined by the local minima at 0.92 to separate BAFF-low and BAFF-high populations. (**g**) Density plots of the BAFF-low and -high populations, showing dense regions on transcriptomic landscape for both categories. The highlighted area represents the region where the M1 macrophages reside.

CD1C+ dendritic cells transform into an active and pro-inflammatory phenotype along disease progression

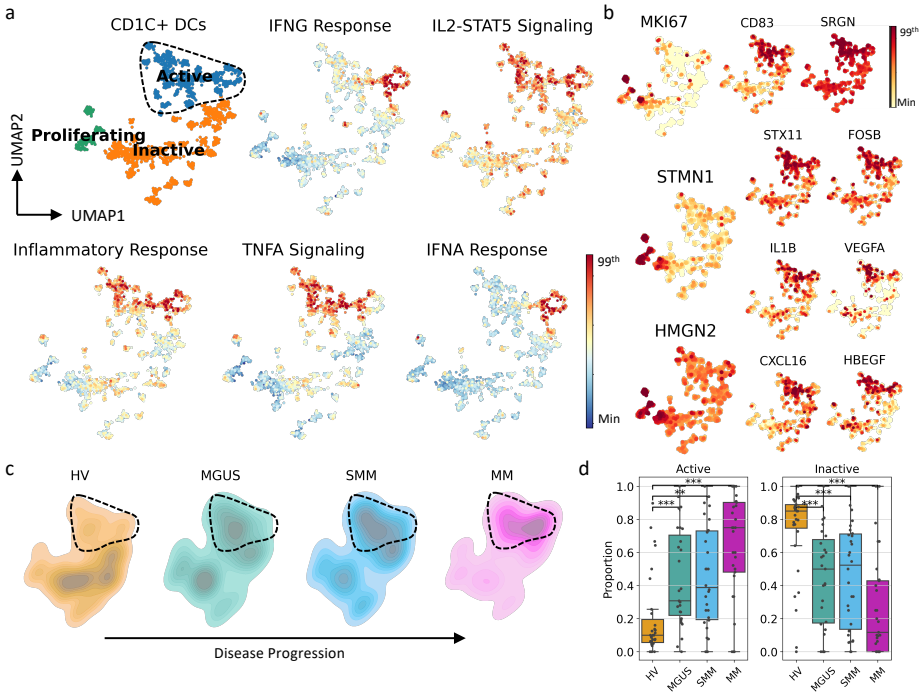

Fig. 6 CD1C+ DCs activation and maturity increase in parallel with disease progression. (**a**) UMAP representation of transcriptome of the CD1C+ DC population colored by CD1C+ DC subtypes and gene set scores of various inflammation-related pathways. The figure colors range from minimum value

(blue) to the 99th percentile of the value distribution (red). (**b**) Expression profiles of marker genes define CD1C+ DC subpopulations. The figure colors range from minimum value (yellow) to the 99th percentile of the value distribution (red). (**c**) Density plots showing transcriptomic landscape of CD1C+ DCs per cohort. Highlighted area represents the region where the activated CD1C+ DCs reside. (**d**) Proportional differences among cohorts for CD1C+ DC subtypes. Each dot represents an individual subject. The proportional differences between each disease state vs HV are compared and the significance was calculated using the Mann–Whitney U test: *P <0.05; **P ≤ 0.005; ***P ≤ 0.005.

We identified CD1C+ dendritic cells by the expression of HLA-DR at the protein level and CLEC10A and CD1C expression at transcriptional level. After clustering, we identified three subtypes of CD1C+ DCs which we designated as proliferating, active, and inactive (Figure 6a). The proliferating subtype consisted of a small number of cells (n=167) and had high expression of cell cycle-related genes MKI67, STMN1 and HMGN2, as well as similar gene expression levels for the marker genes used to define the active subtype (Figure S4b). The active group expressed CD83, SRGN, STX11, NR4A family genes, activator protein 1 (AP1) related genes FOSB, JUNB and anti-apoptotic genes MCL1 and CDKN1A, and showed a more mature and active phenotype (Figure 6b). In this population we also observed activation of inflammatory pathways, i.e., inflammatory response, TNFα signaling, IFNα response, IFNγ response and IL2-STAT5 signaling, as well as T-cell activation pathways (Figure 6a and S5). In addition to this highly inflammatory phenotype, in active CD1C+ DCs, we also observed expression of other pro-inflammatory genes, such as IL1B [51], CXCL16 [52,53], VEGFA [54], HBEGF [55] (Figure 6b), that can facilitate tumor progression and survival. The cluster with no/low proliferation or activation marker gene expression was annotated as inactive CD1C+ DCs. Investigating proportional changes, we observed a population shift from inactive to active CD1C+ DCs along disease progression (Figures 6c-d).

Similar observations were made for CD14+ DCs (Figures S4c and S6). Taken together, these findings suggest that there is increased maturation and activation of the classical DCs (cDC) along disease progression.

External public datasets validate population shifts in immune populations

To validate our observed population shifts in immune populations, we used external datasets from similar studies including Zavidij et al. [12], de Jong et al. [14] and the MMRF CoMMpass study [7]. We used data from Zavidij et al. and de Jong et al. to validate our findings on population shifts from HV to MM, and time to event data from the CoMMpass study to investigate their relationship with progression-free and overall survival (Table 2).

The de Jong et al. dataset allowed us to evaluate the transcriptional differences in cDC and CD8+ ATC populations between HV and MM. Unfortunately, in this study macrophages were not retained due to the sample processing methodology. For both cDC and CD8+ ATC populations, similar trends to our findings were detected (Figure S7). Within cDCs, we identified two clusters where cluster 1 showed increased TNFα signaling, IFNα response and IFNγ response as well as higher levels of activated DC markers (Figure S7a). Although not significant (possibly due to the low number of samples), higher proportions of cluster 1 were observed in MM. Similarly, within CD8+ ATCs, we identified two clusters, where cluster 0 showed increased TNFα signaling as well as higher levels of activated pre-dysfunctional CD8+ T-cell markers (Figure S7b). Higher proportions of cluster 0 were observed in MM patients, compared to HVs.

Compared to both our and the de Jong et al. dataset, the Zavidij et al. dataset included a smaller number of cells. This resulted in an insufficient number of DCs for further subtyping. We identified the main CD8+ ATC population but

failed to detect similar subpopulations. For macrophages, highly similar findings to ours were observed (Figure S8) and we identified two clusters where cluster 1 showed increased IFN signaling, as well as higher levels of M1 markers. This cluster was identified as M1 macrophages. Cluster 0 showed expression of macrophage markers FCGR3A (CD16) and MS4A7 and lacked the M1 and M2 markers as well as CD14. Therefore, this cluster was annotated as M0 macrophages. The proportional analysis showed a significant population shift from M0 to M1 macrophages from HV to MM. Moreover, when BAFF expression was categorized into BAFF-low and -high categories based on the median cut-off at 0.68, we observed the association between high BAFF expression and M1 polarization.

Table 2. Summary of the validation study using external dataset.

	Zavidij et al. 2020	De Jong et al. 2021	CoMMpass Cell Type	CoMMpass Survival (OS)	CoMMpass Survival (PFS)
DCs	NA	✓	✓	X	X
Macrophages	✓	NA	✓	✓	X
CD8 ATC	X	✓	✓	✓	X

Supported or validated cell types are marked by a check mark (✓), while unsupported cell types are marked by an X. Data which were not feasible to analyze are marked by NA.

Population shifts in CD8+ T-cells and Macrophages are associated with poor overall survival in CoMMpass dataset

The CoMMpass immune dataset does not include HV, MGUS, or SMM samples but is instead composed of samples collected from active MM patients with accompanying metadata. Thus, we used this dataset to evaluate whether

differences in the proportions of identified population shifts were related to time to event (PFS and OS). For CD8+ ATC, macrophages and cDCs, where population shifts were detected, we observed great transcriptomic similarities with our findings in the CoMMpass dataset. Within cDCs, we identified two clusters where cluster 1 showed increased TNFα signaling as well as higher levels of activated DC markers (Figure S9a). Similarly, within CD8+ ATCs, we identified three clusters, where the cluster showing increased TNFα signaling as well as higher levels of activated pre-dysfunctional CD8+ T-cell markers were annotated as pre-dysfunctional (Figure S9b). For macrophages, all the subtypes identified in our study were also detected in the CoMMpass dataset based on the marker gene expression and increased BAFF expression in the M1 phenotype could be observed (Figure S10).

We classified CoMMpass patients according to their proportion of pre-dysfunctional CD8+ ATC. Distribution of the proportion of pre-dysfunctional cells was generated and patients were grouped into pre-dysfunctional-low and -high groups using the cut-off value as the median at 0.4 (Figure 7a). Higher proportions of pre-dysfunctional cells were found to be significantly ($p=0.002$) negatively associated with OS (Figure 7b). Similarly, patients are grouped into M1 macrophage-low and -high groups using the cut-off value as the median at 0.55 (Figure 7c). Patients with a high proportion of M1 macrophages were found to have significantly ($p=0.036$) worse OS (Figure 7d). For both pre-dysfunctional CD8+ ATC and M1 populations, no association with PFS was observed (Figures S9b and S10a). Finally, no association was observed between high activated cDC proportions and survival (Figure S9a).

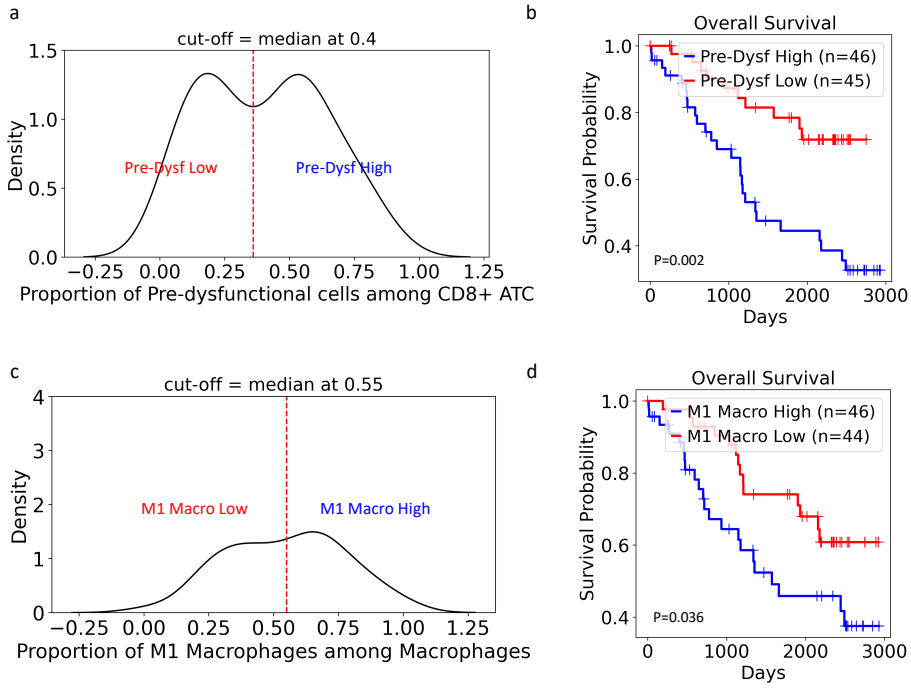

Fig. 7 Survival analyses reveal associations between proportions of pre-dysfunctional cells and M1 macrophages with overall survival. (**a**) Distribution of the proportion of pre-dysfunctional CD8+ T-cells within the CD8+ ATC population in the CoMMpass dataset among NDMM samples. The samples were categorized into pre-dysfunctional high and low groups using the median cut-off (median = 0.4). (**b**) Kaplan-Meier survival curve demonstrate the association between CD8+ ATC proportion and OS (Pre-dys high median = 1160, Pre-dys low median = 1933). (**c**) Distribution of the proportion of M1 macrophages within the macrophage population in the CoMMpass dataset among NDMM samples. The samples were further categorized into M1 macrophage high and low groups using the median cut-off (median = 0.55). (d) Kaplan-Meier survival curve demonstrate the association between the proportion of M1 macrophages and OS (M1 high median = 893, M1 low median = 1945).

Ligand-receptor interaction modelling demonstrates dynamic interplay between the tumor and micro-environment

To better understand the molecular mechanisms and changes in the cell-cell interactions that take place during the transformation of precursor stages to MM cells, we used MultiNichenet for ligand-receptor interaction analysis. We analyzed the top 12 cell types that had the most significantly differentially expressed genes between MGUS and SMM versus MM. This method allows the modeling and prioritization of potential ligand-receptor interactions between cell types by evaluating known ligand-receptor interactions from public databases, along with their gene expression abundance and differential expression of the downstream genes in the contrast groups. We investigated the outcome of both directions of tumoral-immune cell and immune-tumoral cell interactions.

First, we focused on the effect of the plasma cells on their surrounding immune cells (Figure 8a). Among the top 50 interactions we identified 11 plasma cell ligands interacting with 21 receptors from various immune cell types. We found that only ITGB1 in MAIT Cytotoxic T-cells and CD44 in CD1C+ DCs were differentially expressed upon disease progression in the immune micro-environment. Most of the ligands in the plasma cells showed up-regulation in MM patients, including RELN, HGF, MIF, CD320, and ADM. Among these ligands, MIF, CD320 and HGF have potential interactions with many immune cell types via multiple receptors. Additional interesting ligands include FAM3C, ADM and IL15. These ligands, although not identified as significantly up-regulated, can be found in a secreted form.

We also investigated how the immune cells in the micro-environment communicate differentially with the plasma cells upon MM progression (Figure

8b). Through our analysis, 18 immune cell ligands interacting with 15 plasma cell receptors were identified. Likewise, the greatest pre-malignancy vs MM gene expression difference was observed in the plasma cells. Among the identified receptors, F12, CD138 (SDC1) and BCMA (TNFRSF17) were observed to interact with multiple ligands from multiple immune cell types. We also observed many other ligands that were up-regulated within the plasma cells, including HGF, CD320, NCAM1, and ADM.

We further investigated ligands and their potential downstream effects in plasma cells. Interestingly, BAFF (TNFSF13B), for which expression was found to be associated with population shifts in macrophages, was amongst the top predicted ligands with potential to alter the expression of genes that are differentially expressed between MM cells and plasma cells in the precursor stages. In this context, we also observed that two key myeloma markers, MYC and DKK1, as well as many other cancer-associated genes including ADM, HDGF, IL15, HGF, STMN1, CDKN1B and CD82, were potentially regulated by the predicted ligands (Figure 8c). Particularly, ADM, MYC and CDKN1B were predicted to be regulated by numerous ligands. Consequently, observed ligand-receptor interaction cascades shed light on complete succession of events potentially involved in or arriving as a consequence of progression from precursor stages to MM.

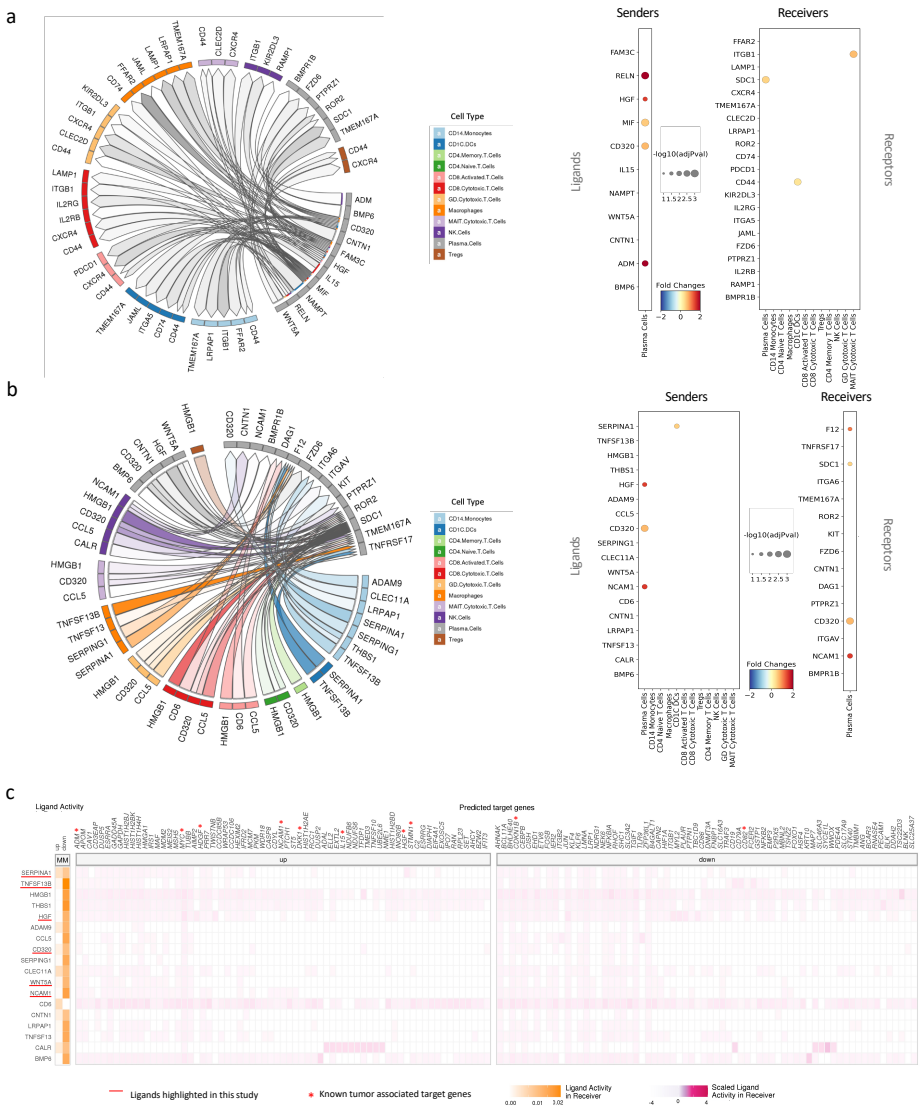

Fig. 8 Ligand-receptor interaction modelling reveals potential interplay between tumoral plasma cells and immune populations. (**a**) The circos plot (left) shows the interactions when plasma cells are selected as senders and the immune cells as receivers. The dot plot (right) shows significantly differentially expressed ligands/receptors in sender/receiver cells ($p<0.05$). (**b**) The circos plot (left) shows the interactions when the immune cells are selected as senders and

plasma cells as receivers. The dot plot (right) shows significantly differentially expressed ligands/receptors in sender/receiver cells ($p<0.05$). (**c**) The activity of the ligands from immune cells and their regulatory potential over significantly up-regulated and down-regulated genes in plasma cells are shown. The order of the ligands (top to bottom) represents their rank on the prioritization. The highlighted ligands either had significant differential expression in the cell types of interest or were observed in our population shift study. All the plots in this figure are obtained using the results from the differential expression analysis of MM vs precursor stages (MGUS&SMM) contrast.

Discussion

Despite recent advancements in its treatment, MM remains an incurable disease. Comprehensive and deep molecular profiling of the tumor plasma cells and surrounding immune populations advance our understanding of disease progression and can inform the identification of novel therapeutic targets. In this study, we generated a single cell transcriptomic atlas comprising more than 120 subjects from 4 cohorts including HV, MGUS, SMM, and MM patients. We applied a multi-modal single cell omics approach to investigate the molecular changes that take place in tumoral plasma cells and immune populations present in the tumor micro-environment during disease progression.

Identification of immune populations from single cell multi-omics data in the bone marrow is a challenging task. Cells can be identified into different subgroups based on phenotypic and/or functional characteristics. Phenotypic cell surface markers and their abundance are key determinants for an accurate classification. On the other hand, functional markers can provide a deep understanding of the current functional state of the cells. In this study, we combined both transcriptomics and proteomics to optimize the identification of distinct cell types.

In the plasma cells collected from HV, MGUS, SMM, and MM patients, we observed both transcriptional similarity and heterogeneity among patients of the same disease stage. Although transcriptional sub-clonality was observed for some subjects, within patient plasma cell transcriptomes were found to be highly similar. As in previous studies, differential expression analysis confirmed the altered expression of MM marker genes, including FRZB, DKK1, MYC, CCND1, and down-regulation of some tumor suppressor genes including CD81 and CD99. Interestingly, analysis of signaling pathways revealed that, despite

inter-patient heterogeneity, some differentially expressed pathways, such as MYC signaling, initiate early at precursor stages, while others, such as oxidative phosphorylation, are only observed in active MM. Other pathways, such as WNT signaling and NOTCH signaling are subject-specific and can be observed at all stages.

Differential expression analysis of cells in the tumor micro-environment revealed activation of inflammatory pathways increasing from HV to MM. Although we profiled numerous cell types, in future studies, it may be interesting to profile additional cell types in the tumor micro-environment, such as granulocytes, myeloid-derived suppressor cells (MDSCs), stromal cells, osteoblasts and osteoclasts, to investigate changes from HV to MM and assess whether they are also affected by the increased inflammation. Activation of TNFα was observed in many cell types at MGUS, indicating that the initial response from the immune cells is triggered by TNF release, followed by IFN release as the disease becomes symptomatic. Moreover, among the immune-related pathways enriched in the immune micro-environment, only IFNα was observed to be activated by the plasma cells in MM. In future studies, it may be of interest to investigate whether activation of IFN pathways is a driver, or consequence, of disease progression. Although IFNα was investigated as a therapeutic molecule in early myeloma treatment trials [56], it was shown that co-cultures with IFNα-producing pDCs demonstrated higher plasma and multiple myeloma cell proliferation [57,58].

Among the different inflammatory and immune subpopulations, significant population shifts were observed in CD8+ T-cells, DCs and macrophages, and we further validated each of these observations using a set of independent validation datasets of Zavidij et al., de Jong et al. and CoMMpass. In CD8+ T-cells, we observed a gradual population shift towards a highly active state, where these cells also exhibited gene expression that suggest emerging

signals of dysfunctionality. This pre-dysfunctional T-cell population was also recently described by Yan et al. and Leun et al., who investigated transcriptional changes during CD8+ T-cell differentiation [45,59]. Leun et al. worked with data from various cancers and proposed an elegant differentiation model for intra-tumoral CD8+ T-cells. The authors described a differentiation trajectory from a naive-like state towards GZMK+ pre-dysfunctional and cytotoxic states, where the cells in these two states can interchange. Pre-dysfunctional T-cells acquire additional markers of dysfunctionality and finally transform into defective T-cells. Our study suggests that this activation trajectory also occurs in MM, confirming the findings of other previous reports on T-cell dysfunctionality [60–63]. In addition, we also found that T-cell dysfunctionality is prognostic, as igh proportions of pre-dysfunctional T-cells were associated with worse OS in CoMMpass patients. In line with our findings, Pilcher et al. has recently shown GZMK+ CD8+ exhausted T-cells to be associated with rapid progression in MM patients [64].

In addition to the changes in the T-cell compartment upon disease progression, we observed alterations in macrophages. Previously, tumor-associated macrophages (TAMs) have been shown to play a pivotal role in MM, contributing to proliferation, angiogenesis, immunosuppression and drug resistance [65,66]. In this study, we detected a population shift towards a highly pro-inflammatory M1 population with increased BAFF expression and found evidence that this shift is initiated at MGUS and SMM stages. Further, a high proportion of these cells was associated with poor OS in CoMMpass patients. A potential mechanism for such a negative effect could be explained by BAFF expression. BAFF is a known inducer of proliferation and survival in MM cells [67–69] Our ligand-receptor interaction analysis prioritized BAFF as one of the top-ranked ligands which can alter many genes that have been dysregulated along the transformation from precursor stages to MM. Although M1 macrophages are considered to be pro-inflammatory or anti-tumoral, whereas M2 macrophages are

anti-inflammatory or pro-tumoral in cancer research [70], BAFF-expressing M1 macrophages were found to be associated with bortezomib resistance [71,72]. Considering the further role of macrophages in bone formation [73,74], the role of macrophages in MM progression may be more broad than pro- or anti-tumoral categorization. Overall, additional studies are needed to understand the impact of macrophages on MM.

Similar to what was reported in previous studies, we observed a proportional decrease in cDCs in bone marrow samples of MM patients [75,76]. Although cDCs in the MM micro-environment are thought to be functionally deficient [75–79], some studies have shown that these cells have the capacity to activate CD8+ T-cells and to promote MM tumor progression *in vitro* [80–82]. Although the proportion of cDCs decreased during disease progression, we observed a shift towards an active and mature phenotype with production of pro-tumorigenic molecules including IL1B, CXCL16, VEGFA and HBEGF.

Finally, we predicted cell-cell interactions to investigate their role in disease progression from the precursor stages to MM. We applied differential expression analysis, followed by cell-cell interaction analysis, and predicted through which ligands and receptors the plasma cells may be interacting with cells in the tumor micro-environment, and vice versa. Our study highlights the potential effect of MIF, IL15, CD320, HGF and FAM3C on the adjustments in immune populations during precursor stages transition to MM. Interaction of MIF with its receptors (CD44, CD74, CXCR4) are known drivers in late stage multiple myeloma and other cancers [83,84] and involved in a variety of mechanisms including homing to bone marrow [85], pro-tumoral M0 macrophage differentiation [86] and resistance to therapy [87,88]. Likewise, IL15 [89–91] and HGF [92–94] are known regulators of inflammatory response in cancer. Although CD320 is known to be associated with B-cell survival and proliferation [95,96] and FAM3C is a known inducer of osteoblast differentiation [97,98], their effect on the tumor micro-

environment and their role in MM progression is subject to further research. Concerning the impact of the immune compartment on MM progression, we identified SERPINA1 and BAFF (TNFSF13B) as ligands that may play a role in MM development. It is well known that BAFF has the potential to enhance growth and survival of plasma cells, however, the role of SERPINA1 in MM requires further investigation. In addition to immune populations, we also identified potential interactions between plasma cells that can influence MM progression. These interactions possibly generate a positive feedback loop where the expression of signaling molecules, such as HGF, CD320 and WNT5A, induce expression of MYC, STMN1, CD82, while an increase in adhesion molecules, such as MIF and NCAM1, facilitate these interactions by enabling proximity between the malignant cells. An increase in intercellular adhesion may also cause bone lesions [99,100], increase cellular mobility and contribute to resistance to therapy [101].

Conclusion

In this study, we have generated an atlas of bone marrow micro-environment of MM and investigated the differences between HV, MGUS, SMM and MM. We identified an increased inflammatory response across the immune populations in the bone marrow and illustrated the dynamic relationship that exists between plasma cells and the micro-environment (Figure S11), revealing the changes that occur at different stages of the disease. Our study suggests that early intervention to modulate the inflammatory response observed at precursor stages of the disease may help to limit disease complexity and progression to MM.

References

1. Bianchi G, Anderson KC. Understanding biology to tackle the disease: Multiple myeloma from bench to bedside, and back. CA Cancer J Clin. 2014;64(6):422–44.

2. Braunlin M, Belani R, Buchanan J, Wheeling T, Kim C. Trends in the multiple myeloma treatment landscape and survival: a U.S. analysis using 2011–2019 oncology clinic electronic health record data. Leuk Lymphoma [Internet]. 2021;62(2):377–86. Available from: https://doi.org/10.1080/10428194.2020.1827253

3. Neumeister P, Schulz E, Pansy K, Szmyra M, Deutsch AJA. Targeting the Microenvironment for Treating Multiple Myeloma. Int J Mol Sci. 2022;23(14):1–19.

4. Rajkumar SV. Multiple myeloma: 2022 update on diagnosis, risk stratification, and management. Am J Hematol. 2022;97(8):1086–107.

5. Rajkumar SV. Multiple myeloma: 2022 update on diagnosis, risk stratification, and management. Am J Hematol. 2022;(May):1086–107.

6. van de Donk NWCJ, Pawlyn C, Yong KL. Multiple myeloma. The Lancet [Internet]. 2021;397(10272):410–27. Available from: http://dx.doi.org/10.1016/S0140-6736(21)00135-5

7. Skerget. Genomic Basis of Multiple Myeloma Subtypes from the MMRF CoMMpass Study. medRxiv. 2021;1–45.

8. Zhan F, Huang Y, Colla S, Stewart JP, Hanamura I, Gupta S, et al. The molecular classification of multiple myeloma. Blood. 2006;108(6):2020–8.

9. Bustoros M, Anand S, Sklavenitis-Pistofidis R, Redd R, Boyle EM, Zhitomirsky B, et al. Genetic subtypes of smoldering multiple myeloma are associated with distinct pathogenic phenotypes and clinical outcomes. Nat Commun. 2022;13(1):14–23.

10. Bustoros M, Sklavenitis-Pistofidis R, Park J, Redd R, Zhitomirsky B, Dunford AJ, et al. Genomic profiling of smoldering multiple myeloma identifies patients at a high risk of disease progression. Journal of Clinical Oncology. 2020;38(21):2380–9.

11. Oben B, Froyen G, Maclachlan KH, Leongamornlert D, Abascal F, Zheng-lin B, et al. Whole-genome sequencing reveals progressive versus stable myeloma precursor conditions as two distinct entities. Nat Commun [Internet]. 2021;1–11. Available from: http://dx.doi.org/10.1038/s41467-021-22140-0

12. Zavidij O, Haradhvala NJ, Mouhieddine TH, Sklavenitis-Pistofidis R, Cai S, Reidy M, et al. Single-cell RNA sequencing reveals compromised immune microenvironment in precursor stages of multiple myeloma. Nat Cancer [Internet]. 2020;1(5):493–506. Available from: http://dx.doi.org/10.1038/s43018-020-0053-3

13. Ledergor G, Weiner A, Zada M, Wang SY, Cohen YC, Gatt ME, et al. Single cell dissection of plasma cell heterogeneity in symptomatic and asymptomatic myeloma [Internet]. Vol. 24, Nature Medicine. Springer US; 2018. 1867–1876 p. Available from: http://dx.doi.org/10.1038/s41591-018-0269-2

14. de Jong MME, Kellermayer Z, Papazian N, Tahri S, Hofste op Bruinink D, Hoogenboezem R, et al. The multiple myeloma microenvironment is defined by an inflammatory stromal cell landscape. Nat Immunol [Internet]. 2021;22(6):769–80. Available from: http://dx.doi.org/10.1038/s41590-021-00931-3

15. Jang JS, Li Y, Mitra AK, Bi L, Abyzov A, van Wijnen AJ, et al. Molecular signatures of multiple myeloma progression through single cell RNA-Seq. Blood Cancer J [Internet]. 2019;9(1). Available from: http://dx.doi.org/10.1038/s41408-018-0160-x

16. Boiarsky R, Haradhvala N, Sklavenitis-Pistofidis R, Mouhieddine TH, Alberge JB, Zavidij O, et al. Single Cell Characterization of Myeloma and Its Precursor Conditions Reveals Transcriptional Signatures of Early Tumorigenesis. Blood. 2021;138(Supplement 1):2219–2219.

17. Liu R, Gao Q, Foltz SM, Fowles JS, Yao L, Wang JT, et al. Co-evolution of tumor and immune cells during progression of multiple myeloma. Nat Commun [Internet]. 2021;12(1):1–18. Available from: http://dx.doi.org/10.1038/s41467-021-22804-x

18. Rajkumar SV, Dimopoulos MA, Palumbo A, Blade J, Merlini G, Mateos MV, et al. International Myeloma Working Group updated criteria for the diagnosis of multiple myeloma. Lancet Oncol [Internet]. 2014;15(12):e538–48. Available from: http://dx.doi.org/10.1016/S1470-2045(14)70442-5

19. Wolf FA, Angerer P, Theis FJ. SCANPY: Large-scale single-cell gene expression data analysis. Genome Biol. 2018 Feb 6;19(1).

20. Wolock SL, Lopez R, Klein AM. Scrublet: Computational Identification of Cell Doublets in Single-Cell Transcriptomic Data. Cell Syst [Internet]. 2019;8(4):281-291.e9. Available from: https://doi.org/10.1016/j.cels.2018.11.005

21. Satija R, Farrell JA, Gennert D, Schier AF, Regev A. Spatial reconstruction of single-cell gene expression data. Nat Biotechnol. 2015;33(5):495–502.

22. Kowalczyk MS, Tirosh I, Heckl D, Rao TN, Dixit A, Haas BJ, et al. Single-cell RNA-seq reveals changes in cell cycle and differentiation programs upon aging of hematopoietic stem cells. Genome Res. 2015;25(12):1860–72.

23. Stoeckius M, Hafemeister C, Stephenson W, Houck-Loomis B, Chattopadhyay PK, Swerdlow H, et al. Simultaneous epitope and transcriptome measurement in single cells. Nat Methods. 2017;14(9):865–8.

24. Sturm1 G, Szabo T, Fotakis G, Haider1 M, Rieder D, Trajanoski Z, et al. Scirpy: A Scanpy extension for analyzing single-cell T-cell receptor-sequencing data. Bioinformatics. 2020;36(18):4817–8.

25. Korsunsky I, Millard N, Fan J, Slowikowski K, Zhang F, Wei K, et al. Fast, sensitive and accurate integration of single-cell data with Harmony. Nat Methods. 2019 Dec 1;16(12):1289–96.

26. McInnes L, Healy J, Melville J. UMAP: Uniform Manifold Approximation and Projection for Dimension Reduction. 2018; Available from: http://arxiv.org/abs/1802.03426

27. Traag VA, Waltman L, van Eck NJ. From Louvain to Leiden: guaranteeing well-connected communities. Sci Rep. 2019 Dec 1;9(1).

28. Aran D, Looney AP, Liu L, Wu E, Fong V, Hsu A, et al. Reference-based analysis of lung single-cell sequencing reveals a transitional profibrotic macrophage. Nat Immunol [Internet]. Available from: http://dx.doi.org/10.1038/s41590-018-0276-y

29. Crowell HL, Soneson C, Germain PL, Calini D, Collin L, Raposo C, et al. Muscat Detects Subpopulation-Specific State Transitions From Multi-Sample Multi-Condition Single-Cell Transcriptomics Data. Nat Commun [Internet]. 2020;11(1):1–12. Available from: http://dx.doi.org/10.1038/s41467-020-19894-4

30. Robinson MD, McCarthy DJ, Smyth GK. edgeR: A Bioconductor package for differential expression analysis of digital gene expression data. Bioinformatics. 2009;26(1):139–40.

31. Liberzon A, Subramanian A, Pinchback R, Thorvaldsdóttir H, Tamayo P, Mesirov JP. Molecular signatures database (MSigDB) 3.0. Bioinformatics. 2011;27(12):1739–40.

32. Sergushichev AA. An algorithm for fast preranked gene set enrichment analysis using cumulative statistic calculation. bioRxiv [Internet]. 2016;060012. Available from: https://www.biorxiv.org/content/10.1101/060012v1%0Ahttps://www.biorxiv.org/content/10.1101/060012v1.abstract

33. MultiNicheNet [Internet]. [cited 2022 Jun 28]. Available from: https://github.com/saeyslab/multinichenetr

34. Browaeys R, Saelens W, Saeys Y. NicheNet: modeling intercellular communication by linking ligands to target genes. Nat Methods [Internet].

2020;17(2):159–62. Available from: http://dx.doi.org/10.1038/s41592-019-0667-5

35. Jovanović KK, Roche-Lestienne C, Ghobrial IM, Facon T, Quesnel B, Manier S. Targeting MYC in multiple myeloma. Leukemia. 2018;32(6):1295–306.

36. Rizzieri D, Paul B, Kang Y. Metabolic alterations and the potential for targeting metabolic pathways in the treatment of multiple myeloma. J Cancer Metastasis Treat. 2019;2019.

37. Derksen PWB, Tjin E, Meijer HP, Klok MD, Mac Gillavry HD, Van Oers MHJ, et al. Illegitimate WNT signaling promotes proliferation of multiple myeloma cells. Proc Natl Acad Sci U S A. 2004;101(16):6122–7.

38. Colombo M, Galletti S, Garavelli S, Platonova N, Paoli A, Basile A, et al. Notch signaling deregulation in multiple myeloma: A rational molecular target. Oncotarget. 2015;6(29):26826–40.

39. van Andel H, Kocemba KA, Spaargaren M, Pals ST. Aberrant Wnt signaling in multiple myeloma: molecular mechanisms and targeting options. Leukemia [Internet]. 2019;33(5):1063–75. Available from: http://dx.doi.org/10.1038/s41375-019-0404-1

40. Ashman LK, Griffith R. Therapeutic targeting of c-KIT in cancer. Expert Opin Investig Drugs. 2013;22(1):103–15.

41. Tohami T, Drucker L, Shapiro H, Radnay J, Lishner M. Overexpression of tetraspanins affects multiple myeloma cell survival and invasive potential. The FASEB Journal. 2007;21(3):691–9.

42. Gao Q, Yellapantula V, Fenelus M, Pichardo J, Wang L, Landgren O, et al. Tumor suppressor CD99 is downregulated in plasma cell neoplasms lacking CCND1 translocation and distinguishes neoplastic from normal plasma cells and B-cell lymphomas with plasmacytic differentiation from primary plasma cell neoplasms. Modern Pathology. 2018;31(6):881–9.

43. Blank CU, Haining WN, Held W, Hogan PG, Kallies A, Lugli E, et al. Defining 'T-cell exhaustion.' Nat Rev Immunol [Internet]. 2019;19(11):665–74. Available from: http://dx.doi.org/10.1038/s41577-019-0221-9

44. Zhao Y, Liao P, Huang S, Deng T, Tan J, Huang Y, et al. Increased TOX expression associates with exhausted T-cells in patients with multiple myeloma. Exp Hematol Oncol [Internet]. 2022;11(1):1–5. Available from: https://doi.org/10.1186/s40164-022-00267-0

45. Yan M, Hu J, Yuan H, Xu L, Liao G, Jiang Z, et al. Dynamic regulatory networks of T-cell trajectory dissect transcriptional control of T-cell state transition. Mol Ther Nucleic Acids [Internet]. 2021;26(December):1115–29. Available from: https://doi.org/10.1016/j.omtn.2021.10.011

46. Wherry EJ, Ha SJ, Kaech SM, Haining WN, Sarkar S, Kalia V, et al. Molecular Signature of CD8+ T-cell Exhaustion during Chronic Viral Infection. Immunity. 2007;27(4):670–84.

47. Fercoq F, Carlin LM. "Mind the GAP": RGS1 hinders antitumor lymphocytes. Nat Immunol. 2021 Jul 1;22(7):801–2.

48. Mikulasova A, Smetana J, Wayhelova M, Janyskova H, Sandecka V, Kufova Z, et al. Genomewide profiling of copy-number alteration in monoclonal gammopathy of undetermined significance. Eur J Haematol. 2016;97(6):568–75.

49. Novak AJ, Darce JR, Arendt BK, Harder B, Henderson K, Kindsvogel W, et al. Expression of BCMA, TACI, and BAFF-R in multiple myeloma: A mechanism for growth and survival. Blood. 2004;103(2):689–94.

50. Benson MJ, Dillon SR, Castigli E, Geha RS, Xu S, Lam KP, et al. Cutting Edge: The Dependence of Plasma Cells and Independence of Memory B-cells on BAFF and APRIL. The Journal of Immunology. 2008;180(6):3655–9.

51. Biology C, Fran CG, Umr ILNC, Franche-comt B. Interleukin-1 β and Cancer. Cancers (Basel). 2020;12(7):1791.

52. Deng L, Chen N, Li Y, Zheng H, Lei Q. CXCR6/CXCL16 functions as a regulator in metastasis and progression of cancer. Biochim Biophys Acta Rev

Cancer [Internet]. 2010;1806(1):42–9. Available from: http://dx.doi.org/10.1016/j.bbcan.2010.01.004

53. Korbecki J, Bajdak-Rusinek K, Kupnicka P, Kapczuk P, Simińska D, Chlubek D, et al. The Role of CXCL16 in the Pathogenesis of Cancer and Other Diseases. Int J Mol Sci. 2021;22(7).

54. Carpini JD, Karam AK, Montgomery L. Vascular endothelial growth factor and its relationship to the prognosis and treatment of breast, ovarian, and cervical cancer. Angiogenesis. 2010;13(1):43–58.

55. Cartoni C, Antonio G, Federico V, Efficace F, Grammatico S, Tendas A, et al. HB-EGF–EGFR Signaling in Bone Marrow Endothelial Cells Mediates Angiogenesis Associated with Multiple Myeloma. Cancers (Basel). 2012;12(1):173.

56. Zhang L, Tai YT, Ho MZG, Qiu L, Anderson KC. Interferon-alpha-based immunotherapies in the treatment of B-cell-derived hematologic neoplasms in today's treat-to-target era. Exp Hematol Oncol. 2017;6(1):1–9.

57. Knight A, Rihova L, Kralova R, Penka M, Adam Z, Pour L, et al. Plasmacytoid dendritic cells in patients with mgus and multiple myeloma. J Clin Med. 2021;10(16).

58. Jego G, Palucka AK, Blanck JP, Chalouni C, Pascual V, Banchereau J. Plasmacytoid dendritic cells induce plasma cell differentiation through type I interferon and interleukin 6. Immunity. 2003;19(2):225–34.

59. van der Leun AM, Thommen DS, Schumacher TN. CD8+ T-cell states in human cancer: insights from single-cell analysis. Nat Rev Cancer. 2020;20(4):218–32.

60. Guillerey C, Harjunpää H, Carrié N, Kassem S, Teo T, Miles K, et al. TIGIT immune checkpoint blockade restores CD81 T-cell immunity against multiple myeloma. Blood. 2018;132(16):1689–94.

61. Zelle-Rieser C, Thangavadivel S, Biedermann R, Brunner A, Stoitzner P, Willenbacher E, et al. T-cells in multiple myeloma display features of exhaustion

and senescence at the tumor site. J Hematol Oncol [Internet]. 2016;9(1):1–12. Available from: http://dx.doi.org/10.1186/s13045-016-0345-3

62. Hallett WHD, Jing W, Drobyski WR, Johnson BD. Immunosuppressive Effects of Multiple Myeloma Are Overcome by PD-L1 Blockade. Biology of Blood and Marrow Transplantation [Internet]. 2011;17(8):1133–45. Available from: http://dx.doi.org/10.1016/j.bbmt.2011.03.011

63. Tan J, Chen S, Huang J, Chen Y, Yang L, Wang C, et al. Increased exhausted CD8 + T-cells with programmed death-1, T-cell immunoglobulin and mucin-domain-containing-3 phenotype in patients with multiple myeloma. Asia Pac J Clin Oncol. 2018;14(5):e266–74.

64. Pilcher W, Thomas BE, Bhasin SS, Jayasinghe RG, Yao L, Gonzalez-Kozlova E, et al. Cross center single-cell RNA sequencing study of the immune microenvironment in rapid progressing multiple myeloma. NPJ Genom Med. 2023;8(1).

65. Sun J, Park C, Guenthner N, Gurley S, Zhang L, Lubben B, et al. Tumor-associated macrophages in multiple myeloma: Advances in biology and therapy. J Immunother Cancer. 2022;10(4).

66. Berardi S, Ria R, Reale A, De Luisi A, Catacchio I, Moschetta M, et al. Multiple myeloma macrophages: Pivotal players in the tumor microenvironment. J Oncol. 2013;2013.

67. Moreaux J, Legouffe E, Jourdan E, Quittet P, Rème T, Lugagne C, et al. BAFF and APRIL protect myeloma cells from apoptosis induced by interleukin 6 deprivation and dexamethasone. Blood. 2004;103(8):3148–57.

68. Li W, Li J, Su C, Zou WY, Luo S. New targets of PS-341: BAFF and APRIL. Medical Oncology. 2010;27(2):439–45.

69. Hengeveld PJ, Kersten MJ. B-cell activating factor in the pathophysiology of multiple myeloma: A target for therapy? Blood Cancer J. 2015;5(2).

70. Mantovani A, Allavena P, Marchesi F, Garlanda C. Macrophages as tools and targets in cancer therapy. Nat Rev Drug Discov. 2022;0123456789.

71. Chen J, He D, Chen Q, Guo X, Yang L, Lin X, et al. BAFF is involved in macrophage-induced bortezomib resistance in myeloma. Cell Death Dis. 2017;8(11).
72. Beyar-Katz O, Magidey K, Reiner-Benaim A, Barak N, Avivi I, Cohen Y, et al. Proinflammatory macrophages promote multiple myeloma resistance to bortezomib therapy. Molecular Cancer Research. 2019;17(11):2331–40.
73. Abdelmagid SM, Barbe MF, Safadi FF. Role of inflammation in the aging bones. Life Sci. 2015;123:25–34.
74. Schlundt C, Fischer H, Bucher CH, Rendenbach C, Duda GN, Schmidt-Bleek K. The multifaceted roles of macrophages in bone regeneration: A story of polarization, activation and time. Acta Biomater. 2021;133:46–57.
75. Brimnes MK, Svane IM, Johnsen HE. Impaired functionality and phenotypic profile of dendritic cells from patients with multiple myeloma. Clin Exp Immunol. 2006;144(1):76–84.
76. Ratta M, Fagnoni F, Curti A, Vescovini R, Sansoni P, Oliviero B, et al. Dendritic cells are functionally defective in multiple myeloma: The role of interleukin-6. Blood. 2002;100(1):230–7.
77. Verheye E, Melgar JB, Deschoemaeker S, Raes G, Maes A, De Bruyne E, et al. Dendritic Cell-Based Immunotherapy in Multiple Myeloma: Challenges, Opportunities, and Future Directions. Int J Mol Sci. 2022;23(2).
78. Hoang MD, Jung SH, Lee HJ, Lee YK, Nguyen-Pham TN, Choi NR, et al. Dendritic Cell-Based Cancer Immunotherapy against Multiple Myeloma: From Bench to Clinic. Chonnam Med J. 2015;51(1):1.
79. Nguyen-Pham TN, Lee YK, Kim HJ, Lee JJ. Immunotherapy using dendritic cells against multiple myeloma: How to improve? Clin Dev Immunol. 2012;2012.
80. Leone P, Berardi S, Frassanito MA, Ria R, De Re V, Cicco S, et al. Dendritic cells accumulate in the bone marrow of myeloma patients where they protect tumor plasma cells from CD8+ T-cell killing. Blood. 2015;126(12):1443–51.

81. Vasir B, Borges V, Wu Z, Grosman D, Rosenblatt J, Irie M, et al. Fusion of dendritic cells with multiple myeloma cells results in maturation and enhanced antigen presentation. Br J Haematol. 2005;129(5):687–700.

82. Dhodapkar M V., Krasovsky J, Olson K. T-cells from the tumor microenvironment of patients with progressive myeloma can generate strong, tumor-specific cytolytic responses to autologous, tumor-loaded dendritic cells. Proc Natl Acad Sci U S A. 2002;99(20):13009–13.

83. Soumoy L, Kindt N, Ghanem G, Saussez S, Journe F. Role of macrophage migration inhibitory factor (Mif) in melanoma. Cancers (Basel). 2019;11(4):1–11.

84. Jäger B, Klatt D, Plappert L, Golpon H, Lienenklaus S, Barbosa PD, et al. CXCR4/MIF axis amplifies tumor growth and epithelial-mesenchymal interaction in non-small cell lung cancer. Cell Signal [Internet]. 2020;73(May):109672. Available from: https://doi.org/10.1016/j.cellsig.2020.109672

85. Xu J, Yu N, Zhao P, Wang F, Huang J, Cui Y, et al. Intratumor Heterogeneity of MIF Expression Correlates With Extramedullary Involvement of Multiple Myeloma. Front Oncol. 2021;11(June):1–13.

86. Gutiérrez-González A, Martínez-Moreno M, Samaniego R, Arellano-Sánchez N, Salinas-Muñoz L, Relloso M, et al. Evaluation of the potential therapeutic benefits of macrophage reprogramming in multiple myeloma. Blood. 2016;128(18):2241–52.

87. Yuhuan Z, Qiang W, Li T, Qian J, Lu Y, Li Y, et al. Role of myeloma-derived MIF in myeloma cell adhesion to bone marrow and chemotherapy response. J Natl Cancer Inst. 2016;108(11):1–11.

88. Wang Q, Zhao D, Xian M, Wang Z, Bi E, Su P, et al. MIF as a biomarker and therapeutic target for overcoming resistance to proteasome inhibitors in human myeloma. Blood. 2020;136(22):2557–73.

89. Zhang S, Zhao J, Bai X, Handley M, Shan F. Biological effects of IL-15 on immune cells and its potential for the treatment of cancer. Int

Immunopharmacol [Internet]. 2021;91(December 2020):107318. Available from: https://doi.org/10.1016/j.intimp.2020.107318

90. Doedens AL, Rubinstein MP, Gross ET, Adam Best J, Craig DH, Baker MK, et al. Molecular programming of tumor-infiltrating CD8+ T-cells and IL15 resistance. Cancer Immunol Res. 2016;4(9):799–811.

91. Knudson KM, Hicks KC, Alter S, Schlom J, Gameiro SR. Mechanisms involved in IL-15 superagonist enhancement of anti-PD-L1 therapy. J Immunother Cancer. 2019;7(1):1–16.

92. Mahtouk K, Tjin EPM, Spaargaren M, Pals ST. The HGF/MET pathway as target for the treatment of multiple myeloma and B-cell lymphomas. Biochim Biophys Acta Rev Cancer [Internet]. 2010;1806(2):208–19. Available from: http://dx.doi.org/10.1016/j.bbcan.2010.07.006

93. Spina A, De Pasquale V, Cerulo G, Cocchiaro P, Morte R Della, Avallone L, et al. HGF/c-MET axis in tumor microenvironment and metastasis formation. Biomedicines. 2015;3(1):71–88.

94. Owusu BY, Galemmo R, Janetka J, Klampfer L. Hepatocyte growth factor, a key tumor-promoting factor in the tumor microenvironment. Cancers (Basel). 2017;9(4):1–16.

95. Li L, Zhang X, Kovacic S, Long AJ, Bourque K, Wood CR, et al. Identification of a human follicular dendritic cell molecule that stimulates germinal center B-cell growth. Journal of Experimental Medicine. 2000;191(6):1077–83.

96. Zhang X, Li L, Jung J, Xiang S, Hollmann C, Choi YS. The Distinct Roles of T-cell-Derived Cytokines and a Novel Follicular Dendritic Cell-Signaling Molecule 8D6 in Germinal Center-B-cell Differentiation. The Journal of Immunology. 2001;167(1):49–56.

97. Bendre A, Büki KG, Määttä JA. Fam3c modulates osteogenic differentiation by down-regulating Runx2. Differentiation. 2017;93(May 2016):50–7.

98. Määttä JA, Bendre A, Laanti M, Büki KG, Rantakari P, Tervola P, et al. Fam3c modulates osteogenic cell differentiation and affects bone volume and cortical bone mineral density. Bonekey Rep. 2016;5(APRIL).

99. Du JS, Yen CH, Hsu CM, Hsiao HH. Management of myeloma bone lesions. Int J Mol Sci. 2021;22(7):1–14.

100. Terpos E, Christoulas D, Gavriatopoulou M, Dimopoulos MA. Mechanisms of bone destruction in multiple myeloma. Eur J Cancer Care (Engl). 2017;26(6):1–11.

101. Janiszewska M, Primi MC, Izard T. Cell adhesion in cancer: Beyond the migration of single cells. Journal of Biological Chemistry [Internet]. 2020;295(8):2495–505. Available from: http://dx.doi.org/10.1074/jbc.REV119.007759

Supplementary Information

Subject cohorts

All participants were above age 18. Any potential participant who met any of the following criteria were excluded from participating in the study:

- History of drug or alcohol abuse.
- Female who might be pregnant or was breast-feeding at the time of enrollment.
    - Active/other malignancy or history of malignancy (other than MM) within 3 years prior to screening. Exceptions were squamous and basal cell carcinomas of the skin and carcinoma in situ of the cervix, or malignancy which in the opinion of the investigator were cured.
    - Active auto-immune disorder
    - Signs of active infection, at the discretion of the investigator
    - Concomitant immune-suppressive medication including prednisone > 5 mg daily

Prospective SMM or symptomatic multiple myeloma participants:

- No history of or current anti-myeloma therapy
- No prior use of bisphosphonates or denosumab

The following criterion were used for inclusion in the specific cohorts.

HV

- >50 years of age

MGUS

IgG or A MGUS [All criteria must be met]:

- Serum monoclonal protein (IgG or IgA or IgM) <3 g/dL **AND**

- Clonal BM plasma cells <10% **AND**
- No myeloma-defining events (see below)

OR Light chain MGUS [All criteria must be met]:

- Abnormal sFLC ratio (<0.26 or >1.65) **AND**
- Increased level of the appropriate involved light chain (increased κ sFLC in patients with ratio >1.65 and increased λ sFLC patients with ratio <0.26) **AND**
- No immunoglobulin heavy chain on immunofixation **AND**
- Clonal BM plasma cells <10% **AND**
- Urinary monoclonal protein <500 mg/24h **AND**
- No myeloma-defining events (see below)

SMM

-
- Serum monoclonal protein (IgG or IgA) ≥3 g/dL **OR**
- Urinary monoclonal protein ≥500 mg/24 h **AND/OR**
- Clonal BM plasma cells 10% - 60%
- **AND** No myeloma-defining events or amyloidosis (no CRAB and no SliM as detailed below)

Symptomatic Multiple Myeloma

Myeloma-defining events are evidence of end-organ damage that can be attributed to the underlying plasma cell proliferative disorder, especially:

- **C**: Calcium elevation (> 11 mg/dL or > 1 mg/dL higher than ULN)
- **R**: Renal insufficiency (creatinine clearance < 40 mL/min or serum creatinine > 2 mg/dL)
- **A**: Anemia (Hb < 10 g/dL or 2 g/dL < normal)

- **B**: Bone disease (≥ 1 lytic lesions on skeletal radiography, CT, or PET-CT). If bone marrow had less than 10% clonal plasma cells, more than one bone lesion was required to distinguish from solitary plasmacytoma with minimal marrow involvement.

OR, in the absence of CRAB, any one or more of the following biomarkers of malignancy, referred to here as the SliM criteria: S=≥Sixty percent (≥60%) clonal BM plasma cells; Li=serum free Light chain ratio involved:uninvolved ≥100; M=>1 focal lesion (≥5 mm each) detected by MRI studies

BM=bone marrow; PET-CT (18F-fluorodeoxyglucose PET with CT); FLC=free light chain; MGUS=monoclonal gammopathy of unknown significance. Note: Clonality should be established by showing κ/λ-light-chain restriction on flow cytometry, immunohistochemistry, or immunofluorescence. BM plasma cell percentage should preferably be estimated from a core biopsy specimen; in case of a disparity between the aspirate and core biopsy, the highest value should be used.

Table S1: CITE-seq ADTs

ADT	Protein	Gene
CD11b_TotalSeqC	CD11b	ITGAM
CD11c_TotalSeqC	CD11c	ITGAX
CD123_TotalSeqC	CD123	IL3RA
CD127_TotalSeqC	CD127	IL7R
CD137_TotalSeqC	CD137	TNFRSF9
CD138_TotalSeqC	CD138	SDC1
CD14_TotalSeqC	CD14	CD14
CD15_TotalSeqC	CD15	FUT4
CD152_TotalSeqC	CD152	CTLA4
CD16_TotalSeqC	CD16	FCGR3A
CD19_TotalSeqC	CD19	CD19
CD197_TotalSeqC	CD197	CCR7

CD20_TotalSeqC	CD20	MS4A1
CD223_TotalSeqC	CD223	LAG3
CD24_TotalSeqC	CD24	CD24
CD244_TotalSeqC	CD244	CD244
CD25_TotalSeqC	CD25	IL2RA
CD269_TotalSeqC	CD269	TNFRSF17
CD27_TotalSeqC	CD27	CD27
CD270_TotalSeqC	CD270	TNFRSF14
CD272_TotalSeqC	CD272	BTLA
CD274_TotalSeqC	CD274	CD274
CD278_TotalSeqC	CD278	ICOS
CD279_TotalSeqC	CD279	PDCD1
CD28_TotalSeqC	CD28	CD28
CD3_TotalSeqC	CD3	CD3D
CD3_TotalSeqC	CD3	CD3E
CD33_TotalSeqC	CD33	CD33
CD357_TotalSeqC	CD357	TNFRSF18
CD366_TotalSeqC	CD366	HAVCR2
CD38_TotalSeqC	CD38	CD38
CD4_TotalSeqC	CD4	CD4
CD45_TotalSeqC	CD45	PTPRC
CD45RA_TotalSeqC	CD45RA	
CD45RO_TotalSeqC	CD45RO	
CD56_TotalSeqC	CD56	NCAM1
CD66b_TotalSeqC	CD66b	CEACAM8
CD69_TotalSeqC	CD69	CD69
CD8_TotalSeqC	CD8	CD8A
CD8_TotalSeqC	CD8	CD8B

CD80_TotalSeqC	CD80	CD80
GPRC5D_TotalSeqC	GPRC5D	GPRC5D
HLA-DR_TotalSeqC	HLA-DR	HLA-DRA
HLA-DR_TotalSeqC	HLA-DR	HLA-DRB1
TIGIT_TotalSeqC	TIGIT	TIGIT

Figure S1

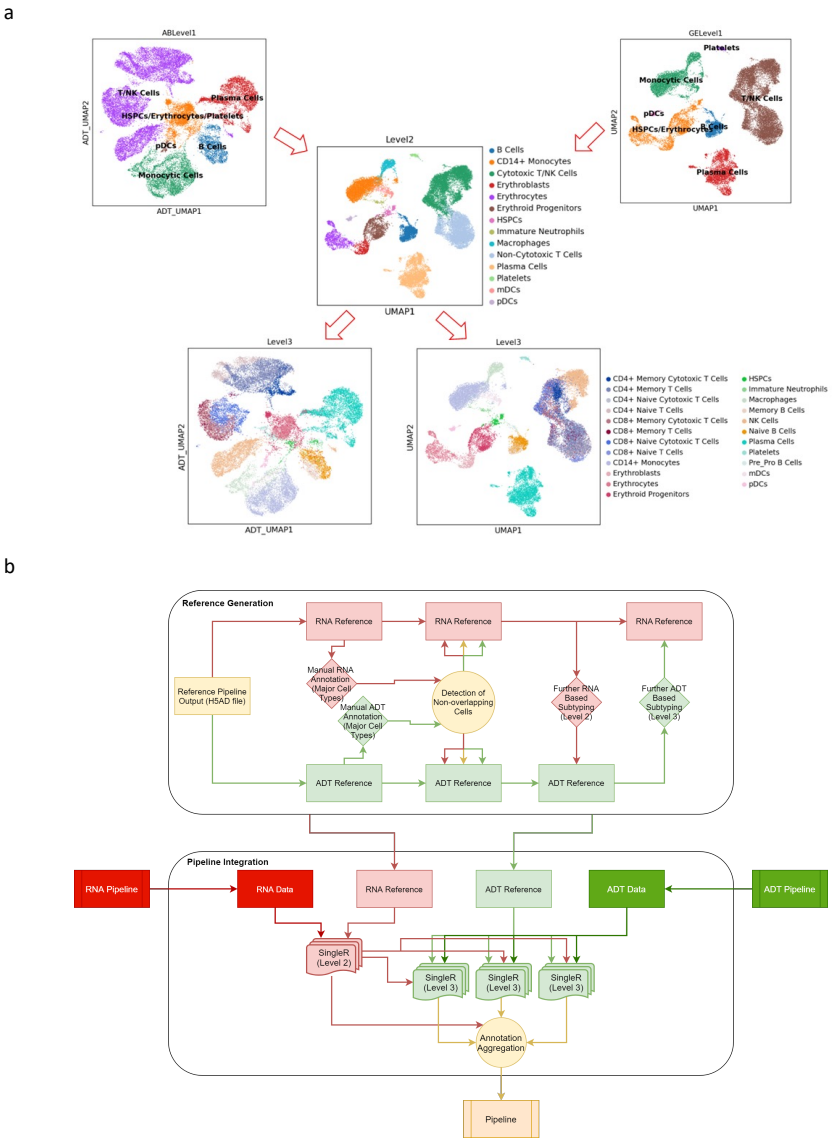

Figure S1. Reference-based automated cell typing strategy. (**a**) Reference data generation steps, visualized by ADT and RNA UMAPs using the colors of cell types at different annotation levels. The data was generated using 12 initial samples, where each cohort was represented with 3 samples. (**b *top***) Reference data generation steps are demonstrated. (**b *bottom***) The integration step of automated cell typing strategy into the

data processing pipeline is demonstrated. Light red: reference RNA data; dark red: query RNA data; light green: reference ADT data; dark green: query ADT data; light yellow: integrated dataset of RNA and ADT.

Figure S2

a

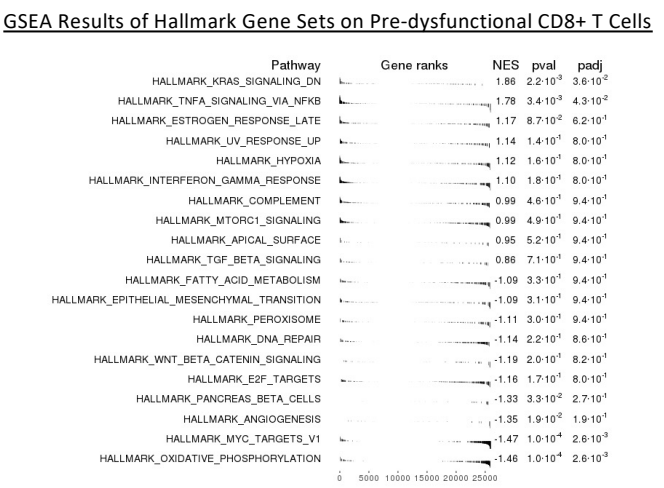

b

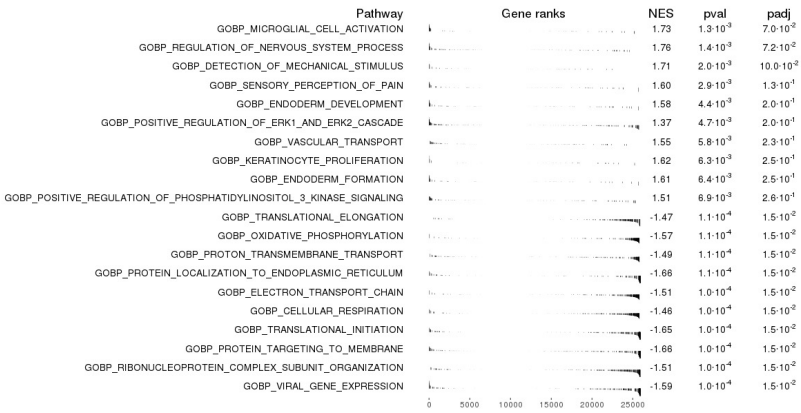

Figure S2. GSEA results of pre-dysfunctional CD8+ ATCs. (**a**) Top 10 up- and down-regulated hallmark gene sets. (**b**) Top 10 up- and down-regulated biological processes (BP) gene sets. For both subsections, the GSEA analyses are conducted contrasting pre-dysfunctional CD8+ ATCs with other CD8+ ATCs.

Figure S3

a

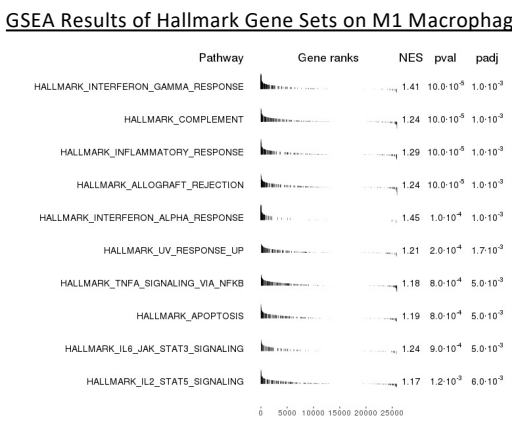

b

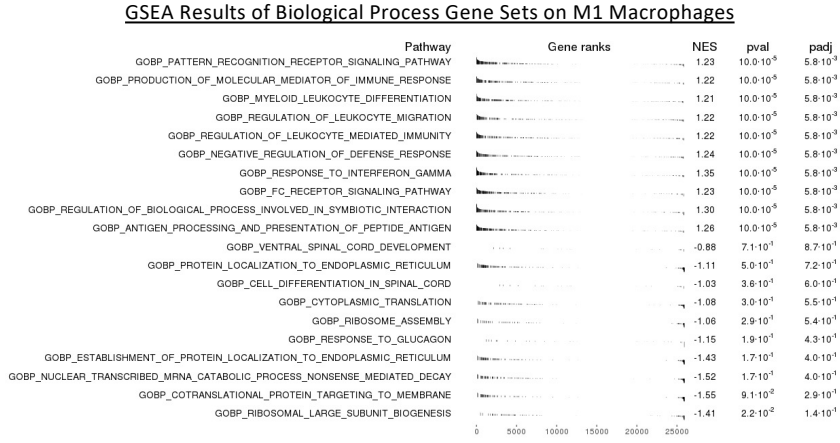

Figure S3. **GSEA results of M1 Macrophages**. (**a**) Top 10 up-regulated hallmark gene sets. No significantly down-regulated gene sets have been identified. (**b)** Top 10 up- and down-regulated biological processes (BP) gene sets. For both subsections, the GSEA analyses are conducted contrasting M1 macrophages with other macrophages

Figure S4

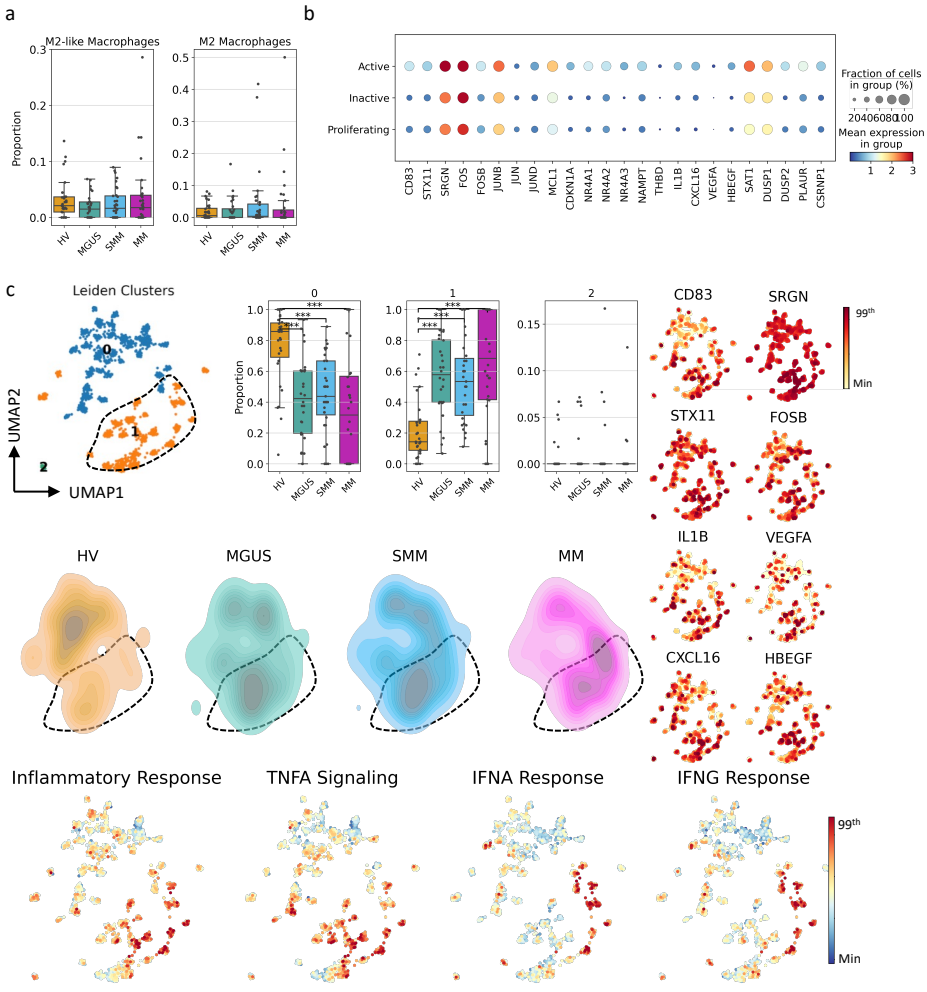

Figure S4. Additional figures on Macrophage, CD1C+ DC and CD14+ DC populations. (**a**) Proportional differences among cohorts for M2 macrophages. Each dot represents an individual subject. The proportional differences between each disease state vs HV are compared and the significance was calculated using the Mann–Whitney U test: *P <0.05; **P ≤ 0.005; ***P ≤ 0.005. (**b**) Expression profiles of proliferation markers define the proliferating cell group. (**c**) Investigation of CD14+ DCs. (**c *top & center***) UMAP of CD14+DCs, colored by the obtained clusters, the proportional difference and density plots among subject cohorts show transcriptional shifts. Highlighted area represents the region where the cells in cluster 1 reside. (**c *right***) Expression profile of the

markers defining active CD1C+ DC subgroup. The figure colors range from minimum value (yellow) to the 99th percentile of the value distribution (red). (**c *bottom***) Gene set scores of inflammatory pathways highlight inflammation responsive regions on the CD14+ DCs UMAP. The figure colors range from minimum value (blue) to the 99th percentile of the value distribution (red).

Figure S5

a

GSEA Results of Hallmark Gene Sets on Activated CD1C+ DCs

Pathway	NES	pval	padj
HALLMARK_INTERFERON_ALPHA_RESPONSE	1.91	$4.5 \cdot 10^{-4}$	$3.3 \cdot 10^{-3}$
HALLMARK_KRAS_SIGNALING_DN	1.84	$5.4 \cdot 10^{-4}$	$3.3 \cdot 10^{-3}$
HALLMARK_APOPTOSIS	1.80	$5.5 \cdot 10^{-4}$	$3.3 \cdot 10^{-3}$
HALLMARK_KRAS_SIGNALING_UP	1.82	$6.2 \cdot 10^{-4}$	$3.3 \cdot 10^{-3}$
HALLMARK_INFLAMMATORY_RESPONSE	2.14	$6.4 \cdot 10^{-4}$	$3.3 \cdot 10^{-3}$
HALLMARK_INTERFERON_GAMMA_RESPONSE	2.11	$6.5 \cdot 10^{-4}$	$3.3 \cdot 10^{-3}$
HALLMARK_TNFA_SIGNALING_VIA_NFKB	2.40	$6.6 \cdot 10^{-4}$	$3.3 \cdot 10^{-3}$
HALLMARK_IL6_JAK_STAT3_SIGNALING	1.70	$8.6 \cdot 10^{-4}$	$3.9 \cdot 10^{-3}$
HALLMARK_HYPOXIA	1.55	$1.2 \cdot 10^{-3}$	$4.3 \cdot 10^{-3}$
HALLMARK_ALLOGRAFT_REJECTION	1.57	$1.3 \cdot 10^{-3}$	$4.3 \cdot 10^{-3}$
HALLMARK_SPERMATOGENESIS	-1.18	$1.7 \cdot 10^{-1}$	$2.6 \cdot 10^{-1}$
HALLMARK_MYC_TARGETS_V2	-1.27	$1.1 \cdot 10^{-1}$	$1.7 \cdot 10^{-1}$
HALLMARK_G2M_CHECKPOINT	-1.21	$1.1 \cdot 10^{-1}$	$1.7 \cdot 10^{-1}$
HALLMARK_FATTY_ACID_METABOLISM	-1.24	$8.0 \cdot 10^{-2}$	$1.4 \cdot 10^{-1}$
HALLMARK_GLYCOLYSIS	-1.27	$5.1 \cdot 10^{-2}$	$9.4 \cdot 10^{-2}$
HALLMARK_DNA_REPAIR	-1.29	$4.8 \cdot 10^{-2}$	$9.4 \cdot 10^{-2}$
HALLMARK_ADIPOGENESIS	-1.29	$3.6 \cdot 10^{-2}$	$7.6 \cdot 10^{-2}$
HALLMARK_MYC_TARGETS_V1	-1.84	$1.2 \cdot 10^{-4}$	$2.0 \cdot 10^{-3}$
HALLMARK_E2F_TARGETS	-1.63	$1.2 \cdot 10^{-4}$	$2.0 \cdot 10^{-3}$
HALLMARK_OXIDATIVE_PHOSPHORYLATION	-1.86	$1.2 \cdot 10^{-4}$	$2.0 \cdot 10^{-3}$

b

GSEA Results of Biological Process Gene Sets on Activated CD1C+ DCs

Pathway	NES	pval	padj
GOBP_POSITIVE_REGULATION_OF_PROTEIN_TYROSINE_KINASE_ACTIVITY	1.92	$3.9 \cdot 10^{-4}$	$2.2 \cdot 10^{-2}$
GOBP_INTERFERON_GAMMA_MEDIATED_SIGNALING_PATHWAY	1.81	$4.6 \cdot 10^{-4}$	$2.2 \cdot 10^{-2}$
GOBP_CYTOKINE_PRODUCTION_INVOLVED_IN_IMMUNE_RESPONSE	1.79	$4.6 \cdot 10^{-4}$	$2.2 \cdot 10^{-2}$
GOBP_CD4_POSITIVE_ALPHA_BETA_T_CELL_ACTIVATION	1.77	$4.6 \cdot 10^{-4}$	$2.2 \cdot 10^{-2}$
GOBP_REGULATION_OF_ALPHA_BETA_T_CELL_ACTIVATION	1.79	$4.6 \cdot 10^{-4}$	$2.2 \cdot 10^{-2}$
GOBP_REGULATION_OF_CELL_KILLING	1.79	$4.6 \cdot 10^{-4}$	$2.2 \cdot 10^{-2}$
GOBP_REGULATION_OF_OSSIFICATION	1.74	$4.7 \cdot 10^{-4}$	$2.2 \cdot 10^{-2}$
GOBP_FORMATION_OF_PRIMARY_GERM_LAYER	1.71	$4.8 \cdot 10^{-4}$	$2.2 \cdot 10^{-2}$
GOBP_BONE_MINERALIZATION	1.71	$4.8 \cdot 10^{-4}$	$2.2 \cdot 10^{-2}$
GOBP_ALPHA_BETA_T_CELL_DIFFERENTIATION	1.65	$4.8 \cdot 10^{-4}$	$2.2 \cdot 10^{-2}$
GOBP_PROTEIN_LOCALIZATION_TO_ENDOPLASMIC_RETICULUM	-1.71	$1.2 \cdot 10^{-4}$	$9.0 \cdot 10^{-3}$
GOBP_MITOCHONDRIAL_GENE_EXPRESSION	-1.79	$1.2 \cdot 10^{-4}$	$9.0 \cdot 10^{-3}$
GOBP_ELECTRON_TRANSPORT_CHAIN	-1.73	$1.2 \cdot 10^{-4}$	$9.0 \cdot 10^{-3}$
GOBP_CELLULAR_RESPIRATION	-1.59	$1.2 \cdot 10^{-4}$	$9.0 \cdot 10^{-3}$
GOBP_RIBOSE_PHOSPHATE_BIOSYNTHETIC_PROCESS	-1.59	$1.2 \cdot 10^{-4}$	$9.0 \cdot 10^{-3}$
GOBP_TRANSLATIONAL_INITIATION	-1.75	$1.2 \cdot 10^{-4}$	$9.0 \cdot 10^{-3}$
GOBP_PURINE_CONTAINING_COMPOUND_BIOSYNTHETIC_PROCESS	-1.59	$1.2 \cdot 10^{-4}$	$9.0 \cdot 10^{-3}$
GOBP_PROTEIN_TARGETING_TO_MEMBRANE	-1.80	$1.2 \cdot 10^{-4}$	$9.0 \cdot 10^{-3}$
GOBP_RIBONUCLEOPROTEIN_COMPLEX_SUBUNIT_ORGANIZATION	-1.62	$1.2 \cdot 10^{-4}$	$9.0 \cdot 10^{-3}$
GOBP_VIRAL_GENE_EXPRESSION	-1.69	$1.2 \cdot 10^{-4}$	$9.0 \cdot 10^{-3}$

Figure S5. GSEA results of active CD1C+ DCs. (**a**) Top 10 up- and down-regulated hallmark gene sets. (**b)** Top 10 up- and down-regulated biological processes (BP) gene

sets. For both subsections, the GSEA analyses are conducted contrasting active CD1C+ DCs with other CD1C+ DCs.

Figure S6

a

GSEA Results of Hallmark Gene Sets on CD14+ DCs Cluster 1

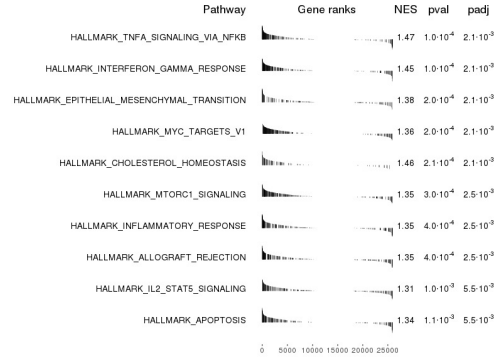

b

GSEA Results of Biological Process Gene Sets on CD14+ DCs Cluster 1

Pathway	Gene ranks	NES	pval	padj
GOBP_PROTEIN_TARGETING_TO_MEMBRANE		1.44	$1.0 \cdot 10^{-4}$	$9.2 \cdot 10^{-3}$
GOBP_VIRAL_GENE_EXPRESSION		1.41	$1.0 \cdot 10^{-4}$	$9.2 \cdot 10^{-3}$
GOBP_T_CELL_RECEPTOR_SIGNALING_PATHWAY		1.41	$1.0 \cdot 10^{-4}$	$9.2 \cdot 10^{-3}$
GOBP_TRANSLATIONAL_INITIATION		1.48	$1.0 \cdot 10^{-4}$	$9.2 \cdot 10^{-3}$
GOBP_RESPONSE_TO_INTERFERON_GAMMA		1.47	$1.0 \cdot 10^{-4}$	$9.2 \cdot 10^{-3}$
GOBP_PROTEIN_LOCALIZATION_TO_ENDOPLASMIC_RETICULUM		1.53	$1.0 \cdot 10^{-4}$	$9.2 \cdot 10^{-3}$
GOBP_NUCLEAR_TRANSCRIBED_MRNA_CATABOLIC_PROCESS_NONSENSE_MEDIATED_DECAY		1.54	$1.0 \cdot 10^{-4}$	$9.2 \cdot 10^{-3}$
GOBP_ESTABLISHMENT_OF_PROTEIN_LOCALIZATION_TO_ENDOPLASMIC_RETICULUM		1.56	$1.0 \cdot 10^{-4}$	$9.2 \cdot 10^{-3}$
GOBP_COTRANSLATIONAL_PROTEIN_TARGETING_TO_MEMBRANE		1.59	$1.0 \cdot 10^{-4}$	$9.2 \cdot 10^{-3}$
GOBP_T_CELL_ACTIVATION_INVOLVED_IN_IMMUNE_RESPONSE		1.48	$1.0 \cdot 10^{-4}$	$9.2 \cdot 10^{-3}$
GOBP_MITOCHONDRIAL_TRANSLATIONAL_TERMINATION		-1.20	$8.6 \cdot 10^{-2}$	$2.7 \cdot 10^{-1}$
GOBP_ZINC_ION_HOMEOSTASIS		-1.32	$7.9 \cdot 10^{-2}$	$2.6 \cdot 10^{-1}$
GOBP_CARDIAC_SEPTUM_DEVELOPMENT		-1.21	$7.1 \cdot 10^{-2}$	$2.5 \cdot 10^{-1}$
GOBP_CELL_DIFFERENTIATION_IN_SPINAL_CORD		-1.38	$6.2 \cdot 10^{-2}$	$2.3 \cdot 10^{-1}$
GOBP_MITOCHONDRIAL_TRANSLATION		-1.20	$4.4 \cdot 10^{-2}$	$1.9 \cdot 10^{-1}$
GOBP_SENSORY_PERCEPTION_OF_CHEMICAL_STIMULUS		-1.20	$4.1 \cdot 10^{-2}$	$1.8 \cdot 10^{-1}$
GOBP_MITOCHONDRIAL_GENE_EXPRESSION		-1.29	$2.9 \cdot 10^{-2}$	$1.6 \cdot 10^{-1}$
GOBP_SYNAPTIC_TRANSMISSION_GLUTAMATERGIC		-1.34	$2.1 \cdot 10^{-2}$	$1.3 \cdot 10^{-1}$
GOBP_REGULATION_OF_SYNAPTIC_TRANSMISSION_GLUTAMATERGIC		-1.68	$5.3 \cdot 10^{-3}$	$7.2 \cdot 10^{-2}$
GOBP_SENSORY_PERCEPTION_OF_TASTE		-1.71	$2.7 \cdot 10^{-3}$	$4.7 \cdot 10^{-2}$

0 5000 10000 15000 20000 25000

Figure S6. GSEA results of cluster1 of CD14+ DCs. (**a**) Top 10 up-regulated hallmark gene sets. No significantly down-regulated gene sets have been identified. (**b)** Top 10 up- and down-regulated biological processes (BP) gene sets. For both subsections, the GSEA analyses are conducted contrasting cluster 1 of CD14+ DCs with other CD14+ DCs.

Figure S7

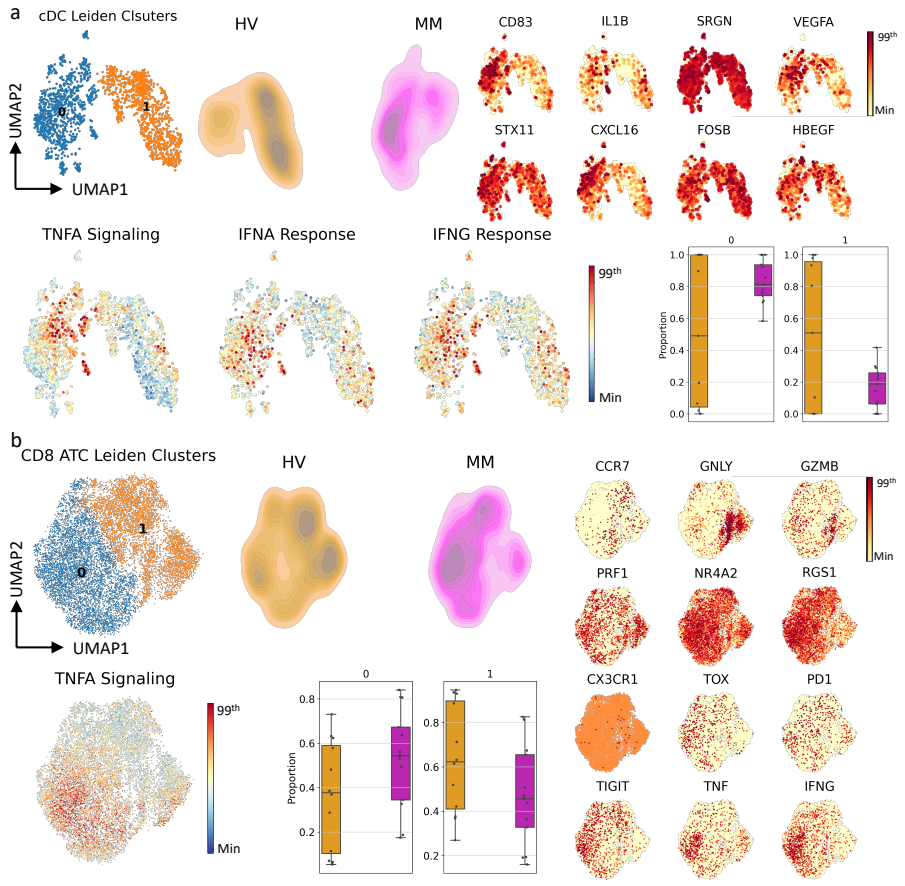

Figure S7. Validation study of de Jong et al. (**a**) Our findings on cDCs (CD1C + & CD14+DCs). (**a *top left***) UMAP of cDCs, colored by the obtained clusters and the dense regions per cohort. (**a *top right***) Expression profile of active CD1C+ DC markers within cDC clusters. The figure colors range from minimum value (yellow) to the 99th percentile of the value distribution (red). (**a *bottom left***) Gene set scores of IFN and TNF pathways demonstrate inflammation-associated regions. The figure colors range from minimum value (blue) to the 99th percentile of the value distribution (red). (**a *bottom right***) Proportional differences among cohorts for CD14+ DC clusters. Each dot represents an individual subject. The proportional differences between each disease state vs HV are compared and the significance was calculated using the Mann–Whitney U test: *P <0.05;

P ≤ 0.005; ***P ≤ 0.005. (b**) Our findings on CD8 ATCs. (**b *top left***) Two clusters are identified. Between HV and MM subjects, the dense regions differ. (**b *right***) Expression profile of CD8+ ATC markers within CD8ATC clusters. The figure colors range from minimum value (yellow) to the 99th percentile of the value distribution (red). (**b *left***) Gene set score of TNFα pathway demonstrates inflammation-associated regions. The figure colors range from minimum value (blue) to the 99th percentile of the value distribution (red). (**b *bottom center***) Proportional differences among cohorts for CD8+ ATC clusters. Each dot represents an individual subject. The proportional differences between each disease state vs HV are compared and the significance was calculated using the Mann–Whitney U test: *P <0.05; **P ≤ 0.005; ***P ≤ 0.005.

Figure S8

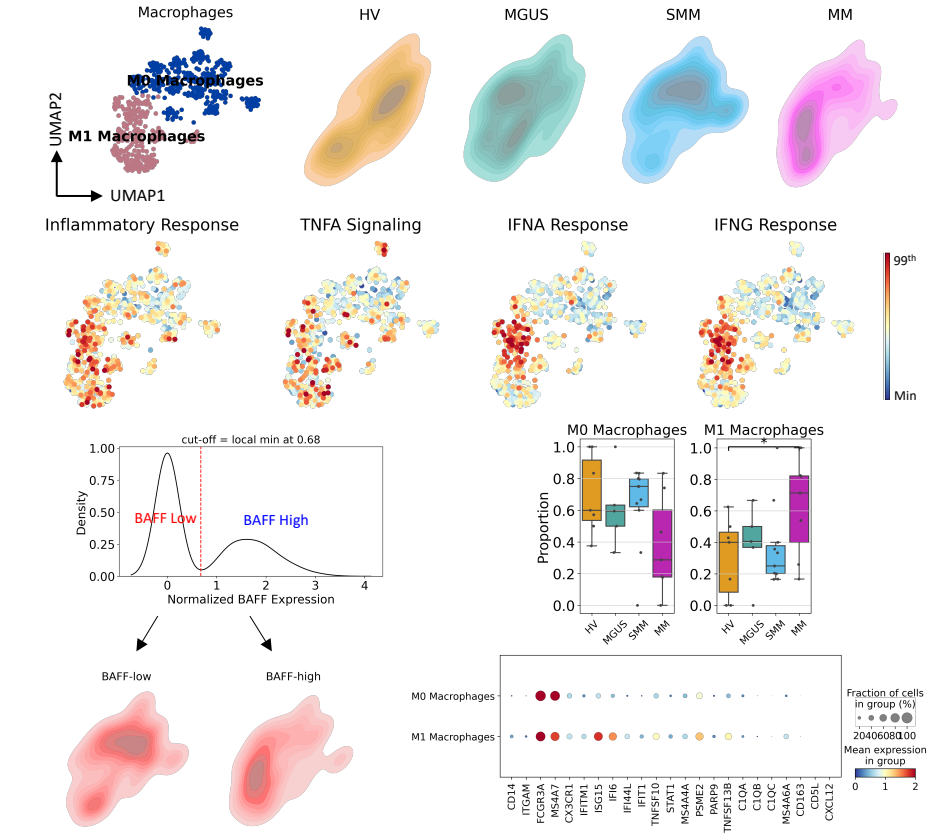

Figure S8. Validation study of Zavidij et al. Our findings on macrophage population. (***top***) UMAP of cDCs, colored by subgroups as well as the dense regions per cohort.

(***center***) Gene set scores of inflammatory pathways highlight inflammation-responsive regions on the macrophage UMAP. The figure colors range from minimum value (blue) to the 99th percentile of the value distribution (red). (***bottom left***) Distribution of BAFF expression. The cells are categorized by the local minimum at 0.68 into BAFF-high and BAFF-low categories. Density UMAP highlights the dense regions of each group on the translation landscape of macrophages. (***right center***) Proportional differences among cohorts for macrophage subtypes. Each dot represents an individual subject. The proportional differences between each disease state vs HV are compared and the significance was calculated using the Mann–Whitney U test: *P <0.05; **P ≤ 0.005; ***P ≤ 0.005. (***bottom right***) Expression profiles of marker genes that define macrophage subpopulations.

Figure S9

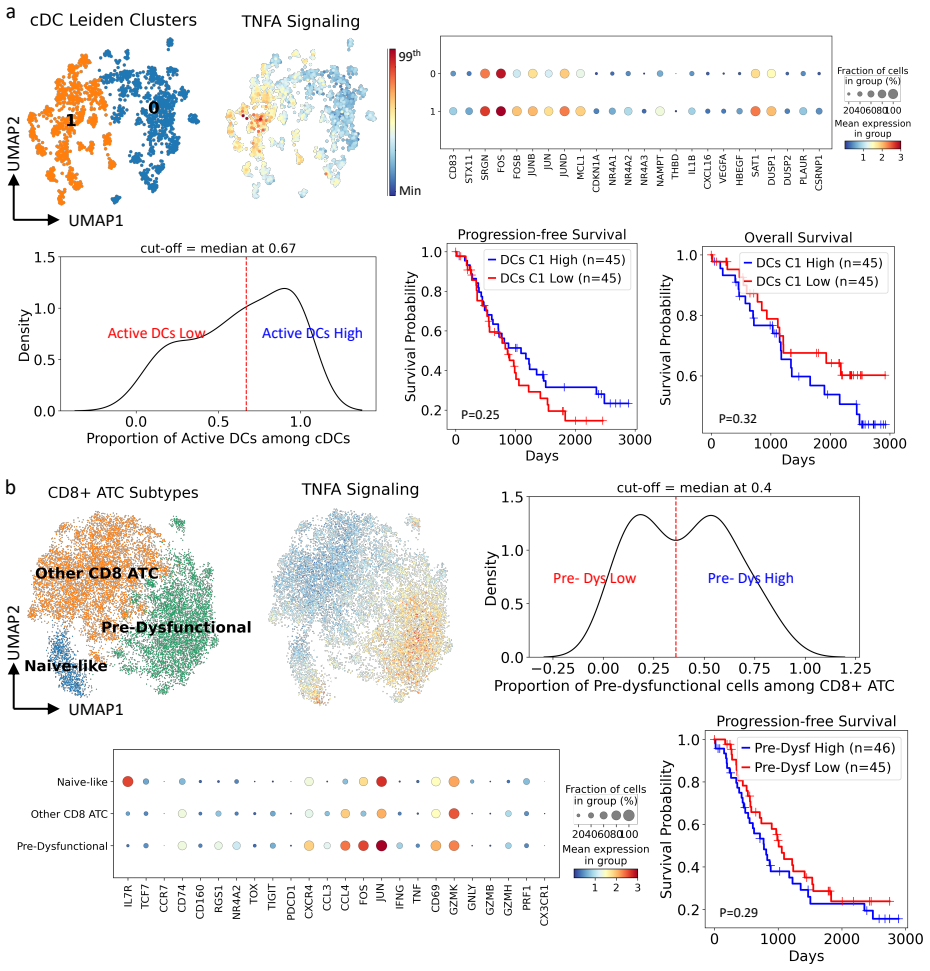

Figure S9. Validation study of CoMMpass dataset. (**a**) Our findings on cDCs (CD1C + & CD14+DCs). (**a *top left***) UMAP of cDCs, colored by identified clusters as well as the gene set scores of inflammatory response and TNFα signaling. The figure colors range from minimum value (blue) to the 99th percentile of the value distribution (red). (**a *top right***) Expression profile of marker genes, used to identify active and inactive CD1C+ DCs, within cDC clusters. (**a *bottom***) The subjects are categorized based on the distribution of proportion of cells in cluster 1 (cDC C1). The median value of 0.67 is used as a cut off to group subjects into cDC C1 high and low categories. Kaplan-Meier survival curves demonstrate the association between cDC C1 proportion and PFS (C1 high median

= 715, C1 low median = 758) as well as OS (C1 high median = 1412, C1 low median = 1273) . (**b**) Our findings on CD8+ ATCs. (**b *top***) UMAP representation of the CD8+ ATCs colored by CD8+ ATC subgroups and TNFα signaling. The figure colors range from minimum value (blue) to the 99th percentile of the value distribution (red). (**b *bottom***) The expression profile of marker genes that define each CD8+ ATC subgroup. (**b *right***) Kaplan-Meier survival curves demonstrate the association between pre-dysfunctional CD8+ ATC proportion and PFS (Pre-dys high median = 670, Pre-dys low median = 900).

Figure S10

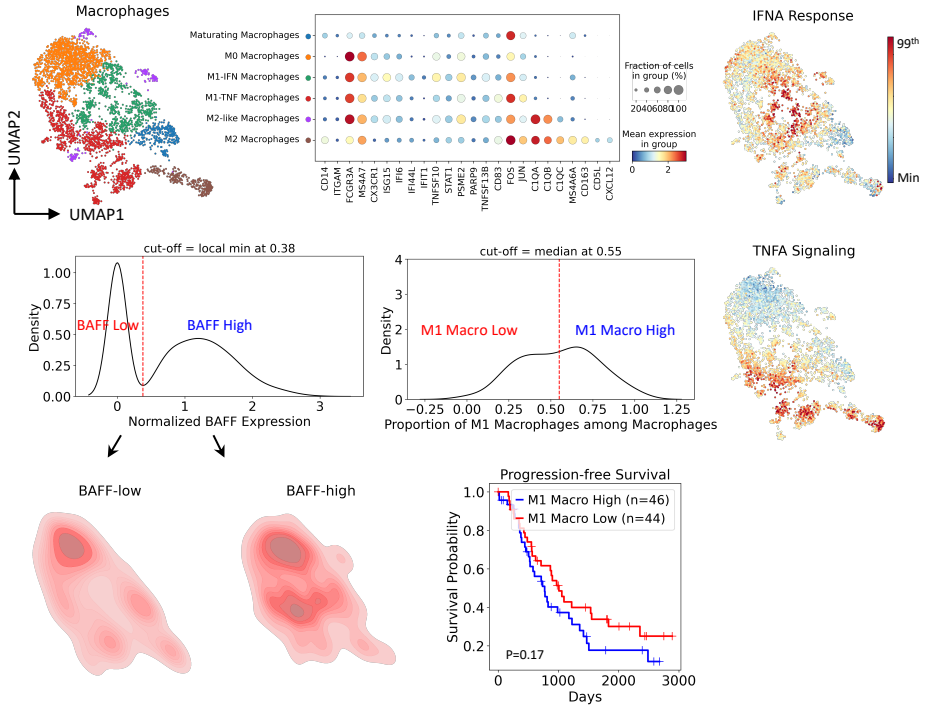

Figure S10. Validation study of CoMMpass dataset. Our findings on macrophages. (***top***) UMAP representation of the macrophages colored by macrophage subgroups and the expression profile of marker genes define each macrophage subgroup. (***right***) UMAP representation of the macrophages colored IFNα and TNFα signaling. The figure colors range from minimum value (blue) to the 99th percentile of the value distribution (red). (***center***) The subjects are categorized based on the distribution of proportion of cells in

M1 macrophages. The local minimum at 0.38 is used as a cut off to group subjects into M1-high and -low categories. Kaplan-Meier survival curves demonstrate the association between M1 macrophage proportion and PFS (M1 high median = 593, M1 low median = 892). (***bottom left***) Distribution of BAFF expression. The cells are categorized by the local minimum at 0.68 into BAFF-high and BAFF-low categories.

Figure S11

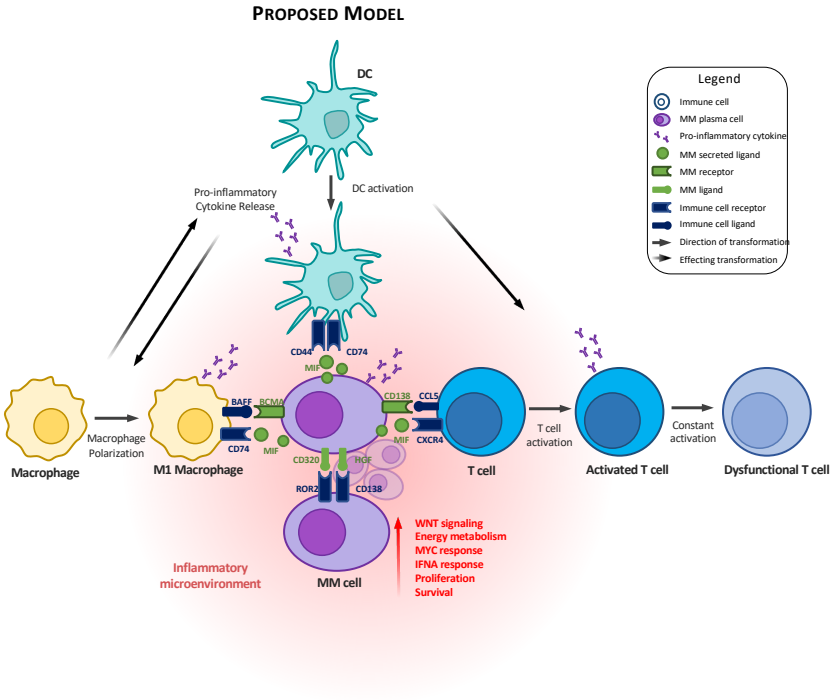

Figure S11. Proposed model of MM progression involves dynamic interplay between malignant plasma cells and the immune populations. Each cell type is represented with a different color, MM: purple; DCs: turquoise; Macrophages: yellow, T-cells: blue. The MM plasma cell ligands and receptors are represented in green. Ligands and receptors from the immune populations are represented in dark blue. The straight arrows show the direction of the transformation. The arrows with descending color represent the direction

of the effect on transformation. The orange cloud represents the inflammatory environment. MM: multiple myeloma; DC: dendritic cell; IFNA: interferon alpha.

Chapter II: Alternative Targeting Strategies

Integrative Analysis of Proteomics and Transcriptomics Reveals Endothelin Receptor B as Novel single Target and Identifies New Combinatorial Targets for Multiple Myeloma

Margaux Lejeune[1*], Murat Cem Köse[1*], Mégane Jassin,[1] Marie-Jia Gou[2], Amaury Herbet[3], Elodie Duray[1], Gaël Cobraiville[2], Jacques Foguenne[4], Didier Boquet[3], André Gothot[4], Yves Beguin[1,5], Marianne Fillet[2], Jo Caers[1,5**]**

[1] Laboratory of Hematology, GIGA I3, University of Liège, Liège, Belgium

[2] Laboratory for the Analysis of Medicines, Center for Interdisciplinary Research on Medicines (CIRM), University of Liège, Liège, Belgium

[3] Université Paris-Saclay, CEA, Département Médicaments et Technologies pour la Santé (DMTS), SPI, 91191 Gif-sur-Yvette, France

[4] Department of Hematobiology and Immunohematology, CHU de Liège, Liège, Belgium

[5] Department of Hematology, CHU de Liège, Liège, Belgium

[*] These authors are co-first authors

[**] These authors are co-senior authors

List of abbreviations

MM	Multiple myeloma
RNA	Ribonucleic acid RNA
CAR	Chimeric Antigen Receptor
BsAbs	Bispecific antibodies (BsAbs)
BCMA	B-Cell Maturation Antigen
DHE	Differentially highly expressed genes
RB49	Rendomab49
GPRC5D	G-protein coupled receptor family C group 5 member D
FCRL5	Fc Receptor-Like 5
BM	Bone marrow
DSMZ	Deutsche Sammlung von Mikroorganismen und Zellkulturen
PBS	Phosphate-buffered saline
TBS	Tris-buffered saline
BSA	Bovine serum albumin
LC	Liquid chromatography
MS	Mass spectrometry
DDA	Data-dependent acquisition
DIA	Data-independent acquisition
IM	Ion mobility
IMFE	Ion mobility feature extraction
SPI	Spectrum purity index
HPA	Human Protein Atlas (HPA)
HPM	Human Proteome Map (HPM)
PDB	Proteomics Database (PDB)
SD	Standard deviation

Abstract

Despite the recent introduction of next-generation immunotherapeutic agents, multiple myeloma (MM) remains incurable. New strategies targeting multiple myeloma-specific antigens may result in a more effective therapy by preventing antigen escape, clonal evolution and tumor resistance. In this work, we adapted an algorithm that integrates proteomic and transcriptomic results of myeloma cells to identify new antigens and possible antigen combinations. We performed cell surface proteomics on six myeloma cell lines and combined these results with gene expression studies. Our algorithm identified 209 overexpressed surface proteins from which 23 proteins could be selected for combinatorial pairing. Flow cytometry analysis of 20 primary samples confirmed the expression of FCRL5, BCMA and ICAM2 in all samples and IL6R, ET_B and SLCO5A1 in more than 60% of myeloma cases. Analyzing possible combinations, we found 6 combinatorial pairs that can target myeloma cells and avoid toxicity on other organs. In addition, our studies identified ET_B as a tumor-associated antigen that is overexpressed on myeloma cells. This antigen can be targeted with a new monoclonal antibody RB49 that recognizes an epitope located in a region that becomes highly accessible after activation of ET_B by its ligand. In conclusion, our algorithm identified several candidate antigens that can be used for either single-antigen targeting approaches or for combinatorial targeting in new immunotherapeutic approaches in MM.

Background

In the past decade, the survival of multiple myeloma (MM) patients has improved with the introduction of novel agents. The 5-year survival rates of a global myeloma population increased from 37% to 52% in a recent registry study, an increase that was mainly seen in young transplant-eligible patients.[1] With the introduction of the monoclonal anti-CD38 antibodies daratumumab and isatuximab, improvement of survival rates is likely to continue. When used in monotherapy, daratumumab showed clinical activity in 37% of refractory MM patients.[2] When combined with lenalidomide or bortezomib, the response rates increased to 92% and 85%, respectively.[3,4] Daratumumab is currently approved as first-line treatment for both transplant-eligible and -ineligible patients.[5,6].

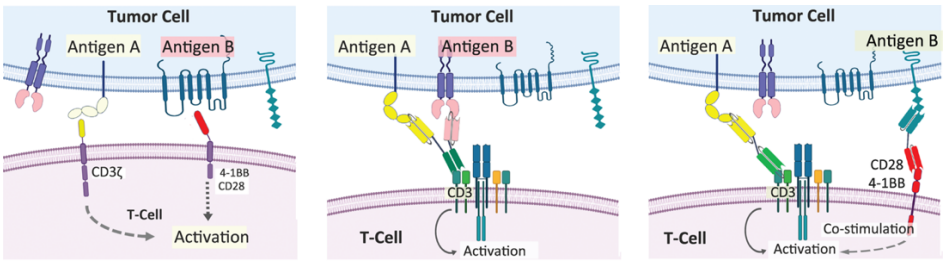

A. Combinatorial CAR-T B. Hemibodies C. Costimulatory bispecifics

Figure 1: Recently developed combinatorial strategies. These strategies require that two antigens are present to activate immune effector cells. (A) They are based on activation of co-stimulatory pathways in CAR-T-cells, (B) the use of hemibodies with alignment of the CD3 binding VH and VL parts and (C) the co-administration of bispecific antibodies that bind to a costimulatory receptor.

Following monoclonal antibodies, more potent immunotherapeutic approaches are developed. Similar to other lymphoproliferative malignancies, Chimeric Antigen Receptor (CAR) T-cell therapies and bispecific antibodies (BsAbs) have been introduced and successfully tested in early clinical trials.[7,8] For MM, these strategies targeted a limited set of antigens (B-Cell Maturation

Antigen (BCMA), G-protein coupled receptor family C group 5 member D (GPRC5D) and Fc Receptor-Like 5 (FCRL5)).[9] Nonetheless, malignant cells can escape immune recognition by employing a number of antigen-evasion strategies, including antigen mutation, down-regulation of target antigens, and the selective survival of antigen-negative cell subpopulations.[10] Such immune escape has been well studied for patients relapsing after anti-BCMA CAR-T therapy or bispecific antibodies. Homozygous deletions of chromosome 16p (where the BCMA gene is located) or a biallelic loss of BCMA have been reported in relapsing patients.[11,12] Hence, increasing the number of targeted antigens may result in a more effective therapy by preventing antigen escape and disease progression. This strategy is particularly relevant in patients with refractory disease, those relapsing after immunotherapy and/or rapid and aggressive disease progression.

On the other hand, immunotherapy should avoid activation towards antigens expressed on healthy tissues and cells (often termed on-target, off-tumor), particularly in patients with minimal bone marrow (BM) infiltration (e.g., minimal residual disease), and thus highly selective and effective treatments are needed.[13] Tumor-specific targeting can also be increased by simultaneously targeting two antigens; even if neither antigen is expressed exclusively by the tumor, the tumor cells — but not healthy cells — are likely to express both antigens.[14] Figure 1 illustrates different forms of immunotherapy that are based on combinatorial approaches, such as CAR-T-cells[15] and bispecific antibodies[16,17].

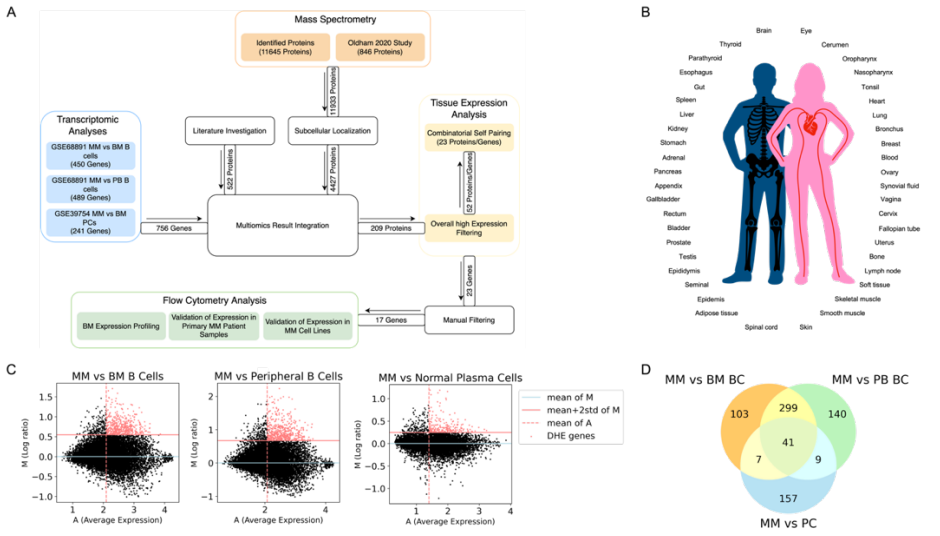

Figure 2: Combinatorial target identification strategy. (A) Analysis workflow. **(B)** The consensus tissue list. **(C)** MA plots (mean vs ratio) illustrating the identified differentially highly expressed (DHE) genes in different contrasts. DHE genes are genes with higher log ratios of mean+2SD and having higher expression than average expression among all patients. **(D)** Venn diagram representing the overlap of identified DHE genes in different contrasts. MM: multiple myeloma; BM BC: bone marrow B-cell; PB BC: peripheral blood B-cell; PC: plasma cell.

In this study, we aimed to identify optimal antigen pairs for selective MM cell targeting. These pairs were identified by combining proteomic and genomic results from myeloma and normal cell populations and their expression profiles were subsequently validated by flow cytometry (Figure 2.A). We could propose different antigen combinations for immunotherapeutic approaches. Moreover, our algorithm revealed Endothelin Receptor B (ET_B) as a potential new target for MM that is overexpressed compared to normal plasma cells and B-lymphocytes and absent on hematopoietic stem cells.

Methods

Cell lines

Human MM cell lines KMS-12-BM, NCI-H929, MOLP-2 and RPMI-8226 were obtained from the German Collection of Microorganisms and Cell Cultures (DSMZ; Braunschweig, Germany). U266, OPM-2 and LP-1 cell lines were obtained from H. Jernberg-Wiklund (Uppsala University, Uppsala, Sweden) and MM1.S was obtained from A. Bolomsky (Wilhelminen Cancer Research Institute, Vienna, Austria). LP-1 cells were cultured in Dulbecco's Modified Eagle's Medium (DMEM) (Lonza, Verviers, Belgium) supplemented with 10% fetal bovine serum (FBS; Sigma-Aldrich, St-Louis, MO, USA), 2 mM L-glutamine (Lonza) and 100 U/mL penicillin-streptomycin (P/S; Lonza). RPMI-8226 cells, KMS-12-BM cells, U266 cells, MOLP-2 cells, OPM-2 cells, NCI-H929 cells and MM1.S cells were cultured in Roswell Park Memorial Institute (RPMI 1640) (Lonza) supplemented with 10% FBS, 2 mM L-glutamine and 100 U/mL P/S. All cell lines were cultured at 37°C in 5% CO_2 humidity.

Cell surface proteomics

Six myeloma cell lines, including OPM-2, LP-1, MOLP-2, U266, MM1.S and KMS-12-BM were selected for cell surface biotinylation and isolation. For this purpose, the Pierce™ Cell Surface Protein Isolation Kit (Thermo Fisher, Waltham, MA, USA) was used for biotinylation, lysis and isolation of labelled proteins. Three biological replicates of each above-mentioned cell lines were cultured in 75 cm^2 flasks to obtain 10^7 cells. For the biotinylation, cell lysis and recovery of biotinylated proteins, we followed the instructions provided by the manufacturer. Eluted bead-free proteins were alkylated by incubating the samples with iodoacetamide (Sigma-Aldrich) and were subsequently subjected digested using trypsin (Promega, Madison, WI,

USA) at 4 µg/µL at 37°C. The following day, the reaction was stopped using 0.5% formic acid (Biosolve, Valkenswaard, the Netherlands) and peptides were subsequently evaporated at 30°C. Protein quantification was performed using the NanoOrange protein quantitation kit (Invitrogen, Waltham, MA, USA).

LC-MS/MS

A 1290 Infinity II ultra-high-performance LC system (Agilent Technologies, Waldbronn, Germany) coupled with 6560 Ion mobility quadrupole time-of-flight (IM-qTOF; Agilent Technologies, Waldbronn, Germany) were used for all LC-MS analyses. Separation was carried out on an Aeris™ Peptide XB-C18 column (150 x 2.1 mm ID; 1.7 µm) (Phenomenex, Torrance, CA, USA) thermostated at 40°C. Mobile phase A and B consisted of H_2O + 0.1% FA and ACN/H_2O/FA (acetonitrile/water/formic acid; 90:10:0, v/v/v), respectively. Peptides were dissolved with an adequate volume of ACN/H_2O/FA to reach 0.5 µg/µL per sample and 5 µg of peptides were injected on the column for each run. MS experiments were operated using positive electrospray ionization. For each sample, data were acquired using two acquisition modes, namely data-dependent acquisition (DDA) and data-independent acquisition (DIA), as previously described.[18]

Data treatment and protein identification

Before protein identification, DIA MS/MS files were first reprocessed to recalibrate the mass axis using the reference masses. Then, LC and IM dimensions were smoothed using PNNL PreProcessor software (Pacific Northwest National Laboratory, Richland, WA, USA). Afterward, a 4D-ion mobility feature extraction (IMFE) algorithm was applied on the datafile using "peptides" as isotope model, charge state no more than 7 and ion intensity above 50 in order to generate a list of ion features. Finally, extraction and alignment of

MS/MS spectra with similar retention time (± 10 s) and drift time (± 0.5 ms) as the features were exported in PKL file.

DDA MS/MS files and pkl format files generated from DIA MS/MS were imported into Spectrum Mill Software (Agilent Technologies; Santa Clara, CA, USA) for peptide sequencing. Carbamidomethylation of cysteines was selected as fixed modification and oxidation of methionines, deamidation of asparagines and glutamines as well as carbamidomethylthio-propanoylation of lysines were selected as variable modifications. Trypsin was set as digestion enzyme and a maximum of 2 missed cleavages was allowed. Mass tolerance for precursor and product ions were set at 20 and 50 ppm, respectively. Peptides were considered as reliable hit by having a fragmentation score > 5 and spectrum purity index (SPI) > 50%. These peptides were exported for further statistical analysis.

Subcellular localization and tissue distribution

To define the subcellular localization and the protein expression in different organs, different databases (resumed in table 1) were consulted. The Panther, COMPARTMENTS and the Human Protein Atlas were used to confirm the cellular localization. For the Human Protein Atlas, the results with enhanced, approved and supported reliabilities were retained for further analysis. To create a protein tissue distribution, expression values for different human tissues were obtained from the Human Protein Atlas, the Human Proteome Map (HPM) (http://www.humanproteomemap.org/download.php, access date: 29/05/2019), the Proteomics Database (PDB) (https://www.proteomicsdb.org/proteomicsdb/#api, access date: 17/06/2019) and a database composed of 29 healthy human tissues (PXD010154, access date: 23/06/2019).

Table 1: The different databases that were consulted to define the exact cellular localization of proteins.

Database name	Website and Access Date	Retained parameters	Additional excluded parameters
Panther Database	www.pantherdb.org 24/09/2019	membrane, cell junction, extracellular membrane and synapse	NA
COMPARTMENTS Database	compartments.jensenlab.org 23/02/2019	plasma membrane, extracellular matrix, periphery, synapse, integrin complex, cell adhesion, cell surface and extracellular region	Exclusion of cytoplasmic, cytoplasm, endosome, mitochondria, nuclear, nucleus and exon were excluded
Human Protein Atlas	www.proteinatlas.org 29/05/2019	cell junction, plasma membrane, focal adhesion sites and peroxisomes	NA

Expression binning and data aggregation

To visualize the tissue expression of these proteins, we merged information coming from proteomic studies performed on organ biopsies and further studied by immunohistochemistry or mass spectrometry. The protein expression values were categorized into 4 categories ("Not detected", "Low", "Medium" and "High") based on thresholds determined by mean-SD, mean and mean+SD of Gaussian distribution fitted to log10 values. All identifiers were converted into UniProt ID's. A consensus list of the different organs is shown in Figure 2.B. For each dataset, tissues were binned into relative categories from the consensus list. Finally, all datasets were aggregated into a single dataset. All nomenclature conversions were applied by BioMart (https://www.ensembl.org/biomart/martview/). For nomenclature conversion and binning, in case of multiple annotations for the same entity, the higher value was always kept.

Transcriptomics data retrieval and analysis

Experiment-normalized GSE68891 and GSE83503 (IFM) microarray datasets were downloaded.[19,20] GSE68891 dataset consists of MM cells (n=126), peripheral blood B-cells (n=11) and bone marrow B-cells (n=7).[19] Gene expression levels were compared between MM samples and two B-cell populations, respectively. On the other hand, in the IFM GSE83503 dataset, MM (n=602) and plasma cell (n=9) populations were compared.[20] For all comparisons, (MM vs normal plasma cells, MM vs peripheral B-cells and MM vs bone marrow B-cells), MA (log ratio vs average) plots of MM vs control condition were generated. After fitting a Gaussian distribution with M values, the genes with higher values of M from mean+2 standard deviation (SD), together with A values above the mean, were selected as differentially highly expressed genes (DHE).

Pairing strategy

Initially, the list of 11645 candidate proteins, identified by mass spectrometry, was merged with the proteins identified in the Oldham 2020 study.[21] We analyzed articles, published between 1995 and 2021 and identified on Medline by using the keywords “antigen”, “membrane”, “surface” and “myeloma”. This literature search retained 552 additional surface proteins. Our final list was filtered based upon the subcellular localization. Furthermore, the proteins that were not coded by any of the DHE genes, those having a high expression in any non-immune tissue and those having overall high expression in all tissues were excluded. The remaining 52 proteins were paired with each other. The pairs which, in combination, had no expression in vital tissues and had at most low expression in non-vital tissues were selected as viable pairs (NA values were ignored).

Identification of patient subgroups

The patients were categorized into transcriptomic subgroups using gene set variation analysis (GSVA) with signature genes identified by Zhan *et al.*[22] Copy number variation (CNV) information of homologous recombination deficiency, t(4;14), t(11;14), t(14;16), CKS1B_Gain (1q gain), CDKN2C_Loss (1p loss), RB1_Loss (Monosomy 13), BI_TP53 (TP53 del), obtained from the supplementary information provided by COMMPASS data, is used to classify patients into low/high risk categories based on cytogenetic abnormalities.[23] Samples having two of the abnormalities t(4;14), 1q gain, 1p loss or 17p del, were categorized as double hit. Any sample having three of them is categorized as triple hit.

Gene expression data scaling for visualization

To visualize the multiple datasets comparably, all expression values in each dataset were min-max scaled. In order to prevent any outlier effects on the

high end of the distribution, the max value was replaced by the 99th percentile of the distribution.

Staining by flow cytometry

Hemolysis (NH_4Cl, 15 minutes) on the bone marrow aspirates was first performed before carrying out membrane staining. These membrane staining were performed on different MM cell lines (LP-1, RPMI-8226, KMS-12-BM, U266, MOLP-2, OPM-2, NCI-H929, MM1.S) and bone marrow cells using the same protocol. Cells were incubated for 20 minutes at room temperature in the presence of predefined antibody concentrations. The cells were then fixed (PAF 3%; paraformaldehyde) before being analyzed by flow cytometry. The anti-human antibodies used are listed in Suppl Table 1. The anti-ET_B mAb RB49 was produced after DNA-immunization of C57BL/6 mice and its affinities and binding epitopes determined. [24,25] For our flow cytometry studies, RB49 was directly conjugated to Alexa Fluor 488. Flow cytometry analyses were performed on a FACSCanto II flow cytometer (BD Biosciences, Franklin Lakes, NJ, USA) and data were analyzed using BD FACSDiva Software V10 (BD Biosciences) or Kaluza V2.1 (Beckman Coulter, Brea, CA, USA). Bone marrow samples from 13 newly diagnosed MM patients, 7 patients with relapsed/refractory disease and 18 healthy persons were obtained and used for the validation of the antigen expression. Clinical data of the MM patients can be found in Suppl Table 2. The RB49, conjugated to Alexa Fluor 488, was used confirm ET_B expression on 10 samples of newly diagnosed myeloma patients (Suppl Table 6).

Results

Immunotherapeutic candidates detected by integrated analysis of proteomics and transcriptomics

By applying surface proteomics on 6 different cell lines and subsequent mass spectrometry, we identified 11645 proteins. We added 846 proteins identified in the Oldham 2020 study.[21] Three data sources that describe the subcellular protein localization (Human Protein Atlas, Compartment and PantherDB) were able to reduce this list to 4427 proteins that are known to be expressed on the cell membrane. A literature search identified 522 proteins that were added to this list.

An ideal target for immunotherapy should be (over)expressed on tumor cells and absent on normal tissue counterparts. We accessed the GSE83503 dataset that included microarray data of malignant plasma cells taken from 602 MM patients and normal plasma cells from 9 healthy volunteers. Contrasting expression profiles of MM cells with normal plasma cells resulted in 214 DHE genes in MM cells (Figure 2.C right panel). We further analyzed the GSE68891 dataset comparing transcriptomics of MM cells from 144 MM patients with non-malignant B-cells, isolated from the peripheral blood (n=11) and bone marrow (n=7), yielding 450 (Figure 2.C left panel) and 489 (Figure 2.C middle panel) DHE genes respectively. Combining the results from both datasets, we obtained 756 genes (Figure 2.D) encoding 2818 proteins. Mapping these results on cell surface proteins identified in proteomics analysis further narrowed down this list to 209 surface proteins that are overexpressed in myeloma cells.

Table 2: List of the 23 proteins identified by the algorithm.

Gene names	Protein names	
UBE2QL1	A1L167	E2Q-like ubiquitin-conjugating enzyme 1
PLXNC1	O60486	Plexin-C1
PRL3	O75365	Protein-tyrosine phosphatase of regenerating liver 3
DKK1	O94907	Dickkopf-related protein 1
IL6R	P08887	Interleukin-6 receptor subunit alpha (IL-6 receptor subunit alpha)
VDR	P11473	Vitamin D3 receptor
ICAM2	P13598	Intercellular adhesion molecule 2
EPOR	P19235	Erythropoietin receptor
NR1D1	P20393	Nuclear receptor subfamily 1 group D member 1
ETRB	P24530	Endothelin receptor type B
CD27	P26842	CD27 antigen
MC4R	P32245	Melanocortin receptor 4
IL5RA	Q01344	Interleukin-5 receptor subunit alpha (IL-5 receptor subunit alpha)
BCMA	Q02223	Tumor necrosis factor receptor superfamily member 17 (B-cell maturation protein)
FRMD6	Q96NE9	FERM domain-containing protein 6
ZNF385A	Q96PM9	Zinc finger protein 385A
TRB1	Q96RU8	Tribbles homolog 1
TAPBPL	Q9BX59	Tapasin-related protein (TAPASIN-R)
SLCO5A1	Q9H2Y9	Solute carrier organic anion transporter family member 5A1
SPAG4	Q9NPE6	Sperm-associated antigen 4 protein
PPARGC1A	Q9UBK2	Peroxisome proliferator-activated receptor gamma coactivator 1-alpha
DEXRAS1	Q9Y272	Dexamethasone-induced Ras-related protein 1
CEACAM8	P31997	Carcinoembryonic antigen-related cell adhesion molecule 8

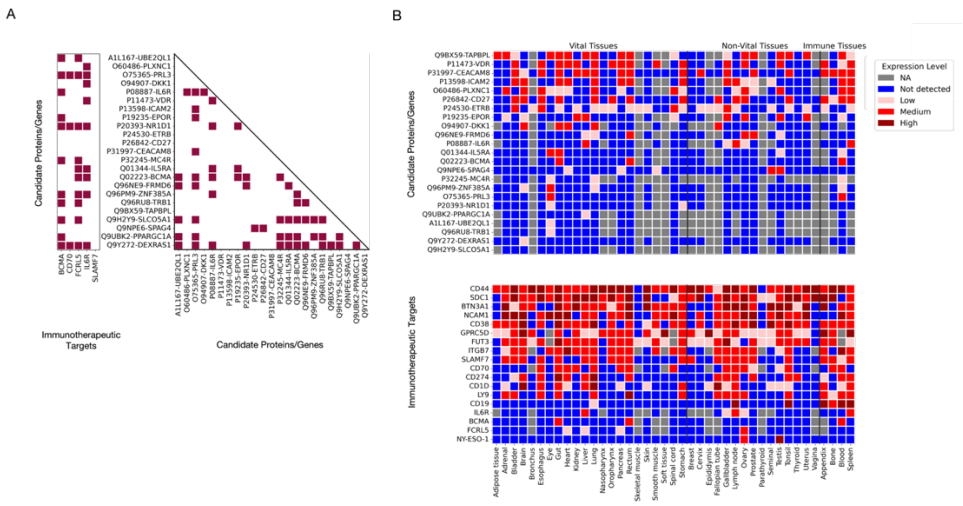

Figure 3: Tissue expression and pairing of candidate and existing immunotherapeutic targets. (A) Viable pairs between candidate proteins/genes and existing immunotherapeutic targets (left) as well as self-combinations (right). Viable pairs are selected based on having no expression in vital tissues and at most low expression in non-vital tissues as pairs. **(B)** Tissue expression of candidate proteins/genes (top) and existing immunotherapeutic targets (bottom).

In order to assess the expression levels of identified proteins throughout the body, a consensus list of 42 organ entities was created that was further subdivided in vital, non-vital and immune tissues. Based on their tissue distribution, we removed proteins with a high protein expression in any tissue, except for immune tissues. We retained 52 proteins that could be used for further combinatorial pairing. Protein pairs were selected if one of the partner proteins showed 'no detection' in a vital tissue. Similar selection criteria were proposed for non-vital tissues with the exception that a low expression of both antigens was allowed in these tissues. To prevent exclusion of candidates due to missing information, NA values were ignored. After applying these criteria, we identified 23 proteins (Table 2) with 55 possible combinations (Figure 3.A right panel). The tissue distribution of these 23 proteins can be found in Figure 3.B top panel. We further checked the tissue distribution of existing immunotherapeutic targets

(Figure 3.B bottom panel) and obtained possible pairs between our candidates and existing targets (Figure 3.A left panel). From this list, we removed the secreted protein DKK1 and 8 other proteins with a suspected intracellular localization, including UBE2QL1, VDR, NR1D1, ZNF385A, TRB1, PPARGC1A, TAPBPL and FRMD6.

Identification of 6 novel combinatorial targets

With flow cytometry, we checked the surface expression of the 14 remaining proteins and of 3 proteins with favorable tissue distribution already used in immunotherapeutic strategies (NY-ESO-1, CD70 and FCRL5) on 8 MM cell lines. Nevertheless, FCRL5 was not analyzed at this stage as it is known to be expressed by only one MM cell line namely MOLP-2 cell line. Table 3 summarizes the presence and expression levels of these proteins on the cell lines. The expression of IL5RA, SPAG4, NY-ESO-1 and EPOR could not be confirmed. ET_B was expressed by all cell lines, PLXNC1 by 7, BCMA, MC4R and SLCO5A1 by 6, PRL3, IL6R and ICAM2 by 5, DEXRAS1 by 4, CD70 by 3, and CD27 and CEACAM8 by only one of the cell lines. Targets that were not detected or that were only detected in one cell line were eliminated. Thus, based on these expression profiles, the list of potential candidates was narrowed down to 10 remaining proteins for further studies on primary patient samples.

Indeed, the expression of individual proteins was subsequently checked on bone marrow samples of 20 MM patients (Table 4). FCRL5 was included in the analysis at this step. All the targets could be detected but with variable expression frequencies. FCRL5, BCMA and ICAM2 were expressed by all patients, IL6R by 85%, ET_B by 75%, SLCO5A1 by 65% and PRL3 by 50%, while MC4R, DEXRAS1, CD70 and PLXNC1 were only expressed by 14-36% of patients.

To avoid toxicity on hematopoietic stem cells or immune effector cells (T and NK cells), we evaluated the expression of these 11 proteins on samples of normal plasma cells, T and NK cells as well as $CD34^{+}$ HSC from 18 healthy donors (Figure 4.A and Suppl Tables 3,4 and 5).

Table 3: Frequencies of expression of 16 target antigens on 8 MM cell lines.

	LP-1	RPMI-8226	MOLP-2	U266	OPM-2	KMS-12-BM	NCI-H929	MM1.S	Freq. of exp. (%)	Freq. of exp. among positive cells (%)		
										+++	++	+
ETRB	+	++	++	+++	+	+	+	+	**100**	12.5	25	62.5
MC4R	+	-	+	++	-	+	+	+	**75**	0	16.7	83.3
ICAM2	+++	+++	+++	+++	-	+++	-	-	**62.5**	100	0	0
EPOR	-	-	-	-	-	-	-	-	**0**	0	0	0
DEXRAS1	+	-	-	+	-	-	+	+	**50**	0	0	100
NY-ESO-1	-	-	-	-	-	-	-	-	**0**	0	0	0
CEACAM8	-	-	-	-	-	-	-	+	**12.5**	0	0	100
CD70	+++	-	-	+++	-	++	-	-	**37.5**	66.7	33.3	0
IL5RA	-	-	-	-	-	-	-	-	**0**	0	0	0
SLCO5A1	+	+	+	+++	+	++	-	-	**75**	16.7	33.3	66.7
IL6R	+	++	+++	++	-	++	-	-	**62.5**	20	60	20
BCMA	++	+	+	-	-	+++	+++	++	**75**	33.3	33.3	33.3
CD27	-	-	-	-	-	+	-	-	**12.5**	0	0	100
PLXNC1	+	++	++	+	-	++	++	++	**87.5**	0	71.4	28.6
PRL3	++	-	-	++	-	+	++	+++	**62.5**	20	60	20
SPAG4	-	-	-	-	-	-	-	-	**0**	0	0	0

-: negative cells; +: low positive cells; ++: intermediate positive cells; +++: high positive cells; Freq. of exp.: frequency of expression

An additional selection criterion for pairing was based on the protein expression on these normal BM populations. Indeed, potential pairs that showed a potential expression on normal BM cells were filtered out. Moreover, only the pairs with viable combinatorial tissue expression were retained. The remaining pairs were further investigated for their combined expression frequency on MM cells (Figure 4.B). The pairs with a combined expression frequency of >40% (2 of which were >70%) were selected as top findings (Figure 4.C).

Table 4: Frequencies of expression of 11 target antigens on myeloma plasma cells from the bone marrow of MM patients. The last two lines of the table show the distribution of the expression frequencies between the positive cells and the partial positive cells among the total positive cells.

		ETRB	MC4-R	ICAM-2	DEXRAS1	CD70	FCRL5	SLCO5A1	IL6R	BCMA	PLXNC1	PRL-3
Patient 1		ND	ND	ND	ND	ND	+	+	+	+	ND	ND
Patient 2		+	+	ND	ND	-	+	+	+	+	ND	+
Patient 3		ND	ND	ND	ND	-	+	+	+	+	ND	+/-
Patient 4		+	-	ND	ND	-	+/-	+/-	-	+	ND	+/-
Patient 5		ND	ND	ND	ND	-	+	+	+	+	ND	+/-
Patient 6		+/-	-	ND	ND	-	+	-	+/-	+/-	ND	+/-
Patient 7		+/-	-	ND	ND	-	+	+	+	+	ND	-
Patient 8		ND	ND	ND	ND	-	+	+/-	+	+	ND	-
Patient 9		+/-	+/-	ND	ND	-	+	+	+	+	ND	+
Patient 10		+	+/-	ND	ND	-	+	+	+	+	ND	-
Patient 11		+/-	+/-	ND	ND	-	+	-	+	+/-	ND	-
Patient 12		ND	ND	ND	ND	-	+	+	+	+	ND	+/-
Patient 13		ND	ND	ND	ND	-	+	+/-	+	+	ND	ND
Patient 14		+	-	+	-	+	+	+/-	-	+	+	+
Patient 15		-	-	+	+	+/-	+	+/-	-	+	-	-
Patient 16		+/-	-	+	-	+	+	-	+	+	-	-
Patient 17		-	-	+	-	+/-	+	-	+/-	+	-	+/-
Patient 18		-	+	+	ND	-	+	-	+	+	-	-
Patient 19		ND	-	+	+/-	-	+	-	+	+	-	-
Patient 20		ND	-	+	-	-	+	-	+	+	-	-
Freq. of exp. (%)		**75**	**35.7**	**100**	**33.3**	**21.1**	**100**	**65**	**85**	**100**	**14.3**	**50**
Freq. of exp. among + cells (%)	+	44.4	40	100	50	50	95	61.5	88.2	90	100	33.3
	+/-	55.6	60	0	50	50	5	38.5	11.8	10	0	66.7

-: negative cells; +/-: partial positive cells; +: positive cells; Freq. of exp.: frequency of expression; ND: not determined

Concerning off target toxicity, we prioritized no expression in any vital organs and tolerated at most low expression in non-vital organs. However, a more stringent analysis where the target expression is not tolerated in any tissue, except

for immune tissues, is valuable. Increasing the stringency of the selection criteria removed 7 possible pairs identified at the initial step of our analysis (Suppl Figure 1) but did not affect the final results obtained validating the antigen expression on primary myeloma cells by flow cytometry.

Transcriptional profiles of target antigens in transcriptional and cytogenic patient subgroups

MM remains a heterogeneous disease with biological differences in tumor development and associated clinical outcomes. From a molecular point of view, the transcriptional profiles of patients can be categorized based on the UAMS classification proposed by Zhan *et al*.[22] Using the GSE83503 dataset, we categorized patients into UAMS categories and compared gene expression in plasma cells from healthy donors and myeloma patients (Figure 5.A). We observed a heterogeneous expression of our identified proteins ET_B, MC4R, PRL3, as well as the current targets for immunotherapy CD44, ITGB7, NCAM1. This heterogeneity was confirmed in the COMMPASS dataset that we used as a validation cohort of our results (Suppl Figure 2).

A more clinically relevant categorization can be made based on cytogenetic abnormalities that are only available in the COMMPASS dataset and have recently been annotated.[23] The identified cytogenetic abnormalities can be categorized into low-risk, standard-risk and high-risk groups. Notably, the heterogeneity observed in the molecular classification was also observed in this patient stratification (Figure 5.B). In both datasets, immunotherapeutic targets BCMA, FCRL5, CD38, GPRC5D, SDC1 (CD138) and SLAMF7 stood out with consistent high expression levels in all patient subgroups. From our candidates, IL6R and PRL3 can also be added to this list.

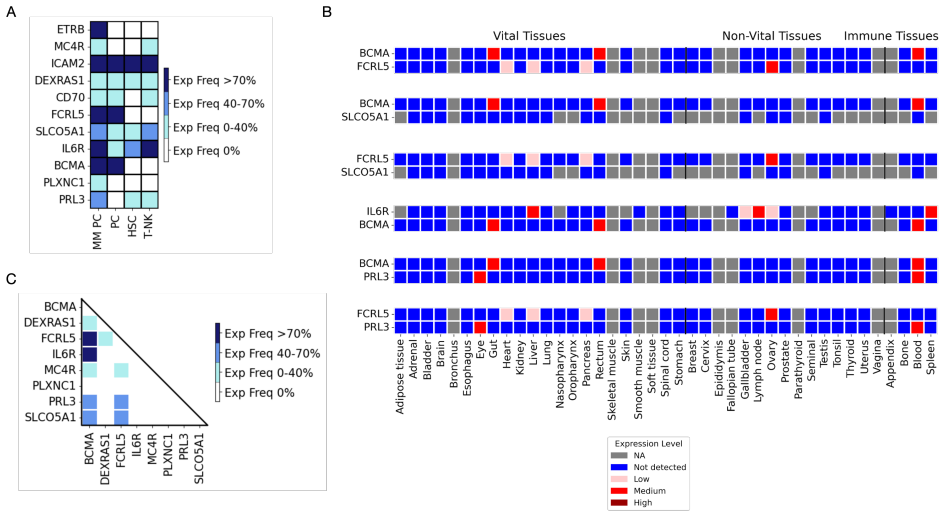

Figure 4: Selection of ideal combinatorial pairs. (A) The frequencies of expression of candidate genes on MM plasma cells (MM PC) from the bone marrow of MM patients and on normal plasma cells (PC), normal $CD34^{+}$ hematopoietic stem cells (HSC), normal T and NK cells (T-NK) from the bone marrow of healthy donors. **(B)** Tissue expression distributions of the genes in the top combinatorial target pairs. **(C)** The combined expression levels for each possible pair in MM cells.

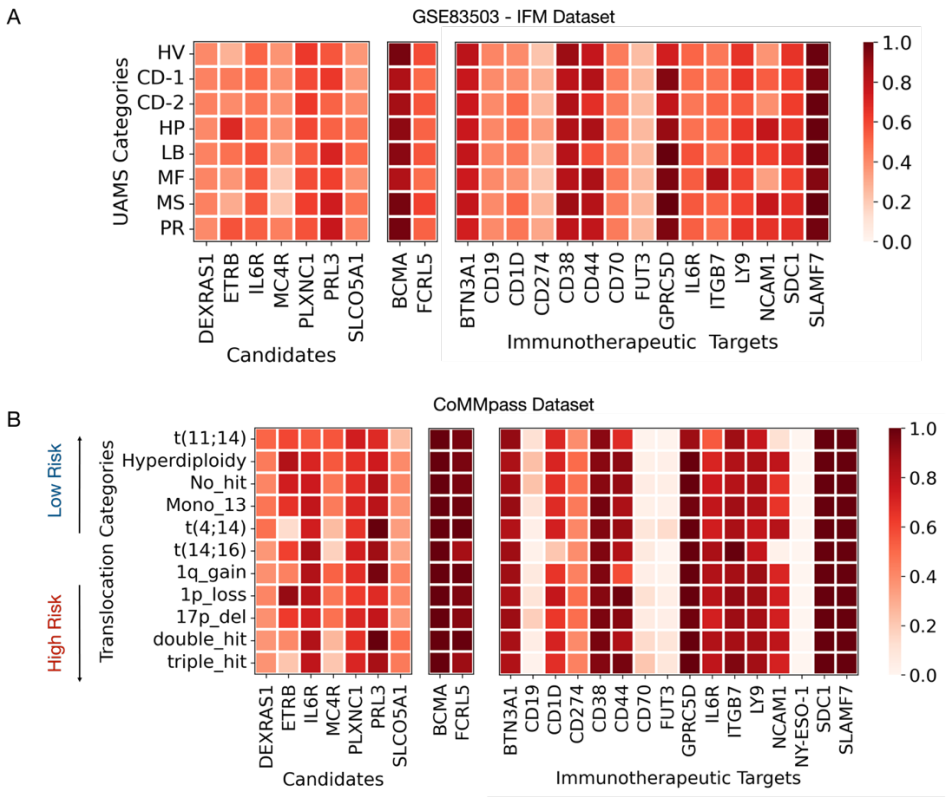

Figure 5: Median expression (scaled) profiles of genes among transcriptional and cytogenetic patient categories. (A) Median expression profiles of candidate and immunotherapeutic target genes over UAMS categories in the IFM dataset (GSE83503). **(B)** Median expression profiles of candidate and immunotherapeutic target genes over cytogenetic categories in the COMMPASS dataset. In both datasets, the data is min-max scaled using 99th percentile as the maximum value.

Endothelin Receptor B as a single target

Our study revealed ET_B as a potential target for MM. This protein was expressed by MM cell lines and primary myeloma cells (results from one of these patients is Illustrated in Figure 6.C). It also presented a global low expression profile throughout the body (Figure 3.B). Inside the bone marrow, ET_B is only expressed by MM plasma cells. These results were confirmed by single cell RNA studies on $CD38^+$ purified myeloma cells and other BM cells from 13 MM

subjects (Figure 6.A).[26] Moreover, the expression of ET_B has prognostic significance. In the COMMPASS data set, patients with a high ET_B mRNA level had better overall survival compared to patients with low ET_B mRNA levels (Figure 6.D). This survival benefit can be explained by a lower mRNA expression in patients with high-risk cytogenetics, such as t(4;14), double hit and triple hit abnormalities (Figure 6.B). When looking at the level of mRNA expression in the different molecular subgroups, the MS-subgroup (overexpression of *FGFR3* and *MMSET* genes induced by t(4;14)) displayed lower expression compared to other subgroups (Suppl Figure 3). ET_B is a G-protein-coupled receptor (GPCR) that changes its confirmation upon activation with new epitopes becoming exposed.[27] Rendomab B49 is a murine IgG1kappa monoclonal antibody that recognizes such an epitope near the N-terminal of the receptor.[25] We obtained the RB49 antibody conjugated to Alexa Fluor 488 and compared its binding to primary myeloma cells with the binding of a control IgG1k antibody. In 8 of the 10 (80%) tested primary MM samples, we could confirm the binding of RB49 to primary malignant plasma cells (results from one of these patients is Illustrated in Figure 6.E). Patient characteristics and obtained flow cytometry results can be found in Supple Table 6.

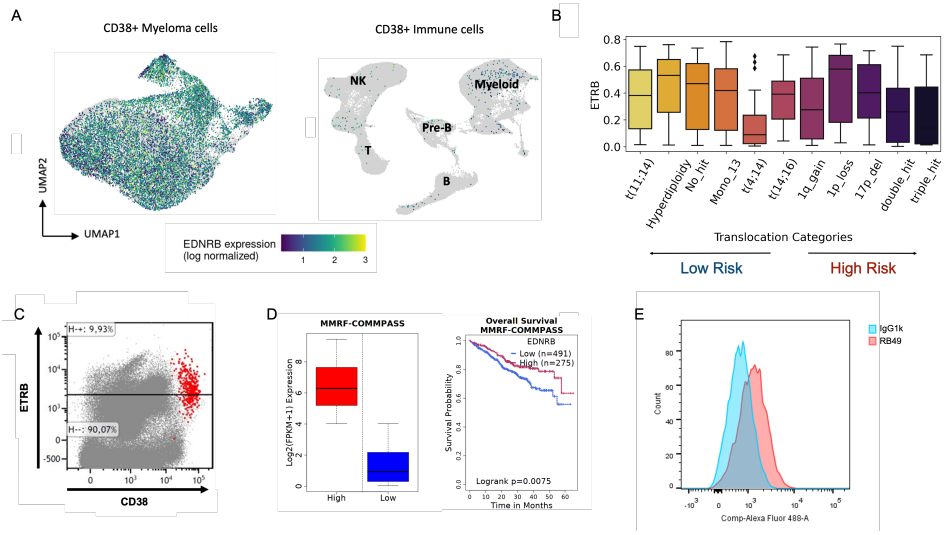

Figure 6: The expression profiles of ET_B gene at proteomic and transcriptional level as well as in different patient subgroups. (A) Transcriptomic expression of ET_B (EDNRB) at single cell level in bone marrow shown among myeloma plasma cells (left) obtained from 13 MM subjects, and $CD38^+$ immune cells (right) obtained from 13 MM and 5 healthy subjects.[28] (B) Expression profile among different cytogenetic categories in COMMPASS dataset. (C) Flow cytometry analysis conducted on the bone marrow sample from MM patient 10, as a sample. The population in red represents $CD38^+$ MM plasma cells. (D) Results of the survival analysis conducted by SurvivalGenie.[29] Patients in the COMMPASS dataset are divided into low- and high-expression categories using the cutp option (left) and survival analysis is performed (right). (E) Histogram illustrating the flow cytometry results with the control IgG1k (in blue) and RB49 (in red), confirming the expression of ET_B.

Discussion

MM is a highly heterogeneous and dynamic disease in which immune dysfunction plays an important role in disease pathogenesis, progression, and drug resistance.[30] Although patients may have long responses to treatment, most of them will eventually develop treatment-resistant disease. Recently, new personalized treatment approaches, such as immunotherapy, that offer the advantage of specifically targeting tumor cells have been developed.

Herein, we present an approach that enables the discovery of new immunotherapeutic targets in MM. We have assembled a comprehensive MM surfaceome dataset, combining previously published protein repositories, transcriptomic data that compared RNA of myeloma cells to normal plasma cells and B-cells, and our own cell surface proteomics performed on six MM cell lines. We added data on tissue distribution to take into account the systemic expression of potential targets and to avoid toxicity in healthy organs.

The expression of 11 candidate targets was verified by flow cytometry on bone marrow samples from 20 MM patients and 18 healthy donors. Seven of them (ET_B, ICAM2, FCRL5, SLCO5A1, IL6R, BCMA) were detected in more than 50% of MM patients' BM. Among these targets, ICAM2, SLCO5A1 and IL6R were found on normal T-NK cells and/or on $CD34^+$ HSC and could potentially lead to fratricide of effector cells or in the elimination of hematopoietic stem cells. The remaining three targets, BCMA, FCRL5 and ET_B, have favorable expression profiles. BCMA and FCRL5 have already been tested in the context of MM in immunotherapeutic strategies, such as CAR-T-cells, antibody-drug conjugates, BsAbs, etc. In contrast, ET_B, a G-protein coupled receptor, has been scarcely studied in the context of MM.

The endothelin axis is involved in the development of an increasing number of tumors, by affecting cell proliferation, migration, invasion, epithelial-mesenchymal transition, osteogenesis and angiogenesis.[31] Vaiou et al. showed that Endothelin-1 (ET-1), supports MM cell viability through both autocrine and paracrine activation, since both myeloma cells and endothelial cells produce ET-1. ET-1 binds to 2 receptors: Endothelin Receptor A (ET_A) and ET_B and its downstream effects are mediated by the MAP kinase pathway and ubiquitin proteasome system.[32] Addition of selective agonists of ETRA or ET_B or with the dual receptor antagonists bosentan or macitentan resulted in a significantly decreased viability of MM cell lines. [33,34] More recently, the same group treated MM xenograft models with macitentan which resulted in reduced tumor load and myeloma-induced angiogenesis; both explained by an inhibitory effect on HIF-1 alpha and secretion of angiogenic cytokines.[35] Although ET-1 supports MM cell survival and antagonists of ET_A and ET_B are able to reduce MM cell growth, CRISPR screens could not confirm a dependency of MM cell lines to ET_B for their survival (Suppl figure 3).

As shown in Figure 6, ET_B is well expressed by MM cells, has a favorable tissue distribution and shows high expression among the majority of patient subgroups. Upon activation and binding of endothelin, this receptor changes its conformation.[27] Hosen *et al.* demonstrated that the active conformer of a protein can serve as a specific therapeutic target, as it is the case with integrin β7. Indeed, these authors identified a mAb specifically targeting the N-terminal region of the β7 chain, which is inaccessible when the integrin is quiescent but exposed in the active conformation.[36] Herbert *et al.* demonstrated that this is also the case with ET_B. They produced different mAbs targeting this receptor, including RB49, which binds to an epitope located in the N-terminal domain of ET_B.[25] In this work, we show that RB49 binds to MM cells and we believe that its sequences can be integrated into different immunotherapy strategies, such as CAR-T-cells, BsAbs, etc., for the treatment of MM.

However, our study has some limitations. Indeed, the selection of potential targets is partially based on flow cytometry results, which can be impacted by several parameters. A major limitation is the need for specific antibodies, preferentially coupled to a fluorochrome. By limiting ourselves to the antibodies available on the market, we had to use monoclonal antibodies for certain targets and polyclonal antibodies for others. In addition, each fluorochrome can potentially influence other fluorochromes and the required compensation may result in a loss of sensitivity and resolution. Thus, weakly expressed antigens may not be detected by flow cytometry analysis. Finally, the brightness of the fluorochromes used also has an impact on the quality of the results.

The restrictive criteria that we proposed to further narrow down our selection is a second limitation of our study. Certain proteins already known and studied at present, which did not meet the selection criteria, were eliminated. For example, CD38 and GPRC5D did not have a favorable tissue expression profile were removed from the list while their use has already been shown to be beneficial for the treatment of MM.

Finally, for practical reasons, we used MM cell lines in order to make a pre-selection of proteins before moving on to primary cell samples. However, cell lines, lacking certain adhesion molecules, growth factor or chemokine receptors, are not completely representative of tumor cells of the patients. Indeed, since FCRL5 is only expressed by a single MM cell line, we did not include it in the validation studies on cell lines, although it is expressed by all patients. Thus, other targets with a limited expression on the different cell lines, are potentially missed at the first stages.

However, our algorithm can become a powerful tool for antigen identification, but researchers should be aware that the selection criteria for retaining potential antigens may eliminate potentially interesting proteins. These criteria were stringent to retain the most suitable targets (based on membrane localization and tissue distribution) and to avoid retention of false-positive proteins. The advantage of such an algorithm is that it can be modified according to tumor type and application: targets of antibody-drug conjugates should internalize after ligation of antibodies and immunotherapeutic targets should have an absent off-tumor expression. Due to the low homogeneity of target expression and the possibility of immune recognition escape and relapse, combinatorial targeting approaches are now being investigated. Our algorithm has highlighted 6 possible pairs that would be interesting to analyze more in depth in strategies, such as CAR-T/NK or BsAb.

MM is an extremely heterogenous disease, with major differences in disease presentation and complications, response to treatment and overall survival. Both molecular and cytogenetic differences drive this heterogeneity. Our results indicate that antigen expression also vary between patients and patient groups: this was particularly true for ET_B, *NCAM1*, *IL6R*, *ITB7* and *CD44*. On the other hand, integration of mRNA expression results from different cytogenetic subgroups allows identification of more specific antigens or antigen pairs. By integrating the COMMPASS dataset and annotating the different molecular or cytogenetic subgroups, we were able to identify combinatorial pairs that could potentially be used for patients in those subgroups. This COMMPASS dataset contains whole genome, whole exome, and RNA sequencing results. Although there is a good correlation between mRNA and protein levels in general in cancer,[37] we find it worth to look at protein levels in future studies on immunotherapeutic targets in specific MM patient subgroups.

The identification of new potential targets is a growing field in MM. Oldham et al.[21] and Ferguson et al.[38] focused on membrane glycoproteins, while

Di Meo et al.[39], Anderson et al.[40] and ourselves analyzed the entire set of surface proteins. The obtained datasets were either used alone or combined with transcriptomic datasets. The initial sample manipulation and sensitivity of mass spectrometry analysis may also differ from assay to assay. Thus, each study will not provide the same list of candidates, and candidates must be confirmed by other analyses. For example, Di Meo et al. demonstrated three proteins (CCR1, LRRC8D, SEMA4A) whose inactivation individually reduces the in vitro growth of MM cells by approximately 60%, 50% and 50%, respectively.[41] Anderson et al. confirmed the unique expression of SEMA4A and found that down-regulating its expression using shRNA decreased myeloma cell proliferation, increased apoptosis and delayed tumor growth. Moreover, an antibody-drug conjugate binding to SEMA4A showed enhanced cytotoxic effects in vitro and in vivo.[40] In our study, the SEMA4A protein was part of the initial list, but was eliminated at the differential expression stage. Our thresholds are probably more stringent than those used in the two previous studies.

Conclusion

By integrating proteomics, transcriptomics and datasets on tissue distribution, we identified several candidate antigens that can be used for either single-antigen targeting approaches or for combinatorial targeting. Endothelin receptor B seems a promising antigen because of its restricted expression on malignant myeloma cells and conformational change in protein structure upon activation. In addition, combinations of either existing or previously unknown antigens could be proposed. These combinations can be integrated into more selective therapies by avoiding on-target, off-tumor toxicity.

References

1. Brink M, Groen K, Sonneveld P, Minnema MC, Broijl A, Dinmohamed AG, et al. Decrease in early mortality for newly diagnosed multiple myeloma patients in the Netherlands: a population-based study. Blood Cancer J. 2021 Nov;11(11):178.

2. Lonial S, Weiss BM, Usmani SZ, Singhal S, Chari A, Bahlis NJ, et al. Daratumumab monotherapy in patients with treatment-refractory multiple myeloma (SIRIUS): an open-label, randomised, phase 2 trial. Lancet. 2016 Apr;387(10027):1551–60.

3. Dimopoulos MA, Oriol A, Nahi H, San-Miguel J, Bahlis NJ, Usmani SZ, et al. Daratumumab, Lenalidomide, and Dexamethasone for Multiple Myeloma. N Engl J Med. 2016 Oct;375(14):1319–31.

4. Palumbo A, Chanan-Khan A, Weisel K, Nooka AK, Masszi T, Beksac M, et al. Daratumumab, Bortezomib, and Dexamethasone for Multiple Myeloma. N Engl J Med. 2016 Aug;375(8):754–66.

5. Facon T, Kumar S, Plesner T, Orlowski RZ, Moreau P, Bahlis N, et al. Daratumumab plus Lenalidomide and Dexamethasone for Untreated Myeloma. N Engl J Med. 2019 May;380(22):2104–15.

6. Voorhees PM, Kaufman JL, Laubach J, Sborov DW, Reeves B, Rodriguez C, et al. Daratumumab, lenalidomide, bortezomib, and dexamethasone for transplant-eligible newly diagnosed multiple myeloma: the GRIFFIN trial. Blood. 2020 Aug;136(8):936–45.

7. Batlevi CL, Matsuki E, Brentjens RJ, Younes A. Novel immunotherapies in lymphoid malignancies. Nat Rev Clin Oncol. 2016 Jan;13(1):25–40.

8. Lejeune M, Köse MC, Duray E, Einsele H, Beguin Y, Caers J. Bispecific, T-Cell-Recruiting Antibodies in B-Cell Malignancies. Front Immunol. 2020;11:762.

9. Cho SF, Xing L, Anderson KC, Tai YT. Promising Antigens for the New Frontier of Targeted Immunotherapy in Multiple Myeloma. Cancers (Basel). 2021 Dec;13(23):6136.

10. Swamydas M, Murphy E V, Ignatz-Hoover JJ, Malek E, Driscoll JJ. Deciphering mechanisms of immune escape to inform immunotherapeutic strategies in multiple myeloma. J Hematol Oncol. 2022 Feb;15(1):17.

11. Samur MK, Fulciniti M, Aktas Samur A, Bazarbachi AH, Tai YT, Prabhala R, et al. Biallelic loss of BCMA as a resistance mechanism to CAR T-cell therapy in a patient with multiple myeloma. Nat Commun. 2021 Feb;12(1):868.

12. Da Già MC, Dietrich O, Truger M, Arampatzi P, Duell J, Heidemeier A, et al. Homozygous BCMA gene deletion in response to anti-BCMA CAR T-cells in a patient with multiple myeloma. Nat Med. 2021 Apr;27(4):616–9.

13. Burgos L, Puig N, Cedena MT, Mateos MV, Lahuerta JJ, Paiva B, et al. Measurable residual disease in multiple myeloma: ready for clinical practice? J Hematol Oncol. 2020 Jun;13(1):82.

14. Kloss CC, Condomines M, Cartellieri M, Bachmann M, Sadelain M. Combinatorial antigen recognition with balanced signaling promotes selective tumor eradication by engineered T-cells. Nat Biotechnol. 2013 Jan;31(1):71–5.

15. Perna F, Berman SH, Soni RK, Mansilla-Soto J, Eyquem J, Hamieh M, et al. Integrating Proteomics and Transcriptomics for Systematic Combinatorial Chimeric Antigen Receptor Therapy of AML. Cancer Cell. 2017 Oct;32(4):506-519.e5.

16. Banaszek A, Bumm TGP, Nowotny B, Geis M, Jacob K, Wölfl M, et al. On-target restoration of a split T-cell-engaging antibody for precision immunotherapy. Nat Commun. 2019 Nov;10(1):5387.

17. Skokos D, Waite JC, Haber L, Crawford A, Hermann A, Ullman E, et al. A class of costimulatory CD28-bispecific antibodies that enhance the

antitumor activity of CD3-bispecific antibodies. Sci Transl Med. 2020 Jan;12(525).

18. Nys G, Nix C, Cobraiville G, Servais AC, Fillet M. Enhancing protein discoverability by data independent acquisition assisted by ion mobility mass spectrometry. Talanta. 2020 Jun;213:120812.

19. Martello M, Poletti A, Borsi E, Solli V, Dozza L, Barbato S, et al. Clonal and subclonal TP53 molecular impairment is associated with prognosis and progression in multiple myeloma. Blood Cancer J. 2022 Jan;12(1):15.

20. Miannay B, Minvielle S, Roux O, Drouin P, Avet-Loiseau H, Guérin-Charbonnel C, et al. Logic programming reveals alteration of key transcription factors in multiple myeloma. Sci Rep. 2017 Aug;7(1):9257.

21. Oldham RAA, Faber ML, Keppel TR, Buchberger AR, Waas M, Hari P, et al. Discovery and validation of surface N-glycoproteins in MM cell lines and patient samples uncovers immunotherapy targets. J Immunother Cancer. 2020 Aug;8(2).

22. Zhan F, Huang Y, Colla S, Stewart JP, Hanamura I, Gupta S, et al. The molecular classification of multiple myeloma. Blood. 2006 Sep;108(6):2020–8.

23. Walker BA, Mavrommatis K, Wardell CP, Ashby TC, Bauer M, Davies FE, et al. Identification of novel mutational drivers reveals oncogene dependencies in multiple myeloma. Blood. 2018 Aug;132(6):587–97.

24. Allard B, Wijkhuisen A, Borrull A, Deshayes F, Priam F, Lamourette P, et al. Generation and characterization of rendomab-B1, a monoclonal antibody displaying potent and specific antagonism of the human endothelin B receptor. MAbs. 2013;5(1):56–69.

25. Herbet A, Costa N, Leventoux N, Mabondzo A, Couraud JY, Borrull A, et al. Antibodies targeting human endothelin-1 receptors reveal different conformational states in cancer cells. Physiol Res. 2018 Jun;67(Suppl 1):S257–64.

26. de Jong MME, Kellermayer Z, Papazian N, Tahri S, Hofste Op Bruinink D, Hoogenboezem R, et al. The multiple myeloma microenvironment is defined

by an inflammatory stromal cell landscape. Nat Immunol. 2021 Jun;22(6):769–80.

27. Shihoya W, Nishizawa T, Okuta A, Tani K, Dohmae N, Fujiyoshi Y, et al. Activation mechanism of endothelin ET(B) receptor by endothelin-1. Nature. 2016 Sep;537(7620):363–8.

28. de Jong MME, Kellermayer Z, Papazian N, Tahri S, Hofste Op Bruinink D, Hoogenboezem R, et al. The multiple myeloma microenvironment is defined by an inflammatory stromal cell landscape. Nat Immunol. 2021 Jun;22(6):769–80.

29. Dwivedi B, Mumme H, Satpathy S, Bhasin SS, Bhasin M. Survival Genie, a web platform for survival analysis across pediatric and adult cancers. Sci Rep. 2022 Feb;12(1):3069.

30. Visram A, Kourelis T V. Aging-associated immune system changes in multiple myeloma: The dark side of the moon. Cancer Treat Res Commun. 2021;29:100494.

31. Rosanò L, Spinella F, Bagnato A. Endothelin 1 in cancer: biological implications and therapeutic opportunities. Nat Rev Cancer. 2013 Sep;13(9):637–51.

32. Vaiou M, Pangou E, Liakos P, Sakellaridis N, Vassilopoulos G, Dimas K, et al. Endothelin-1 (ET-1) induces resistance to bortezomib in human multiple myeloma cells via a pathway involving the ETB receptor and upregulation of proteasomal activity. J Cancer Res Clin Oncol. 2016 Oct;142(10):2141–58.

33. Russignan A, Spina C, Tamassia N, Cassaro A, Rigo A, Bagnato A, et al. Endothelin-1 receptor blockade as new possible therapeutic approach in multiple myeloma. Br J Haematol. 2017 Sep;178(5):781–93.

34. Russignan A, Spina C, Tamassia N, Cassaro A, Rigo A, Bagnato A, et al. In reply to Schäfer et al: new evidence on the role of endothelin-1 axis as a potential therapeutic target in multiple myeloma. Vol. 184, British journal of haematology. England; 2019. p. 1052–5.

35. Russignan A, Dal Collo G, Bagnato A, Tamassia N, Bugatti M, Belleri M, et al. Targeting the Endothelin-1 Receptors Curtails Tumor Growth and Angiogenesis in Multiple Myeloma. Front Oncol. 2020;10:600025.

36. Hosen N, Matsunaga Y, Hasegawa K, Matsuno H, Nakamura Y, Makita M, et al. The activated conformation of integrin β(7) is a novel multiple myeloma-specific target for CAR T-cell therapy. Nat Med. 2017 Dec;23(12):1436–43.

37. Kosti I, Jain N, Aran D, Butte AJ, Sirota M. Cross-tissue Analysis of Gene and Protein Expression in Normal and Cancer Tissues. Sci Rep. 2016 May;6:24799.

38. Ferguson ID, Escobar BP, Tuomivaara ST, Lin YHT, Nix MA, Leung KK, et al. Defining the cell surface proteomic landscape of multiple myeloma reveals immunotherapeutic strategies and biomarkers of drug resistance. bioRxiv. 2021 Jan 1;2021.01.17.427038.

39. Di Meo F, Yu C, Cesarano A, Arafat A, Marino S, Roodman GD, et al. Mapping the High-Risk Multiple Myeloma Cell Surface Proteome Identifies T-Cell Inhibitory Receptors for Immune Targeting. Blood. 2021;138:265.

40. Anderson GSF, Ballester-Beltran J, Giotopoulos G, Guerrero JA, Surget S, Williamson JC, et al. Unbiased cell surface proteomics identifies SEMA4A as an effective immunotherapy target for myeloma. Blood. 2022 Feb;

41. Di Meo F, Yu C, Cesarano A, Arafat A, Marino S, Roodman GD, et al. Mapping the High-Risk Multiple Myeloma Cell Surface Proteome Identifies T-Cell Inhibitory Receptors for Immune Targeting. Blood. 2021;138:265.

Supplementary Information

Suppl Table 1: List of antibodies used for staining by flow cytometry.

Target	Fluorochrome	Clone	Provider
Candidate targets			
BCMA	PE-Cy7	19F2	Biolegend
IL6R	PerCP-Cy5.5	UV4	Biolegend
FCRL5	PE	509F6	BD Biosciences
$ETRBET_B$	AF647	671917	R&D Systems
MC4R	FITC	-	Biorbyt
PLXNC1	AF647	544232	BD Biosciences
SLCO5A1	PE	-	Biorbyt
PRL3	CF647	-	Biorbyt
CD70	PerCP-Cy5.5	113-16	Biolegend
IL5RA	APC	26815	ThermoFisher
EPOR	PE	38409	R&D Systems
DEXRAS1	FITC	-	Biorbyt
ICAM2	FITC	CBR-IC2/2	Biolegend
CD27	PE-Cy7	O323	Sony
CEACAM8	FITC	G10F5	Biolegend
SPAG4	AF647	H-6	Santa Cruz
NY-ESO-1	AF488	HLy9.1.25	BD Biosciences
Rb49	AF488	-	CEA (Paris, France)
Gating strategies			
CD19	APC	J3-119	IOTest (Beckman)

CD38	APC-H7	HB7	BD Biosciences
CD56	BV421	HCD56	Sony
CD16	FITC	3G8	BD Biosciences
CD45	V500	HI30	BD Biosciences
CD3	V450	UCHT1	BD Biosciences
CD34	PE	8G12	BD Biosciences
CD34	PerCP-Cy5.5	8G12	BD Biosciences
Fixable viability dye	APC-Cy7	-	Invitrogen
CD14	PE	REA599	Miltenyi
CD16	APC	B73.1	BD Biosciences
CD45	BV510	H130	BD Biosciences
CD38	Pe-Cy7	HIT2	BD Biosciences
CD56	V450	B159	BD Biosciences
Control isotypes			
Mouse IgG1	FITC	-	BD Biosciences
Mouse IgG1	PE	-	BD Biosciences
Mouse IgG1	PerCP-Cy5.5	-	BD Biosciences
Mouse IgG1	PE-Cy7	-	BD Biosciences
Mouse IgG1	APC	-	BD Biosciences

Suppl Table 2: Clinical data of the 20 MM patients. First 13 represents newly diagnosed MM patients. Later 7 represents relapse/refrectory MM patients.

	Gender	Age	Isotype	Genetics	ISS
1	Female	71 y	Lambda light chain	Not known	1
2	Male	59 y	IgG kappa	Trisomy chrom 9	2
3	Female	66 y	IgG Kappa	t(11 ;14)	3
4	Male	47 y	IgG kappa.	Hyperdiploidy	1
5	Male	65 y	IgG lambda	No abnormalities	2
6	Male	74 y	IgG lambda	+1q	3
7	Male	78 y	Kappa light chain	+1q	3
8	Male	70 y	IgG kappa	Chromotrypsis 1p	3
9	Male	73 y	IgG kappa.	Del 17p	3
10	Male	63 y	IgG kappa	T(11;14)	1
11	Female	71 y	Lambda light chain	Del 1p, +1q	1
12	Male	61 y	IgG kappa	t(11 ;14)	1
13	Male	76 y	IgG kappa	Hyperdiploidy	1

	Gender	Age	Isotype	Genetics	ISS	Prior lines
1	Female	71 y	Lambda light chain	Hyperdiploidy	1	6 (including ASCT)
2	Female	67 y	Kappa light chaine	Del17p, +1q	2	4 (including ASCT)
3	Male	58 y	Lambda light chain	Chromotrypsis chrom 17	1	3 (including ASCT)
4	Female	72 y	IgA kappa	+1q, Del 17p, t(4;14)	3	3 prior lines
5	Female	71 y	IgGkappa.	Not known	1	6 (including ASCT)
6	Female	76 y	IgG lambda	T(4 ;14), +1Q	1	2 prior lines
7	Male	68 y	IgG Lambda	+ 1q	2	2 including ASCT

Suppl Table 3: Frequencies of expression of 11 target antigens on normal plasma cells from the bone marrow of healthy donors. The last two lines of the table show the distribution of the expression frequencies between the positive cells and the partial positive cells among the total positive cells.

	ETRB	MC4-R	ICAM-2	DEXRAS1	CD70	FCRL5	SLCO5A1	IL6R	BCMA	PLXNC1	PRL-3
Donor 1	ND	ND	ND	ND	ND	ND	ND	ND	ND	ND	ND
Donor 2	-	-	+	-	-	+	-	-	+	-	-
Donor 3	-	-	+	-	+/-	+	-	-	+	-	-
Donor 4	-	-	+	-	-	+	-	-	+	-	-
Donor 5	-	-	+	-	+/-	+	-	-	+	-	-
Donor 6	-	-	+	-	-	+	+/-	-	+	-	-
Donor 7	-	-	+	-	-	+	+/-	-	+	-	-
Donor 8	-	-	+	+/-	-	+	+	-	+/-	-	-
Donor 9	-	-	+	-	+/-	+	+	+/-	+	-	-
Donor 10	-	-	+	-	-	+	+	+	+/-	-	-
Donor 11	-	-	+	-	-	+	-	+/-	+/-	-	-
Donor 12	-	-	+	-	-	+	-	-	+/-	-	-
Donor 13	-	-	+	-	-	+	-	-	+	-	-
Donor 14	-	-	+	-	-	+	-	-	+/-	-	-
Donor 15	-	-	+	-	-	+	-	-	+/-	-	-
Donor 16	-	-	+	-	-	+	-	-	+/-	-	-
Donor 17	-	-	+	-	-	+	+	-	+	-	-
Donor 18	-	-	+	-	-	+	-	-	+	-	-
Freq. of exp. (%)	**0**	**0**	**100**	**5.9**	**17.6**	**100**	**35.3**	**17.6**	**100**	**0**	**0**
Freq. of exp. among + cells (%) +	/	/	100	0	0	100	66.7	33.3	58.8	/	/
Freq. of exp. among + cells (%) +/-	/	/	0	100	100	0	33.3	66.7	41.2	/	/

-: negative cells; +/-: partial positive cells; +: positive cells; Freq. of exp.: frequency of expression; ND: not determined

Suppl Table 4: Frequencies of expression of 11 target antigens on normal $CD34^+$ HSC from the bone marrow of healthy donors. The last two lines of the table show the distribution of the expression frequencies between the positive cells and the partial positive cells among the total positive cells.

		ETRB	MC4-R	ICAM-2	DEXRAS1	CD70	FCRL5	SLCO5A1	IL6R	BCMA	PLXNC1	PRL-3
Donor 1		ND	ND	ND	ND	ND	ND	ND	ND	ND	ND	ND
Donor 2		ND	ND	ND	ND	ND	ND	ND	ND	ND	ND	ND
Donor 3		ND	ND	ND	ND	ND	ND	ND	ND	ND	ND	ND
Donor 4		ND	ND	ND	ND	ND	ND	ND	ND	ND	ND	ND
Donor 5		ND	ND	ND	ND	ND	ND	ND	ND	ND	ND	ND
Donor 6		ND	ND	ND	ND	ND	ND	ND	ND	ND	ND	ND
Donor 7		ND	ND	ND	ND	ND	ND	ND	ND	ND	ND	ND
Donor 8		-	-	+	+/-	-	-	+	+	-	-	+/-
Donor 9		-	-	+	-	-	-	+	+	-	-	+/-
Donor 10		-	-	+	-	-	-	+	+	-	-	+/-
Donor 11		-	-	+	-	-	-	-	+/-	-	-	+/-
Donor 12		-	-	+	-	-	-	-	-	-	-	-
Donor 13		-	-	+	-	-	-	-	+/-	-	-	-
Donor 14		-	-	+	-	-	-	-	-	-	-	-
Donor 15		-	-	+	-	-	-	-	-	-	-	-
Donor 16		-	-	+	-	-	-	-	-	-	-	-
Donor 17		-	-	+	-	-	-	+	+/-	-	-	-
Donor 18		-	-	+	-	-	-	-	+/-	-	-	-
Freq. of exp. (%)		**0**	**0**	**100**	**9.1**	**0**	**0**	**36.4**	**63.6**	**0**	**0**	**36.4**
Freq. of exp. among + cells (%)	+	/	/	100	0	/	/	100	42.9	/	/	0
	+/-	/	/	0	100	/	/	0	57.1	/	/	100

-: negative cells; +/-: partial positive cells; +: positive cells; Freq. of exp.: frequency of expression; ND: not determined

Suppl Table 5: Frequencies of expression of 11 target antigens on normal T and/or NK cells from the bone marrow of healthy donors. The last two lines of the table show the distribution of the expression frequencies between the positive cells and the partial positive cells among the total positive cells.

	ETRB	MC4-R	ICAM-2	DEXRAS1	CD70	FCRL5	SLCO5A1	IL6R	BCMA	PLXNC1	PRL-3
Donor 1	-	-	+	-	+/-	-	+/-	+/-	-	-	-
Donor 2	-	-	+	-	-	-	-	+	-	-	-
Donor 3	-	-	+	-	-	-	+/-	+/-	-	-	-
Donor 4	-	-	+	-	-	-	-	+	-	-	-
Donor 5	-	-	+/-	-	-	-	-	+	-	-	-
Donor 6	-	-	+	-	+/-	-	+/-	+/-	-	-	-
Donor 7	-	-	+	-	+/-	-	+/-	+/-	-	-	-
Donor 8	-	-	+	+/-	-	-	+	+/-	-	-	-
Donor 9	-	-	+	-	-	-	+	+/-	-	-	+/-
Donor 10	-	-	+	-	-	-	+	+/-	-	-	+/-
Donor 11	-	-	+	+	-	-	+	+/-	-	-	+/-
Donor 12	-	-	+	-	-	-	+	+/-	-	-	-
Donor 13	-	-	+	-	-	-	+	+/-	-	-	-
Donor 14	-	-	+	+	-	-	+	-	-	-	-
Donor 15	-	-	+	-	-	-	-	-	-	-	-
Donor 16	-	-	+	-	-	-	-	-	-	-	-
Donor 17	-	+/-	+	-	-	-	+	-	-	-	-
Donor 18	-	+/-	+	-	-	-	-	+/-	-	-	-
Freq. of exp. (%)	**0**	**11.1**	**100**	**16.7**	**16.7**	**0**	**66.7**	**77.8**	**0**	**0**	**16.7**
Freq. of exp. among + cells (%) +	/	0	94.4	66.7	0	/	66.7	21.4	/	/	0
Freq. of exp. among + cells (%) +/-	/	100	5.6	33.3	100	/	33.3	78.6	/	/	100

-: negative cells; +/-: partial positive cells; +: positive cells; Freq. of exp.: frequency of expression; ND: not determined

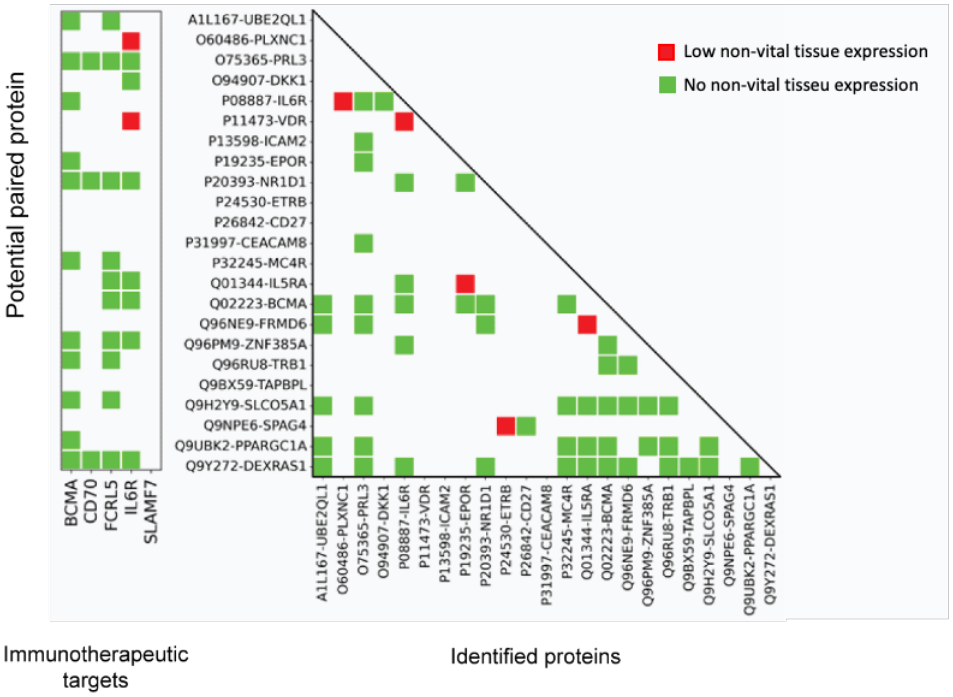

Suppl Figure 1: Identified pairs for combinatorial pairing with or without low expression in non-vital tissues. Red squares, the pairs that have low expression in at least one non-vital tissue; Green squares, the pairs that shown no expression in non-vital tissues.

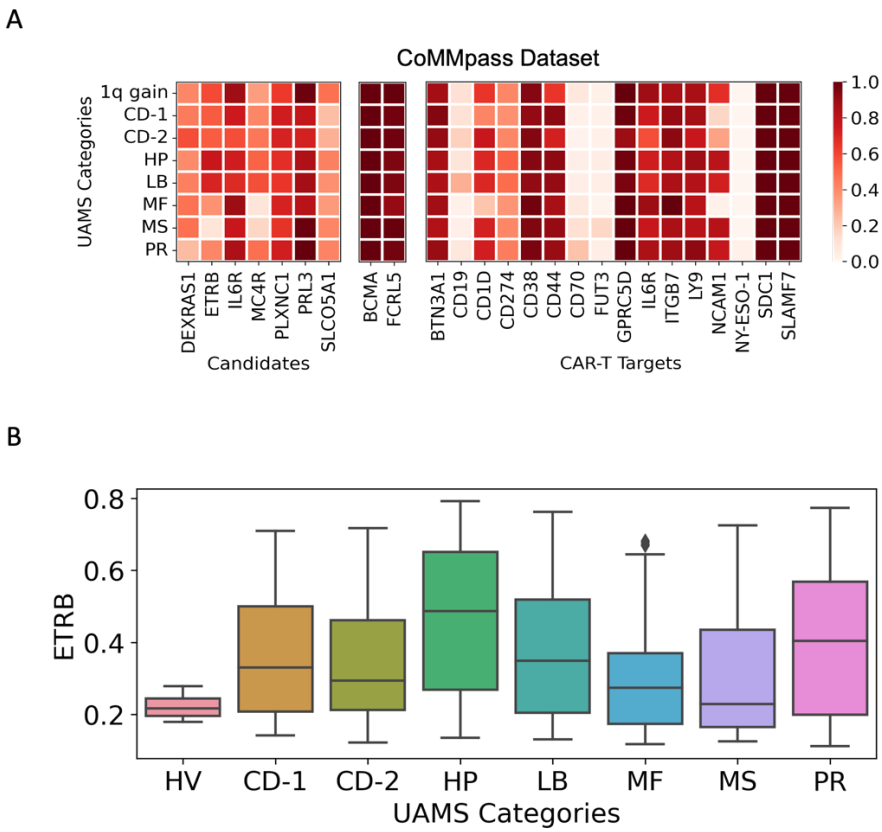

Suppl Figure 2: (A) Median expression (scaled) profiles of genes among transcriptional patient categories in the COMMPASS dataset. The transcriptional categories were obtained from the metadata of the original study. The subgroups defined in the study were binned to their relevant UAMS category. The 1q gain category was not indicated by UAMS; therefore, we have kept this category as an additional group. (**B**) ETRB mRNA expression in the different molecular subgroups. The MS-subgroup (overexpression of FGFR3 and MMSET genes induced by t(4;14)) displayed lower expression compared to other subgroups.

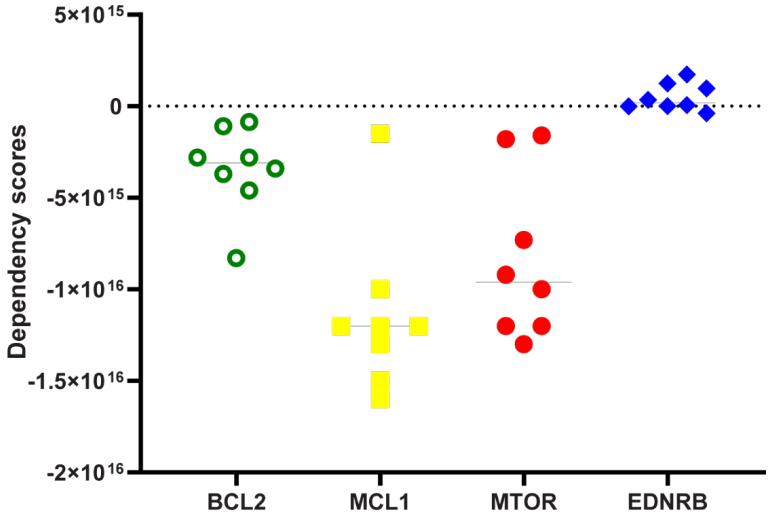

Suppl Figure 3: Gene-dependency of myeloma cell line for their survival. Publically available datasets (Depmap.org) were accessed to identify the dependency (studies by CRISPR/CAS studies) of 8 different myeloma cell lines (AMO1, INA6, JJN3, KMS-11, LP-1, MM1.S, OPM-2 and RPMI-8226) to either BCL2, MCL1, MTOR and ETRB. The more negative the values are, the higher the dependency of this cell line for survival.

Conclusions and Perspectives

Novel immunotherapeutic applications have made a significant impact on the treatment of multiple myeloma. Usage of monoclonal antibodies have been well integrated in different treatment schedules for MM treatment. Meanwhile, the promising outcomes observed in relapse/refractory patients have already led to the approval of bispecific antibodies and CART applications, paving the way for other innovative treatment options. However, despite the recent developments in the diagnostics and therapeutics, the field of multiple myeloma is subject to further improvements. This incurable malignancy is characterized by high relapse rates, demanding continuous research and innovation. The complexity of the disease biology, involving numerous genetic abnormalities and impaired immune response, makes it difficult to comprehensively understand and effectively counter.

In this dissertation, the tumor and tumor micro-environment were investigated to gain more insights for the events that take place during disease development. While the impact of the tumor micro-environment has been studied extensively, the use of next-generation sequencing provides an opportunity to gain a more comprehensive insight. Our study has revealed that dysregulation in the tumor micro-environment initiates early on during the progression of multiple myeloma and develops further as the disease progress. These findings involve increase of pro-inflammatory pathways in the tumor micro-environment, as well as certain population shifts in some of the key immune populations. Simultaneously, tumor cells exhibit up-regulation of pro-tumorigenic pathways. Exploring inter-cellular interactions, a dynamic interplay was observed between tumor cells and their micro-environment, which can induce changes in the expression of genes that are observed to be altered during transition from precursor stages to MM stage. While our findings provide a detailed

understanding of the bone marrow tumor micro-environment, there is still more to learn about other cell types like granulocytes, MDSCs, stromal cells, osteoblasts, and osteoclasts that were not included in our study.

Our study identified several ligands and receptors that align with existing literature, such as BAFF-BCMA[169,170], IL2-IL15[171] and HGF-MET/CD44[172,173], confirming their involvement in the disease. Additionally, we discovered novel interactions involving CD320, FAM3C and SERPINA1 which provide insights in disease progression and communicate potential targets for future treatment strategies. Focusing on these interactions and their downstream alterations, first in vitro and later in mouse models, may lead to a better understanding of the disease and novel therapeutics. Another interesting finding in our research was related to MIF gene. There are studies that focused on the MIF expression in cancer, including MM.[174–176] However, many of these studies focus on myeloma cells and therapeutic resistance. Yet, a recent study by Lewinsky et al.[177] showed that increased expression of CD84 in the tumor micro-environment, as a result of MIF induction, results in an immunosuppressive tumor micro-environment. Another study, conducted by Gutiérrez-González et al.[178] showed that inhibiting MIF and inducing granulocyte-macrophage colony-stimulating factor resulted in the generation of an anti-tumoral macrophage population in vitro. Together with our findings regarding the impairment in M1 macrophages and its high interaction potential with other cell types of the tumor micro-environment, further investigation of MIF up-regulation in MM should be conducted.

Our investigation has revealed significant alterations in hallmark pathways as abnormal plasma cells progress to multiple myeloma. One prominent pathway is MYC, which is known to be a prognostic factor in MM and has been extensively studied. Therapeutic approaches targeting MYC inhibition have been developed and show promise.[179,180] Similarly, oxidative phosphorylation has been investigated under metabolic alterations in MM pathogenesis and treatment

strategies have been developed to inhibit metabolic activity.[181,182] Among the identified pathways, E2F targets and G2M checkpoint are both mechanisms related to cell cycle. Dysregulation in cell cycle is a characteristic of cancer. Various factors affecting cell cycle activation and potential inhibition mechanisms can be found in the literature.[183,184] Furthermore, WNT[185–187] and NOTCH[188–190] signaling pathways have been observed in individual MM patients and associated with enhancer roles in many cancers, including MM. They have previously observed to be active in a considerable fraction of MM patients. We have confirmed this observation and demonstrated that their activation can be observed at any stage of the disease. Both mechanisms and their inhibition are studied well in the context of other cancers, as well as in MM. Therefore, their inhibition mechanisms are valuable for future personalized therapy applications. Lastly, TNF and IFN, two pro-inflammatory cytokine families, exhibit complex effects in cancer, with both anti- and pro-tumoral properties.[191–194] In our dataset, we observed early TNF activity in the tumor micro-environment even at the MGUS stage, while IFNα activity was absent in MGUS but significantly increased throughout disease progression in both the tumor micro-environment and abnormal plasma cells. IFNα has been previously associated with B-cell activation and survival.[195] Yet, despite high off-target toxicity, it has also showed potential as a therapeutic agent in MM.[196] It is important to understand the underlying mechanisms of IFNα in MM progression. With the emerging targeted therapeutic applications, its potential in early clinical trials could be explored.

The relation between old age and disease progression is an interesting association. A recent study by Urban et al.[197] focused on the commonalities between accumulation of epigenetic alterations and DNA damage. Additionally, genetic variants of the pro-inflammatory cytokines IL6 and TNFα in MM were found to be associated with age at diagnosis.[198] Moreover, it was previously shown that aging bone marrow favors memory T-cell and plasma cell survival as well as plasma cell recirculation.[199,200] Taken together, focusing the changes on

aging bone marrow could potentially shed light on the events that lead to MM progression.

In this dissertation, we also aimed of identifying novel antigens and antigen pairs for targeted immunotherapeutic applications in MM. Our study successfully identified ETRB as a potential novel target and discovered six antigen pairs that could be utilized for combinatorial targeting in MM. The initial success of our approach is encouraging for overcoming the study's limitations and exploring its further applications. Our findings should be expanded by adaptation of our methodology to different patient groups, such as high-risk, MRD positive and relapse/refractory patients. Additionally, exploring the expression of target antigens in various cytogenic and molecular patient subgroups provides valuable insights into the applicability of these targets. Validation of these findings in transcriptomics with proteomics, using primary cells, should be conducted. Furthermore, applying untargeted mass spectrometry analysis to primary patient samples instead of cell lines may uncover additional potential targets that were not detected due to differences between cell lines and primary samples. Finally, the selection criteria used in this study can be better adapted for a less strict setting, to prevent exclusion of other potential antigens.

ETRB is only targetable when it is in the active form. Although our investigation on targeting ETRB using flow cytometry yielded success in 80% of the patients, the overall abundance of the protein, in both active and inactive form, as well as its quantity, remains unexplored. To address this gap, further exploration can be conducted through targeted mass spectrometry.[201] Moreover, as a therapeutic target, an initial investigation should be conducted in vitro, to test its capability to induce cytotoxicity in MM cell lines.

In addition to ETRB as single target, we have identified six antigen pairs, suitable for combinatorial targeting. These antigens include BCMA, FCRL5,

PRL3, IL6R and SLCO51A. There are existing targeting strategies for BCMA, FCRL5 and PRL3. For the identified combinations between these antigens, combinatorial targeting strategies, can be developed and evaluated for specificity and efficacy in vitro. Particularly, BCMA and FCRL5 showed high expression frequency in both flow cytometry results of primary MM samples and transcriptomic analysis of patient subpopulations. For IL6R and SLCO51A, it is important to first understand their role in MM biology and identify a single targeting strategy, such as monoclonal antibody, which can further be adapted for combinatorial targeting.

Current treatment strategies focus on elimination of tumor cells as well as the suppression of pro-tumorigenic signals. However, these efforts are limited for the duration of the treatment. It is a major concern that if the pro-tumorigenic micro-environment is not fully eradicated, it can host a suitable environment for a rapid development of disease relapse. Therefore, development of novel applications to reshape the tumor micro-environment could potentially achieve disease eradication.

Advances in single cell approaches have been widely and quickly embraced and the increased resolution of single-cell analysis has revolutionized research in many fields. Initially, high-throughput single cell studies were limited by transcriptomics applications. Although transcriptome analysis provides valuable insights into a cell's functional state, it fails to capture crucial information related to mutations, copy number variations, chromatin accessibility, post-transcriptional modifications, spatial localization, and protein localization. These aspects, unfortunately, cannot be assessed by transcriptomics alone, and can have significant impact the functional and structural status of the cell. Recent adaptations in CITE-seq, ATAC-seq, VDJ sequencing, exome sequencing and spatial applications have allowed for the investigation of single cells in a multi-modal fashion. CITE-seq enables the investigation of the cell

surface proteome, which is a crucial information for protein-based cell typing as well as identification and quantification of target cell surface antigens. However, the potential of CITE-seq is limited by the number of antibodies that can be used, and data normalization remains challenging due to the low number of dimensions, leading to difficulties in the assessment of reliable relative abundance. In my perspective, I am optimistic about significant improvements in the application of the CITE-seq approach, which will make it an essential tool for proteomics research in MM.

The field of multiple myeloma treatment is a dynamic and rapidly evolving area of research, with a variety of strategies being developed and evaluated in clinical trials. These include promising approaches, bispecific antibodies and CART strategies. In addition to these, the recent COVID-19 pandemic has drawn attention to the use of mRNA vaccines. Their use in cancer research is a rapidly developing area. Their potential applications include in vivo CART-cell generation, improved antigen presentation by antigen-presenting cells (APCs), and direct targeting of tumor cells.[202] Consequently, mRNA vaccines hold great promise as a potential future treatment for MM.

In conclusion, our work has demonstrated novel findings regarding multiple myeloma progression and treatment. These findings not only contribute to our understanding of the disease but also introduce further research opportunities for us to discover. With hope for new beginnings to shed light over multiple myeloma…

Global References

1. Kumar SK, Rajkumar V, Kyle RA, Duin M van, Sonneveld P. Multiple myeloma. Nature Publishing Group [Internet]. 2017;3:1–20. Available from: http://dx.doi.org/10.1038/nrdp.2017.46
2. Siegel RL, Miller KD, Jemal A. Cancer statistics, 2020. CA Cancer J Clin. 2020;70(1):7–30.
3. Brigle K, Rogers B. Pathobiology and Diagnosis of Multiple Myeloma. Semin Oncol Nurs. 2017;1–12.
4. Benjamin M, Reddy S, Brawley OW. Myeloma and race: A review of the literature. Cancer and Metastasis Reviews. 2003;22(1):87–93.
5. Waxman AJ, Mink PJ, Devesa SS, Anderson WF, Weiss BM, Kristinsson SY, et al. Racial disparities in incidence and outcome in multiple myeloma: A population-based study. Blood. 2010;116(25):5501–6.
6. Raab MS, Podar K, Breitkreutz I, Richardson PG, Anderson KC. Multiple myeloma. The Lancet [Internet]. 2009;374(9686):324–39. Available from: http://dx.doi.org/10.1016/S0140-6736(09)60221-X
7. Lejeune M, Köse MC, Duray E, Einsele H, Beguin Y, Caers J. Bispecific, T-Cell-Recruiting Antibodies in B-Cell Malignancies. Front Immunol. 2020;11(May).
8. Kim D, Park D. Deep sequencing of B cell receptor repertoire. BMB Rep. 2019;52(9):540–7.
9. Bird SA, Boyd K. Multiple myeloma: an overview of management. Palliat Care Soc Pract. 2019;13:1–13.
10. Neumeister P, Schulz E, Pansy K, Szmyra M, Deutsch AJA. Targeting the Microenvironment for Treating Multiple Myeloma. Int J Mol Sci. 2022;23(14):1–19.

11. Cowan AJ, Green DJ, Kwok M, Lee S, Coffey DG, Holmberg LA, et al. Diagnosis and Management of Multiple Myeloma: A Review. JAMA - Journal of the American Medical Association. 2022;327(5):464–77.
12. Fernández De Larrea C, Kyle RA, Durie BGM, Ludwig H, Usmani S, Vesole DH, et al. Plasma cell leukemia: Consensus statement on diagnostic requirements, response criteria and treatment recommendations by the International Myeloma Working Group. Leukemia. 2013;27(4):780–91.
13. Rajkumar SV, Dimopoulos MA, Palumbo A, Blade J, Merlini G, Mateos MV, et al. International Myeloma Working Group updated criteria for the diagnosis of multiple myeloma. Lancet Oncol [Internet]. 2014;15(12):e538–48. Available from: http://dx.doi.org/10.1016/S1470-2045(14)70442-5
14. Rajkumar SV, Kumar S. Multiple Myeloma: Diagnosis and Treatment. Mayo Clin Proc [Internet]. 2016;91(1):101–19. Available from: http://dx.doi.org/10.1016/j.mayocp.2015.11.007
15. Durie BGM, Salmon SE. Clinical staging system for multiple myeloma. Cancer. 1975;36:842–54.
16. Greipp PR, Miguel JS, Dune BGM, Crowley JJ, Barlogie B, Bladé J, et al. International staging system for multiple myeloma. Journal of Clinical Oncology. 2005;23(15):3412–20.
17. Padala SA, Barsouk A, Barsouk A, Rawla P, Vakiti A, Kolhe R, et al. Epidemiology, Staging, and Management of Multiple Myeloma. Medical Sciences. 2021;9(1):3.
18. Rajkumar SV. Updated Diagnostic Criteria and Staging System for Multiple Myeloma. American Society of Clinical Oncology Educational Book. 2016;36:e418–23.
19. Palumbo A, Avet-Loiseau H, Oliva S, Lokhorst HM, Goldschmidt H, Rosinol L, et al. Revised international staging system for multiple

myeloma: A report from international myeloma working group. Journal of Clinical Oncology. 2015;33(26):2863–9.

20. Cardona-benavides IJ, de Ramón C, Gutiérrez NC. Genetic abnormalities in multiple myeloma: Prognostic and therapeutic implications. Cells. 2021;10(2):1–28.
21. Awada H, Thapa B, Awada H, Dong J, Gurnari C, Hari P, et al. A comprehensive review of the genomics of multiple myeloma: Evolutionary trajectories, gene expression profiling, and emerging therapeutics. Cells. 2021;10(8).
22. Wallington-Beddoe CT, Mynott RL. Prognostic and predictive biomarker developments in multiple myeloma. J Hematol Oncol [Internet]. 2021;14(1):1–15. Available from: https://doi.org/10.1186/s13045-021-01162-7
23. Fonseca R, Blood EA, Oken MM, Kyle RA, Dewald GW, Bailey RJ, et al. Myeloma and the t(11;14)(q13;q32); evidence for a biologically defined unique subset of patients. Blood. 2002;99(10):3735–41.
24. Furukawa Y, Kikuchi J. Molecular pathogenesis of multiple myeloma. Int J Clin Oncol. 2015;20(3):413–22.
25. Pei H, Zhang L, Luo K, Qin Y, Chesi M, Fei F, et al. MMSET regulates histone H4K20 methylation and 53BP1 accumulation. Nature. 2011;470(7332):124–8.
26. Xie Z, Chng WJ. MMSET: Role and therapeutic opportunities in multiple myeloma. Biomed Res Int. 2014;2014:6–11.
27. Corre J, Cleynen A, Robiou du Pont S, Buisson L, Bolli N, Attal M, et al. Multiple myeloma clonal evolution in homogeneously treated patients. Leukemia [Internet]. 2018;32(12):2636–47. Available from: http://dx.doi.org/10.1038/s41375-018-0153-6
28. Maura F, Bolli N, Angelopoulos N, Dawson KJ, Leongamornlert D, Martincorena I, et al. Genomic landscape and chronological reconstruction of driver events in multiple myeloma. Nat Commun

[Internet]. 2019;10(1):1–12. Available from: http://dx.doi.org/10.1038/s41467-019-11680-1

29. Kumar SK, Rajkumar SV. The multiple myelomas - Current concepts in cytogenetic classification and therapy. Nat Rev Clin Oncol [Internet]. 2018;15(7):409–21. Available from: http://dx.doi.org/10.1038/s41571-018-0018-y

30. McCubrey JA, Steelman LS, Chappell WH, Abrams SL, Wong EWT, Chang F, et al. Roles of the Raf/MEK/ERK pathway in cell growth, malignant transformation and drug resistance. Biochim Biophys Acta Mol Cell Res. 2007;1773(8):1263–84.

31. Lionetti M, Barbieri M, Todoerti K, Agnelli L, Fabris S, Tonon G, et al. A compendium of DIS3 mutations and associated transcriptional signatures in plasma cell dyscrasias. Oncotarget. 2015;6(28):26129–41.

32. Herrero AB, Rojas EA, Misiewicz-Krzeminska I, Krzeminski P, Gutiérrez NC. Molecular mechanisms of p53 deregulation in cancer: An overview in multiple myeloma. Int J Mol Sci. 2016;17(12).

33. Flynt E, Bisht K, Sridharan V, Ortiz M, Towfic F, Thakurta A. Prognosis, Biology, and Targeting of TP53 Dysregulation in Multiple Myeloma. Cells. 2020;9(2).

34. Zhan F, Huang Y, Colla S, Stewart JP, Hanamura I, Gupta S, et al. The molecular classification of multiple myeloma. Blood. 2006;108(6):2020–8.

35. Broyl A, Hose D, Lokhorst H, De Knegt Y, Peeters J, Jauch A, et al. Gene expression profiling for molecular classification of multiple myeloma in newly diagnosed patients. Blood. 2010;116(14):2543–53.

36. Lopes R, Caetano J, Ferreira B, Barahona F, Carneiro EA, João C. The immune microenvironment in multiple myeloma: Friend or foe? Cancers (Basel). 2021;13(4):1–16.

37. Godfrey J, Benson DM. The role of natural killer cells in immunity against multiple myeloma. Leuk Lymphoma. 2012;53(9):1666–76.

38. Encinas J, Castellano E. The Role of Tumor Microenvironment in Multiple Myeloma. Cancers (Basel). 2021;1–22.
39. Zhang L, Tai YT, Ho M, Xing L, Chauhan D, Gang A, et al. Regulatory B cell-myeloma cell interaction confers immunosuppression and promotes their survival in the bone marrow milieu. Blood Cancer J. 2017;7(3):2–5.
40. Wang JN, Cao XX, Zhao AL, Cai H, Wang X, Li J. Increased activated regulatory T cell subsets and aging Treg-like cells in multiple myeloma and monoclonal gammopathy of undetermined significance: A case control study. Cancer Cell Int [Internet]. 2018;18(1):1–8. Available from: https://doi.org/10.1186/s12935-018-0687-8
41. Ratta M, Fagnoni F, Curti A, Vescovini R, Sansoni P, Oliviero B, et al. Dendritic cells are functionally defective in multiple myeloma: The role of interleukin-6. Blood. 2002;100(1):230–7.
42. Brimnes MK, Svane IM, Johnsen HE. Impaired functionality and phenotypic profile of dendritic cells from patients with multiple myeloma. Clin Exp Immunol. 2006;144(1):76–84.
43. Liu TM. Stemness of Mesenchymal Stem Cells. J Stem Cell Ther Transplant. 2017;1(1):071–3.
44. Maiso P, Mogollón P, Ocio EM, Garayoa M. Bone marrow mesenchymal stromal cells in multiple myeloma: Their role as active contributors to myeloma progression. Cancers (Basel). 2021;13(11):1–28.
45. Bianchi G, Munshi NC. Pathogenesis beyond the cancer clone(s) in multiple myeloma. Blood. 2015;125(1):33–9.
46. Giannakoulas N, Ntanasis-Stathopoulos I, Terpos E. The role of marrow microenvironment in the growth and development of malignant plasma cells in multiple myeloma. Int J Mol Sci. 2021;22(9).
47. Liang Y tzu T, Lijie L, Cho S feng, Yu T, Acharya C, Wen K, et al. APRIL signaling via TACI mediates immunosuppression by T regulatory cells in multiple myeloma : therapeutic implications. Leukemia [Internet].

2019;(324):426–38. Available from: http://dx.doi.org/10.1038/s41375-018-0242-6

48. Anderson KC. Osteoclast immunosuppressive effects in Multiple Myeloma : Role of Programmed Cell Death Ligand 1. 2018;9(August).

49. Morris E V., Edwards CM. Adipokines, adiposity, and bone marrow adipocytes: Dangerous accomplices in multiple myeloma. J Cell Physiol. 2018;233(12):9159–66.

50. Paramore A, Frantz S. Bortezomib. Nat Rev Drug Discov. 2003;2(8):611–2.

51. Uckun FM. Overcoming the immunosuppressive tumor microenvironment in multiple myeloma. Cancers (Basel). 2021;13(9).

52. Robak P, Drozdz I, Szemraj J, Robak T. Drug resistance in multiple myeloma. Cancer Treat Rev [Internet]. 2018;70(August):199–208. Available from: https://doi.org/10.1016/j.ctrv.2018.09.001

53. Burwick N, Sharma S. Glucocorticoids in multiple myeloma: past, present, and future. Ann Hematol. 2019;98(1):19–28.

54. Al Hamed R, Bazarbachi AH, Malard F, Harousseau JL, Mohty M. Current status of autologous stem cell transplantation for multiple myeloma. Blood Cancer J [Internet]. 2019;9(4). Available from: http://dx.doi.org/10.1038/s41408-019-0205-9

55. Lonial S, Durie B, Palumbo A, San-Miguel J. Monoclonal antibodies in the treatment of multiple myeloma: Current status and future perspectives. Leukemia [Internet]. 2016;30(3):526–35. Available from: http://dx.doi.org/10.1038/leu.2015.223

56. Radocha J, van de Donk NWCJ, Weisel K. Monoclonal antibodies and antibody drug conjugates in multiple myeloma. Cancers (Basel). 2021;13(7):1–24.

57. Martino M, Canale FA, Alati C, Vincelli ID, Moscato T, Porto G, et al. Cart-cell therapy: Recent advances and new evidence in multiple myeloma. Cancers (Basel). 2021;13(11):1–19.

58. Rodríguez-Lobato LG, Ganzetti M, Fernández de Larrea C, Hudecek M, Einsele H, Danhof S. CAR T-Cells in Multiple Myeloma: State of the Art and Future Directions. Front Oncol. 2020;10(July):1–21.
59. Shissler SC, Lee MS, Webb TJ. Mixed signals: Co-stimulation in invariant natural killer T cell-mediated cancer immunotherapy. Front Immunol. 2017;8(NOV).
60. Mohyuddin GR, Rooney A, Balmaceda N, Aziz M, Sborov DW, McClune B, et al. Chimeric antigen receptor T-cell therapy in multiple myeloma: A systematic review and meta-analysis of 950 patients. Blood Adv. 2021;5(4):1097–101.
61. Zhou X, Einsele H, Danhof S. Bispecific antibodies: A new era of treatment for multiple myeloma. J Clin Med. 2020;9(7):1–14.
62. Swan D, Routledge D, Harrison S. The evolving status of immunotherapies in multiple myeloma: the future role of bispecific antibodies. Br J Haematol. 2022;196(3):488–506.
63. Susanibar Adaniya S, Stadtmauer EA, Cohen AD. CAR T cell therapy for multiple myeloma: What have we learned? Leukemia. 2022;36(6):1481–4.
64. Kang C. Teclistamab: First Approval. Drugs [Internet]. 2022;82(16):1613–9. Available from: https://doi.org/10.1007/s40265-022-01793-1
65. Van Oekelen O, Aleman A, Upadhyaya B, Schnakenberg S, Madduri D, Gavane S, et al. Neurocognitive and hypokinetic movement disorder with features of parkinsonism after BCMA-targeting CAR-T cell therapy. Nat Med. 2021;27(12):2099–103.
66. Shah UA, Mailankody S. Emerging immunotherapies in multiple myeloma. The BMJ. 2020;370(fig 1).
67. Shah UA, Mailankody S. CAR T and CAR NK cells in multiple myeloma: Expanding the targets. Best Pract Res Clin Haematol. 2020;33(1).

68. Stark R, Grzelak M, Hadfield J. RNA sequencing: the teenage years. Nat Rev Genet [Internet]. 2019;20(11):631–56. Available from: http://dx.doi.org/10.1038/s41576-019-0150-2
69. Weber APM. Discovering new biology through sequencing of RNA. Plant Physiol. 2015;169(3):1524–31.
70. Tang F, Barbacioru C, Wang Y, Nordman E, Lee C, Xu N, et al. mRNA-Seq whole-transcriptome analysis of a single cell. Nat Methods. 2009;6(5):377–82.
71. Svensson V, Vento-tormo R, Teichmann SA. Exponential scaling of single-cell RNA- seq in the last decade. ArXiv. 2017;
72. Baran-Gale J, Chandra T, Kirschner K. Experimental design for single-cell RNA sequencing. Brief Funct Genomics. 2018;17(4):233–9.
73. Hedlund E, Deng Q. Single-cell RNA sequencing: Technical advancements and biological applications. Mol Aspects Med [Internet]. 2018;59:36–46. Available from: https://doi.org/10.1016/j.mam.2017.07.003
74. Nguyen A, Khoo WH, Moran I, Croucher PI, Phan TG. Single cell RNA sequencing of rare immune cell populations. Front Immunol. 2018;9(JUL).
75. Pereira H, Schulze PSC, Schüler LM, Santos T, Barreira L, Varela J. Fluorescence activated cell-sorting principles and applications in microalgal biotechnology. Algal Res [Internet]. 2018;30(December 2017):113–20. Available from: https://doi.org/10.1016/j.algal.2017.12.013
76. Grün D, van Oudenaarden A. Design and Analysis of Single-Cell Sequencing Experiments. Cell. 2015;163(4):799–810.
77. Fan HC, Fu GK, Fodor SPA. Combinatorial labeling of single cells for gene expression cytometry. Science (1979). 2015;347(6222).
78. Hashimshony T, Senderovich N, Avital G, Klochendler A, de Leeuw Y, Anavy L, et al. CEL-Seq2: Sensitive highly-multiplexed single-cell RNA-

Seq. Genome Biol [Internet]. 2016;17(1):1–7. Available from: http://dx.doi.org/10.1186/s13059-016-0938-8

79. Kolodziejczyk AA, Kim JK, Svensson V, Marioni JC, Teichmann SA. The Technology and Biology of Single-Cell RNA Sequencing. Mol Cell [Internet]. 2015;58(4):610–20. Available from: http://dx.doi.org/10.1016/j.molcel.2015.04.005

80. Macosko EZ, Basu A, Satija R, Nemesh J, Goldman M, Tirosh I, et al. Highly parallel genome-wide expression profiling of individual cells using nanoliter droplets. 2016;161(5):1202–14.

81. Vitak SA, Torkenczy KA, Rosenkrantz JL, Fields AJ, Christiansen L, Wong MH, et al. Sequencing thousands of single-cell genomes with combinatorial indexing. Nat Methods. 2017;14(3):302–8.

82. Rosenberg AB, Roco CM, Muscat RA, Kuchina A, Yao Z, Gray L, et al. SPLiT-seq reveals cell types and lineages in the developing brain and spinal cord Alexander. Science (1979). 2018;360(6385):176–82.

83. Smitsman AW, Corbetta D. Library construction for next-generation sequencing: Overviews and challenges. Development [Internet]. 2010;1(2):167–203. Available from: http://www.ncbi.nlm.nih.gov/pubmed/24502796%0Ahttp://www.pubmedcentral.nih.gov/articlerender.fcgi?artid=PMC4351865

84. Ziegenhain C, Vieth B, Parekh S, Reinius B, Guillaumet-Adkins A, Smets M, et al. Comparative Analysis of Single-Cell RNA Sequencing Methods. Mol Cell. 2017;65(4):631-643.e4.

85. Cheng J, Liao J, Shao X, Lu X, Fan X. Multiplexing Methods for Simultaneous Large-Scale Transcriptomic Profiling of Samples at Single-Cell Resolution. Advanced Science. 2021;8(17):1–14.

86. Hicks SC, Townes FW, Teng M, Irizarry RA, Townes FW. Missing Data and Technical Variability in Single-Cell RNA-Sequencing Experiments Keywords. bioRxiv preprint. 2015;

87. Leek JT, Scharpf RB, Bravo HC, Simcha D, Langmead B, Johnson WE, et al. Tackling the widespread and critical impact of batch effects in high-throughput data. Nat Rev Genet [Internet]. 2010;11(10):733–9. Available from: http://dx.doi.org/10.1038/nrg2825

88. Proserpio V, Casale FP, Natarajan KN, Marioni JC, Stegle O, Teichmann SA, et al. Computational analysis of cell-to-cell heterogeneity in single-cell RNA-sequencing data reveals hidden subpopulations of cells. Nat Biotechnol. 2015;33(2):155–60.

89. Brennecke P, Anders S, Kim JK, Kołodziejczyk AA, Zhang X, Proserpio V, et al. Accounting for technical noise in single-cell RNA-seq experiments. Nat Methods. 2013;10(11):1093–8.

90. Stegle O, Teichmann SA, Marioni JC. Computational and analytical challenges in single-cell transcriptomics. Nat Rev Genet [Internet]. 2015;16(3):133–45. Available from: http://dx.doi.org/10.1038/nrg3833

91. Arzalluz-Luque Á, Devailly G, Mantsoki A, Joshi A. Delineating biological and technical variance in single cell expression data. International Journal of Biochemistry and Cell Biology [Internet]. 2017;90(July):161–6. Available from: http://dx.doi.org/10.1016/j.biocel.2017.07.006

92. Zheng GXY, Terry JM, Belgrader P, Ryvkin P, Bent ZW, Wilson R, et al. Massively parallel digital transcriptional profiling of single cells. Nat Commun [Internet]. 2017;8:1–12. Available from: http://dx.doi.org/10.1038/ncomms14049

93. AlJanahi AA, Danielsen M, Dunbar CE. An Introduction to the Analysis of Single-Cell RNA-Sequencing Data. Mol Ther Methods Clin Dev [Internet]. 2018;10(September):189–96. Available from: http://dx.doi.org/10.1016/j.omtm.2018.07.003

94. Williams CR, Baccarella A, Parrish JZ, Kim CC. Trimming of sequence reads alters RNA-Seq gene expression estimates. BMC Bioinformatics

[Internet]. 2016;17(1):1–13. Available from: http://dx.doi.org/10.1186/s12859-016-0956-2

95. Poirion OB, Zhu X, Ching T, Garmire L. Single-cell transcriptomics bioinformatics and computational challenges. Front Genet. 2016;7(SEP):1–11.

96. Luecken MD, Theis FJ. Current best practices in single-cell RNA-seq analysis: a tutorial. Mol Syst Biol. 2019;15(6).

97. Lun ATL, Bach K, Marioni JC. Pooling across cells to normalize single-cell RNA sequencing data with many zero counts. Genome Biol [Internet]. 2016;17(1):1–14. Available from: http://dx.doi.org/10.1186/s13059-016-0947-7

98. Bacher R, Chu LF, Leng N, Gasch AP, Thomson JA, Stewart RM, et al. SCnorm: Robust normalization of single-cell RNA-seq data. Nat Methods [Internet]. 2017;14(6):584–6. Available from: http://dx.doi.org/10.1038/nmeth.4263

99. Tom Sean Smith, Andreas Heger, Ian Sudbery. UMI-tools: Modelling sequencing errors in Unique Molecular Identifiers to improve quantification accuracy. Genome Res. 2017;

100. Parekh S, Ziegenhain C, Vieth B, Enard W, Hellmann I. zUMIs - A fast and flexible pipeline to process RNA sequencing data with UMIs. Gigascience. 2018;7(6):1–9.

101. Petukhov V, Guo J, Baryawno N, Severe N, Scadden DT, Samsonova MG, et al. dropEst: Pipeline for accurate estimation of molecular counts in droplet-based single-cell RNA-seq experiments. Genome Biol. 2018;19(1):1–16.

102. Tian L, Su S, Dong X, Amann-Zalcenstein D, Biben C, Seidi A, et al. scPipe: A flexible R/Bioconductor preprocessing pipeline for single-cell RNA-sequencing data. PLoS Comput Biol [Internet]. 2018;14(8):e1006361. Available from: http://dx.plos.org/10.1371/journal.pcbi.1006361

103. Camara PG. Methods and challenges in the analysis of single-cell RNA-sequencing data. Curr Opin Syst Biol [Internet]. 2018;7:47–53. Available from: https://doi.org/10.1016/j.coisb.2017.12.007

104. Satija R, Farrell JA, Gennert D, Schier AF, Regev A. Spatial reconstruction of single-cell gene expression data. Nat Biotechnol. 2015;33(5):495–502.

105. McCarthy DJ, Campbell KR, Lun ATL, Wills QF. Scater: Pre-processing, quality control, normalization and visualization of single-cell RNA-seq data in R. Bioinformatics. 2017;33(8):1179–86.

106. Wolf FA, Angerer P, Theis FJ. SCANPY: Large-scale single-cell gene expression data analysis. Genome Biol. 2018 Feb 6;19(1).

107. Ilicic T, Kim JK, Kolodziejczyk AA, Bagger FO, McCarthy DJ, Marioni JC, et al. Classification of low quality cells from single-cell RNA-seq data. Genome Biol [Internet]. 2016;17(1):1–15. Available from: http://dx.doi.org/10.1186/s13059-016-0888-1

108. You Y, Tian L, Su S, Dong X, Jabbari JS, Hickey PF, et al. Benchmarking UMI-based single-cell RNA-seq preprocessing workflows. Genome Biol. 2021;22(1):1–32.

109. Lun ATL, Riesenfeld S, Andrews T, Dao TP, Gomes T, Marioni JC. EmptyDrops: Distinguishing cells from empty droplets in droplet-based single-cell RNA sequencing data. Genome Biol. 2019;20(1):1–9.

110. Wolock SL, Lopez R, Klein AM. Scrublet: Computational Identification of Cell Doublets in Single-Cell Transcriptomic Data. Cell Syst [Internet]. 2019;8(4):281-291.e9. Available from: https://doi.org/10.1016/j.cels.2018.11.005

111. McGinnis CS, Murrow LM, Gartner ZJ. DoubletFinder: Doublet Detection in Single-Cell RNA Sequencing Data Using Artificial Nearest Neighbors. Cell Syst [Internet]. 2019;8(4):329-337.e4. Available from: https://doi.org/10.1016/j.cels.2019.03.003

112. Andrews TS, Hemberg M. Dropout-based feature selection for scRNASeq. 2016;1–3.
113. Andrews TS, Hemberg M. Identifying cell populations with scRNASeq. Mol Aspects Med [Internet]. 2018;59:114–22. Available from: https://doi.org/10.1016/j.mam.2017.07.002
114. van der Maaten LJP, Hinton GE. Visualizing high-dimensional data using t-sne. Journal of Machine Learning Research [Internet]. 2008;9:2579–605. Available from: https://lvdmaaten.github.io/publications/papers/JMLR_2008.pdf%0Ahttp://www.ncbi.nlm.nih.gov/entrez/query.fcgi?db=pubmed&cmd=Retrieve&dopt=AbstractPlus&list_uids=7911431479148734548related:VOiAgwMNy20J
115. McInnes L, Healy J, Melville J. UMAP: Uniform Manifold Approximation and Projection for Dimension Reduction. 2018; Available from: http://arxiv.org/abs/1802.03426
116. Becht E, McInnes L, Healy J, Dutertre CA, Kwok IWH, Ng LG, et al. Dimensionality reduction for visualizing single-cell data using UMAP. Nat Biotechnol. 2019;37(1):38–47.
117. Kiselev VY, Andrews TS, Hemberg M. Challenges in unsupervised clustering of single-cell RNA-seq data. Nat Rev Genet [Internet]. 2019; Available from: http://dx.doi.org/10.1038/s41576-018-0088-9
118. Wu Y, Zhang K. Tools for the analysis of high-dimensional single-cell RNA sequencing data. Nat Rev Nephrol [Internet]. 2020;16(7):408–21. Available from: http://dx.doi.org/10.1038/s41581-020-0262-0
119. Carangelo G, Magi A, Semeraro R. From multitude to singularity: An up-to-date overview of scRNA-seq data generation and analysis. Front Genet. 2022;13(October):1–16.
120. Blondel VD, Guillaume JL, Lambiotte R, Lefebvre E. Fast unfolding of communities in large networks. Journal of Statistical Mechanics: Theory and Experiment. 2008;2008(10).

121. Traag VA, Waltman L, van Eck NJ. From Louvain to Leiden: guaranteeing well-connected communities. Sci Rep. 2019 Dec 1;9(1).
122. Anuar SHH, Abas ZA, Yunos NM, Zaki NHM, Hashim NA, Mokhtar MF, et al. Comparison between Louvain and Leiden Algorithm for Network Structure: A Review. J Phys Conf Ser. 2021;2129(1).
123. Polański K, Young MD, Miao Z, Meyer KB, Teichmann SA, Park JE. BBKNN: Fast batch alignment of single cell transcriptomes. Bioinformatics. 2020;36(3):964–5.
124. Korsunsky I, Millard N, Fan J, Slowikowski K, Zhang F, Wei K, et al. Fast, sensitive and accurate integration of single-cell data with Harmony. Nat Methods. 2019 Dec 1;16(12):1289–96.
125. Joshua W, Kozareva V, Ferreira A, Vanderburg C, Martin C, Macosko E. Integrative inference of brain cell similarities and differences from single-cell genomics. bioRxiv. 2018;26(2):107–10.
126. Stuart T, Butler A, Hoffman P, Hafemeister C, Papalexi E, Mauck WM, et al. Comprehensive Integration of Single-Cell Data. Cell [Internet]. 2019;177(7):1888-1902.e21. Available from: https://doi.org/10.1016/j.cell.2019.05.031
127. Tran HTN, Ang KS, Chevrier M, Zhang X, Lee NYS, Goh M, et al. A benchmark of batch-effect correction methods for single-cell RNA sequencing data. Genome Biol. 2020;21(1):1–32.
128. Wagner A, Regev A, Yosef N. Revealing the vectors of cellular identity with single-cell genomics. Nat Biotechnol [Internet]. 2016;34(11):1145–60. Available from: http://dx.doi.org/10.1038/nbt.3711
129. Is W, Type C, Clevers H, Rafelski S, Elowitz M, Lein E. What Is Your Conceptual Definition of "Cell Type" in the Context of a Mature Organism? Cell Syst. 2017;4(3):255–9.
130. Choi YH, Kim JK. Dissecting Cellular Heterogeneity Using Single-Cell RNA Sequencing. Mol Cells [Internet]. 2018;41(10):0–0. Available from: http://dx.doi.org/10.14348/molcells.2018.0446www.molcells.org

131. Papalexi E, Satija R. Single-cell RNA sequencing to explore immune cell heterogeneity. Nat Rev Immunol [Internet]. 2018;18(1):35–45. Available from: http://dx.doi.org/10.1038/nri.2017.76

132. Aran D, Looney AP, Liu L, Wu E, Fong V, Hsu A, et al. Reference-based analysis of lung single-cell sequencing reveals a transitional profibrotic macrophage. Nat Immunol [Internet]. Available from: http://dx.doi.org/10.1038/s41590-018-0276-y

133. Kanter D, K. J, Lijnzaad L, P. P, Candelli C, T. T, et al. CHETAH: a selective, hierarchical cell type identification method for single-cell RNA sequencing. bioRxiv Bioinformatics [Internet]. 2019; Available from: http://biorxiv.org/cgi/content/short/558908v1

134. Kiselev VYu, Yiu A, Hemberg M. scmap - A tool for unsupervised projection of single cell RNA-seq data. bioRxiv [Internet]. 2017;150292. Available from: https://www.biorxiv.org/content/early/2017/11/29/150292

135. Hao Y, Hao S, Andersen-Nissen E, Mauck WM, Zheng S, Butler A, et al. Integrated analysis of multimodal single-cell data. Cell [Internet]. 2021;184(13):3573-3587.e29. Available from: https://doi.org/10.1016/j.cell.2021.04.048

136. Pliner HA, Shendure J, Trapnell C. Supervised classification enables rapid annotation of cell atlases. bioRxiv [Internet]. 2019;538652. Available from: https://www.biorxiv.org/content/10.1101/538652v1

137. Abdelaal T, Michielsen L, Cats D, Hoogduin D, Mei H, Reinders MJT, et al. A comparison of automatic cell identification methods for single-cell RNA sequencing data. Genome Biol. 2019;20(1):1–19.

138. Chen G, Ning B, Shi T. Single-cell RNA-seq technologies and related computational data analysis. Front Genet. 2019;10(APR):1–13.

139. Robinson MD, McCarthy DJ, Smyth GK. edgeR: A Bioconductor package for differential expression analysis of digital gene expression data. Bioinformatics. 2009;26(1):139–40.

140. Love MI, Huber W, Anders S. Moderated estimation of fold change and dispersion for RNA-seq data with DESeq2. Genome Biol. 2014;15(12):1–21.

141. Crowell HL, Soneson C, Germain PL, Calini D, Collin L, Raposo C, et al. Muscat Detects Subpopulation-Specific State Transitions From Multi-Sample Multi-Condition Single-Cell Transcriptomics Data. Nat Commun [Internet]. 2020;11(1):1–12. Available from: http://dx.doi.org/10.1038/s41467-020-19894-4

142. Subramanian A, Tamayo P, Mootha VK, Mukherjee S, Ebert BL, Gillette MA, et al. Gene set enrichment analysis: A knowledge-based approach for interpreting genome-wide expression profiles. Proc Natl Acad Sci U S A. 2005;102(43):15545–50.

143. Sergushichev AA. An algorithm for fast preranked gene set enrichment analysis using cumulative statistic calculation. bioRxiv [Internet]. 2016;060012. Available from: https://www.biorxiv.org/content/10.1101/060012v1%0Ahttps://www.biorxiv.org/content/10.1101/060012v1.abstract

144. Türei D, Valdeolivas A, Gul L, Palacio-Escat N, Klein M, Ivanova O, et al. Integrated intra- and intercellular signaling knowledge for multicellular omics analysis. Mol Syst Biol. 2021;17(3):1–16.

145. Bateman A, Martin MJ, Orchard S, Magrane M, Agivetova R, Ahmad S, et al. UniProt: the universal protein knowledgebase in 2021. Nucleic Acids Res. 2021;49(D1):D480–9.

146. Hermjakob H, Montecchi-Palazzi L, Lewington C, Mudali S, Kerrien S, Orchard S, et al. IntAct: An open source molecular interaction database. Nucleic Acids Res. 2004;32(DATABASE ISS.):452–5.

147. Dimitrov D, Türei D, Garrido-Rodriguez M, Burmedi PL, Nagai JS, Boys C, et al. Comparison of methods and resources for cell-cell communication inference from single-cell RNA-Seq data. Nat Commun. 2022;13(1).

148. Browaeys R, Saelens W, Saeys Y. NicheNet: modeling intercellular communication by linking ligands to target genes. Nat Methods [Internet]. 2020;17(2):159–62. Available from: http://dx.doi.org/10.1038/s41592-019-0667-5

149. Hu Y, Peng T, Gao L, Tan K. CytoTalk: De novo construction of signal transduction networks using single-cell transcriptomic data. Sci Adv. 2021;7(16).

150. Peterson VM, Zhang KX, Kumar N, Wong J, Li L, Wilson DC, et al. Multiplexed quantification of proteins and transcripts in single cells. Nat Biotechnol. 2017;35(10):936–9.

151. Stoeckius M, Hafemeister C, Stephenson W, Houck-Loomis B, Chattopadhyay PK, Swerdlow H, et al. Simultaneous epitope and transcriptome measurement in single cells. Nat Methods. 2017;14(9):865–8.

152. Todorovic V. Single-cell RNA-seq—now with protein. Nat Methods [Internet]. 2017;14(11):1028–9. Available from: http://dx.doi.org/10.1038/nmeth.4488

153. Smibert P, Mimitou E, Stoeckius M. Expanding the CITE-seq tool-kit: Detection of proteins, transcriptomes, clonotypes and CRISPR perturbations with multiplexing, in a single assay. Protoc Exch. 2019;16(5):409–12.

154. Baron M, Yanai I. New skin for the old RNA-Seq ceremony: The age of single-cell multi-omics. Genome Biol. 2017;18(1):17–9.

155. Zheng Y, Jun SH, Tian Y, Florian M, Gottardo R. Robust Normalization and Integration of Single-cell Protein Expression across CITE-seq Datasets. bioRxiv [Internet]. 2022;2022.04.29.489989. Available from: https://www.biorxiv.org/content/10.1101/2022.04.29.489989v1%0Ahttps://www.biorxiv.org/content/10.1101/2022.04.29.489989v1.abstract

156. Aitchison J. Measures of location of compositional data sets. Math Geol. 1989;21(7):787–90.

157. Mulè MP, Martins AJ, Tsang JS. Normalizing and denoising protein expression data from droplet-based single cell profiling. bioRxiv. 2020;2020.02.24.963603.
158. Goldstein LD, Chen YJJ, Wu J, Chaudhuri S, Hsiao YC, Schneider K, et al. Massively parallel single-cell B-cell receptor sequencing enables rapid discovery of diverse antigen-reactive antibodies. Commun Biol [Internet]. 2019;2(1). Available from: http://dx.doi.org/10.1038/s42003-019-0551-y
159. Sturm1 G, Szabo T, Fotakis G, Haider1 M, Rieder D, Trajanoski Z, et al. Scirpy: A Scanpy extension for analyzing single-cell T-cell receptor-sequencing data. Bioinformatics. 2020;36(18):4817–8.
160. Borcherding N, Bormann NL, Kraus G. scRepertoire: An R-based toolkit for single-cell immune receptor analysis. F1000Res. 2020;9:1–17.
161. Team I. immunarch: An R Package for Painless Bioinformatics Analysis of T-Cell and B-Cell Immune Repertoires. Zenodo. 2019;
162. Zavidij O, Haradhvala NJ, Mouhieddine TH, Sklavenitis-Pistofidis R, Cai S, Reidy M, et al. Single-cell RNA sequencing reveals compromised immune microenvironment in precursor stages of multiple myeloma. Nat Cancer [Internet]. 2020;1(5):493–506. Available from: http://dx.doi.org/10.1038/s43018-020-0053-3
163. de Jong MME, Kellermayer Z, Papazian N, Tahri S, Hofste op Bruinink D, Hoogenboezem R, et al. The multiple myeloma microenvironment is defined by an inflammatory stromal cell landscape. Nat Immunol [Internet]. 2021;22(6):769–80. Available from: http://dx.doi.org/10.1038/s41590-021-00931-3
164. Pilcher W, Thomas BE, Bhasin SS, Jayasinghe RG, Yao L, Gonzalez-Kozlova E, et al. Cross center single-cell RNA sequencing study of the immune microenvironment in rapid progressing multiple myeloma. NPJ Genom Med. 2023;8(1).
165. Jin S, Guerrero-Juarez CF, Zhang L, Chang I, Ramos R, Kuan CH, et al. Inference and analysis of cell-cell communication using CellChat. Nat

Commun [Internet]. 2021;12(1):1–20. Available from: http://dx.doi.org/10.1038/s41467-021-21246-9

166. Ledergor G, Weiner A, Zada M, Wang SY, Cohen YC, Gatt ME, et al. Single cell dissection of plasma cell heterogeneity in symptomatic and asymptomatic myeloma [Internet]. Vol. 24, Nature Medicine. Springer US; 2018. 1867–1876 p. Available from: http://dx.doi.org/10.1038/s41591-018-0269-2

167. Boiarsky R, Haradhvala NJ, Alberge JB, Sklavenitis-Pistofidis R, Mouhieddine TH, Zavidij O, et al. Single cell characterization of myeloma and its precursor conditions reveals transcriptional signatures of early tumorigenesis. Nat Commun. 2022;13(1).

168. Liu R, Gao Q, Foltz SM, Fowles JS, Yao L, Wang JT, et al. Co-evolution of tumor and immune cells during progression of multiple myeloma. Nat Commun [Internet]. 2021;12(1):1–18. Available from: http://dx.doi.org/10.1038/s41467-021-22804-x

169. Chen J, He D, Chen Q, Guo X, Yang L, Lin X, et al. BAFF is involved in macrophage-induced bortezomib resistance in myeloma. Cell Death Dis. 2017;8(11).

170. Novak AJ, Darce JR, Arendt BK, Harder B, Henderson K, Kindsvogel W, et al. Expression of BCMA, TACI, and BAFF-R in multiple myeloma: A mechanism for growth and survival. Blood. 2004;103(2):689–94.

171. Sheu BC, Wen-Chun Chang C, Cheng HY, Lin HH, Chang DY, Huang SC, et al. Cytokine regulation networks in the cancer microenvironment. 2008;13(16):6255–68.

172. Gambella M, Palumbo A, Rocci A. MET/HGF pathway in multiple myeloma: From diagnosis to targeted therapy? Expert Rev Mol Diagn. 2015;15(7):881–93.

173. Mahtouk K, Tjin EPM, Spaargaren M, Pals ST. The HGF/MET pathway as target for the treatment of multiple myeloma and B-cell lymphomas.

Biochim Biophys Acta Rev Cancer [Internet]. 2010;1806(2):208–19. Available from: http://dx.doi.org/10.1016/j.bbcan.2010.07.006

174. Babu SN, Chetal G, Kumar S. Macrophage migration inhibitory factor: A potential marker for cancer diagnosis and therapy. Asian Pacific Journal of Cancer Prevention. 2012;13(5):1737–44.

175. Xu J, Yu N, Zhao P, Wang F, Huang J, Cui Y, et al. Intratumor Heterogeneity of MIF Expression Correlates With Extramedullary Involvement of Multiple Myeloma. Front Oncol. 2021;11(June):1–13.

176. Wang Q, Zhao D, Xian M, Wang Z, Bi E, Su P, et al. MIF as a biomarker and therapeutic target for overcoming resistance to proteasome inhibitors in human myeloma. Blood. 2020;136(22):2557–73.

177. Lewinsky H, Gunes EG, David K, Radomir L, Kramer MP, Pellegrino B, et al. CD84 is a regulator of the immunosuppressive microenvironment in multiple myeloma. JCI Insight. 2021;6(4):1–25.

178. Gutiérrez-González A, Martínez-Moreno M, Samaniego R, Arellano-Sánchez N, Salinas-Muñoz L, Relloso M, et al. Evaluation of the potential therapeutic benefits of macrophage reprogramming in multiple myeloma. Blood. 2016;128(18):2241–52.

179. Jovanović KK, Roche-Lestienne C, Ghobrial IM, Facon T, Quesnel B, Manier S. Targeting MYC in multiple myeloma. Leukemia. 2018;32(6):1295–306.

180. John L, Krauth MT, Podar K. Pathway-Directed Therapy in Multiple Myeloma. Cancers (Basel). 2021;13(7):1668.

181. Rizzieri D, Paul B, Kang Y. Metabolic alterations and the potential for targeting metabolic pathways in the treatment of multiple myeloma. J Cancer Metastasis Treat. 2019;2019.

182. Masarwi M, DeSchiffart A, Ham J, Reagan MR. Multiple Myeloma and Fatty Acid Metabolism. JBMR Plus. 2019;3(3):1–10.

183. Petroni G, Formenti SC, Chen-Kiang S, Galluzzi L. Immunomodulation by anticancer cell cycle inhibitors. Nat Rev Immunol [Internet].

2020;20(11):669–79. Available from: http://dx.doi.org/10.1038/s41577-020-0300-y

184. Maes A, Menu E, de Veirman K, Maes K, Vanderkerken K, de Bruyne E. The therapeutic potential of cell cycle targeting in multiple myeloma. Oncotarget. 2017;8(52):90501–20.

185. Derksen PWB, Tjin E, Meijer HP, Klok MD, Mac Gillavry HD, Van Oers MHJ, et al. Illegitimate WNT signaling promotes proliferation of multiple myeloma cells. Proc Natl Acad Sci U S A. 2004;101(16):6122–7.

186. Spaan I, Raymakers RA, Van De Stolpe A, Peperzak V. Wnt signaling in multiple myeloma: A central player in disease with therapeutic potential. J Hematol Oncol. 2018;11(1):1–18.

187. Kim Y, Reifenberger G, Lu D, Endo T, Carson DA, Gast SM, et al. Influencing the Wnt signaling pathway in multiple myeloma. Anticancer Res. 2011;31(2):725–30.

188. Nefedova Y, Sullivan DM, Bolick SC, Dalton WS, Gabrilovich DI. Inhibition of notch signaling induces apoptosis of myeloma cells and enhances sensitivity to chemotherapy. Blood. 2008;111(4):2220–9.

189. Sabol HM, Delgado-Calle J. The multifunctional role of Notch signaling in multiple myeloma. J Cancer Metastasis Treat. 2021;7.

190. Colombo M, Galletti S, Garavelli S, Platonova N, Paoli A, Basile A, et al. Notch signaling deregulation in multiple myeloma: A rational molecular target. Oncotarget. 2015;6(29):26826–40.

191. Montfort A, Colacios C, Levade T, Andrieu-Abadie N, Meyer N, Ségui B. The TNF paradox in cancer progression and immunotherapy. Front Immunol. 2019;10(JULY):1–5.

192. Budhwani M, Mazzieri R, Dolcetti R. Plasticity of type I interferon-mediated responses in cancer therapy: From anti-tumor immunity to resistance. Front Oncol. 2018;8(AUG).

193. Borden EC. Interferons α and β in cancer: therapeutic opportunities from new insights. Nat Rev Drug Discov [Internet]. 2019;18(3):219–34. Available from: http://dx.doi.org/10.1038/s41573-018-0011-2

194. Josephs SF, Ichim TE, Prince SM, Kesari S, Marincola FM, Escobedo AR, et al. Unleashing endogenous TNF-alpha as a cancer immunotherapeutic. J Transl Med [Internet]. 2018;16(1):1–8. Available from: https://doi.org/10.1186/s12967-018-1611-7

195. Vazquez MI, Catalan-Dibene J, Zlotnik A. B cells responses and cytokine production are regulated by their immune microenvironment. Cytokine [Internet]. 2015;74(2):318–26. Available from: http://dx.doi.org/10.1016/j.cyto.2015.02.007

196. Zhang L, Tai YT, Ho MZG, Qiu L, Anderson KC. Interferon-alpha-based immunotherapies in the treatment of B cell-derived hematologic neoplasms in today's treat-to-target era. Exp Hematol Oncol. 2017;6(1):1–9.

197. Urban VS, Cegledi A, Mikala G. Multiple myeloma, a quintessential malignant disease of aging: a geroscience perspective on pathogenesis and treatment. Geroscience [Internet]. 2023;45(2):727–46. Available from: https://doi.org/10.1007/s11357-022-00698-x

198. Martino A, Buda G, Maggini V, Lapi F, Lupia A, Di Bello D, et al. Could age modify the effect of genetic variants in IL6 and TNF-α genes in multiple myeloma? Leuk Res [Internet]. 2012;36(5):594–7. Available from: http://dx.doi.org/10.1016/j.leukres.2012.02.009

199. Pritz T, Weinberger B, Grubeck-Loebenstein B. The aging bone marrow and its impact on immune responses in old age. Immunol Lett [Internet]. 2014;162(1):310–5. Available from: http://dx.doi.org/10.1016/j.imlet.2014.06.016

200. Benet Z, Jing Z, Fooksman DR. Plasma cell dynamics in the bone marrow niche. Cell Rep [Internet]. 2021;34(6):108733. Available from: https://doi.org/10.1016/j.celrep.2021.108733

201. Meng Z, Veenstra TD. Targeted mass spectrometry approaches for protein biomarker verification. J Proteomics [Internet]. 2011;74(12):2650–9. Available from: http://dx.doi.org/10.1016/j.jprot.2011.04.011
202. Miao L, Zhang Y, Huang L. mRNA vaccine for cancer immunotherapy. Mol Cancer. 2021;20(1):1–23.

Publications and Abstracts

1. Ritacco, C., Köse, M. C., Courtois, J., Canti, L., Beguin, C., Dubois, S., ... & Baron, F. (2023). Post-transplant cyclophosphamide prevents xenogeneic graft-versus-host disease while depleting proliferating regulatory T-cells. *Iscience*, *26*(3).
   https://hdl.handle.net/2268/300893

2. Köse, M. C., Lejeune, M., Gou, M. J., Duray, E., Cobraiville, G., Foguenne, J., ... & Caers, J. (2022). Integrative Analysis of Proteomics and Transcriptomics Reveals the Etrb As Novel Single Target and New Combinatorial Targets for Multiple Myeloma. Blood, 140(Supplement 1), 4219-4219.
   https://hdl.handle.net/2268/301610

3. Gou, M. J., Köse, M. C., Crommen, J., Nix, C., Cobraiville, G., Caers, J., & Fillet, M. (2022). Contribution of Capillary Zone Electrophoresis Hyphenated with Drift Tube Ion Mobility Mass Spectrometry as a Complementary Tool to Microfluidic Reversed Phase Liquid Chromatography for Antigen Discovery. International Journal of Molecular Sciences, 23(21), 13350.
   https://hdl.handle.net/2268/299662

4. Köse, M. C., Bergiers, I., Malfait, M., Heidrich, B., De Maeyer, D., Fourneau, N., ... & Casneuf, T. (2022). S170: DYNAMIC INTERPLAY BETWEEN TUMOR AND MICRO-ENVIRONMENT DURING MYELOMA DISEASE PROGRESSION. HemaSphere, 6, 71-72.
https://hdl.handle.net/2268/301609

5. Vrancken, L., Lejeune, M., PIROTTE, M., Duray, E., Köse, M. C., BEGUIN, Y., & CAERS, J. (2021). Le myélome multiple: un tour d'horizon des nouveautés dans sa biologie et son traitement. Revue Médicale de Liège, 76.
https://hdl.handle.net/2268/260541

6. Lejeune, M., Köse, M. C., Duray, E., Einsele, H., Beguin, Y., & Caers, J. (2020). Bispecific, T-cell- recruiting antibodies in B-cell malignancies. Frontiers in Immunology, 11, 762.
https://hdl.handle.net/2268/248987

7. Lejeune, M., Köse, M. C., Duray, E., Beguin, Y., & CAERS, J. (2020). Les anticorps bispécifiques ciblant les lymphocytes T dans le myélome multiple. Onco: Revue Multidisciplinaire d'Oncologie, 14(6).
https://hdl.handle.net/2268/255130

8. Bolomsky, A., Vogler, M., Köse, M. C., Heckman, C. A., Ehx, G., Ludwig, H., & Caers, J. (2020). MCL-1 inhibitors, fast-lane development of a new class of anti-cancer agents. Journal of hematology & oncology, 13(1), 1-19.
https://hdl.handle.net/2268/254099